Electrostatic Analyzers with Application to Electric Propulsion Testing

IEPC-2013-300

Presented at the 33rd International Electric Propulsion Conference,
The George Washington University • Washington, D.C. • USA
October 6 – 10, 2013

Casey C. Farnell[1] and Cody C. Farnell[2]
Colorado State University, Fort Collins, CO 80523, USA
Plasma Controls, LLC, Fort Collins, CO 80526, USA

Shawn C. Farnell[3]
Kenyon College, Gambier, OH 43022, USA
Plasma Controls, LLC, Fort Collins, CO 80526, USA

and

John D. Williams[4]
Colorado State University, Fort Collins, CO 80523, USA
Plasma Controls, LLC, Fort Collins, CO 80526, USA

Abstract: Electrostatic analyzers (ESAs) are used in electric propulsion to measure the energy per unit charge E/q distribution of ion and electron beams, in the downstream region of thrusters for example. This paper serves to give an overview of the most fundamental, yet most widely used, types of ESA designs. Analyzers are grouped into two classifications: (1) mirror-type analyzers and (2) deflector-type analyzers. Common mirror-type analyzers are the parallel-plate mirror analyzer (PMA) and the cylindrical mirror analyzer (CMA). For deflector type analyzers, a generalized toroidal type is first described and the commonly used cylindrical deflector (CDA) and spherical deflector (SDA) analyzers are discussed as special cases. The procedure for energy resolution calculations of ESAs is described, which is a common way of comparing analyzers. Finally, we present ion energy distributions from a SDA, comparing variations in particle energy, particle angle, entrance and exit geometry, and sector angle using both numerical calculation and particle simulation.

[1] Research Scientist, Dept. of Mechanical Engineering, casey.farnell@colostate.edu
[2] Research Scientist, Dept. of Mechanical Engineering, cody.farnell@colostate.edu
[3] Visiting Assistant Professor, Dept. of Mathematics & Statistics, farnells@kenyon.edu
[4] Associate Professor, Dept. of Mechanical Engineering, john.d.williams@colostate.edu

Nomenclature

Symbol	Units	Description
A, B, C, n	-	Constants for FBW/HBW energy resolution equations
a, b, c, n	-	Constants for FWHM energy resolution equations
$a^*, b^*, c^*, \omega, M, D^*, l_n$	-	Constants for energy resolution equations
a_α	-	Angular coordinate for particle motion
$\vec{B}$	(T)	Magnetic field
b	(m)	Half slit width
b_β	-	Angular coordinate for particle motion
C	-	Analyzer constant
c_t	-	Toroidal factor
D_k	(m)	Coefficient of energy dispersion
$\widetilde{D}$	(m)	Axial energy dispersion coefficient for mirror analyzers
d	(m)	Distance
$E \text{ or } E_p$	(eV)	Range of particle energies or a selected particle energy in the beam
E_0	(eV)	Transmission (TE) or pass energy
$\vec{E}$	(V/m) or (N/C)	Electric field
$\Delta E = FWHM$	(eV)	Full width at half of the maximum height of the energy transmission function
$\Delta E_B = FBW$	(eV)	Base energy resolution; full width of the energy transmission function
$\Delta E_h = HBW$	(eV)	Half the base energy resolution
ΔE_p	(eV)	Individual particle energy relative to the pass energy of the analyzer.
$\frac{\Delta E}{E_0}$	-	Energy resolution
$e = 1.6022\ x\ 10^{-19}$	(C)	Elementary charge unit
$\vec{F}$	(N)	Force acting on a charged particle
f	-	Transmission, fraction of transmitted particles
g_0	(m)	Half of the gap width between the analyzer electrodes
h	(m)	Ideal field boundary to electrode separation distance
J	(A)	Beam current
K	-	CMA coefficient
k	-	Calibration factor, reciprocal of the analyzer constant C
k_B	(J/K)	Boltzmann constant
k_T	-	Matsuda plate distance factor
L	(m)	Source to image focusing length
M	-	Linear magnification coefficient
m	(kg)	Mass
$\dot{m}$	(kg/s)	Mass flow rate
n	(m^{-3})	Particle density
P	(torr) or ($A/V^{3/2}$)	Pressure or Perveance
q	(C)	Charge of a particle
R_B	-	Ratio of beam radius to minimum beam radius
r	(m)	Radius
r_m	(m)	Minimum space charge beam radius
T	(N or K)	Thrust or temperature
t_w	(m)	Trace width
V	(Volts)	Voltage
V_s	(Volts)	Analyzer entrance/exit potential
ΔV	(Volts)	Voltage difference across plates/sectors

V_p	(Volts)	Potential of the plasma where ions are created
v	(m/s)	Velocity
w	(m)	Width of the entrance/exit slits of the analyzer
(x, y, z)	(m)	Cartesian coordinates for particle motion
z	-	Charge state of a particle (integer number)
α	(radians,°)	Acceptance half angle of the analyzer in the dispersion plane
β	(radians,°)	Acceptance half angle of the analyzer normal to the dispersion plane
δ	-	Relative deviation of kinetic energy
φ	(°)	Particle beam entrance angle, analyzer angle
λ	(m)	Mean free path
Ω	(Ohms)	Resistor value
ρ	-	Resolving power, reciprocal of energy resolution

I. Introduction

Electrostatic analyzers (ESAs) are used in electric propulsion to measure the energy per unit charge E/q distribution of ion and electron beams, in the downstream region of thrusters for example. The Electric Propulsion Technical Committee (EPTC) of the American Institute of Aeronautics and Astronautics (AIAA) was asked to assemble a Committee on Standards (CoS) for Electric Propulsion Testing. The assembled CoS was tasked with developing Standards and Recommended Practices for various diagnostic techniques used in the evaluation of plasma devices and plasma thrusters. This paper presents a partial summary of the Standard being developed for ESAs.

ESAs have a wide range of designs due to the fact that many configurations can be made which curve the trajectories of particles. This standard serves to give an overview of the most fundamental, yet most widely used, types of ESA designs. Analyzers are grouped into two classifications: (1) mirror-type analyzers and (2) deflector-type analyzers.

Mirror-type analyzers are designed based on electric fields in which particles are first retarded (decelerated), then re-accelerated. Two common mirror-type analyzers are discussed: the parallel-plate mirror analyzer (PMA) and the cylindrical mirror analyzer (CMA).

In deflector-type sector field analyzers, the energy of charged particles remains approximately constant along a circular optic axis. For deflector type analyzers, a generalized toroidal type is first described. Then, the commonly used cylindrical deflector (CDA) and spherical deflector (SDA) analyzers are discussed as special cases of the toroidal type. Many types of ESAs designed for wide field of view and spaceflight are based upon the toroidal ESA.

The pass energy (transmission energy) of an ESA is determined by the voltage potentials applied to the electrodes and the analyzer constant, which depends on its geometry. The procedure for energy resolution calculations of ESAs is described, which is a common way of comparing analyzers.

A. Applicability

In electric propulsion, an electrostatic analyzer is used to measure energy of charged particles in the plumes of thrusters. The beam energy is related to the beam velocity, and, additionally knowing the flux of particles from a thruster enables thrust measurement (Goebel and Katz 2008). Thrust is the force generated by a propulsion device according to the rate of expelled mass $\dot{m}$ multiplied by the exhaust velocity of the particles. In electric propulsion devices, ion beam velocities range from 5000 m/s to above 100,000 m/s, corresponding to typical ion beam energies from the low 10s of eV to above 10,000 eV (Jahn and Choueiri 2002).

Energy measurements of the thruster plume are also of interest for determining how the plume will interact with the surrounding environment. Also, since an electrostatic analyzer is an energy filter, it can also be used in experiments to selectively transmit charged particles of particular energy. This is useful in mass spectrometers for example that require narrow energy bands for mass separation.

There are three basic means of measuring the energy of charged particles in a beam (Moore, et al. 2009). These involve measuring: the time of flight over a known distance, the retarding potential required to stop the particles, or the extent of deflection in an electric, magnetic, or electromagnetic field. This standard will discuss a subset of third method; particle deflection and analysis using static (time invariant) electric fields, thus calling the resulting devices electrostatic analyzers, or ESAs. The use of magnetic fields will not be included. The following is a brief description

of all three methods of charged particle separation, helpful in comparing the use of ESAs in relation to other methods.

1. *Characteristics of time of flight analysis*

The kinetic energy of a charged particle (E_p) can be measured by recording the time it takes the particle to move from one position to another, which is called time of flight analysis. Because the velocities of charged particles are generally high, where the analyzing flight distance is in the range of a few centimeters, the response time of the analyzer's electronics needs to be on the order of a few nanoseconds (Moore, et al. 2009). Time of flight analyzers are generally used for the analysis of electrons with energies less than 10 eV and ions below 1 keV (Moore, et al. 2009).

2. *Characteristics of retarding electrostatic field analysis*

The kinetic energy distribution in a charged particle beam can also be measured by applying a retarding electrostatic field along the beam path (M. Yavor 2009) (Simpson, Design of Retarding Field Energy Analyzers 1961). The energy per unit charge (E/q) analysis of the beam is made by placing a grid or aperture in front of a particle detector (also called a collector) and varying the detector's potential while recording the collected current (Moore, et al. 2009). This device is commonly called a retarding potential analyzer (RPA). The current recorded at the collector is the integrated current of particles whose energy exceeds the potential established by the grid (Moore, et al. 2009), which forms a high-pass filter (Roy and Carette, Electron Spectroscopy for Surface Analysis 1977). To obtain the energy distribution, the integrated current is differentiated as a function of retarding potential. A drawback is that only the component of velocity normal to the retarding grid is selected (Moore, et al. 2009). Other difficulties include the development of focusing effects due to the variable nature of the ratio of the initial energy to the energy at the retarding potential grid, and potential "sag" between discriminating electrodes (Enloe and Shell, Optimizing the energy resolution of planar retarding potential analyzers 1992). Particles that approach the retarding grids at slightly off axis angles are often deflected away from the collector. This makes the transmission of the analyzer unpredictable, especially near the peak energies of interest. Space charge buildup and stray electric and magnetic fields can also be present near the retarding grid that prevents low energy particles from passing through the grid when desired (Green 1970) (Moore, et al. 2009).

3. *Characteristics of electromagnetic (electric or magnetic field) analysis*

The third approach to measuring particle energies is to pass the beam through an electric, magnetic, or electromagnetic field. When using static electric fields, the instrument is called an electrostatic analyzer (ESA). Static electric fields are more commonly used than shaped magnetic fields because they are generally easier to produce. Electrostatic analyzers are used for particle energies up to several keV while magnetic analyzers are used for very high energy particles due to the large electrical biases that would be required for effective particle analysis (Moore, et al. 2009). A wide range of energy analyzer designs exist; however, in all types of electrostatic devices, a charged particle is separated according to its energy per charge E/q rather than its absolute velocity.

II. Schematic / Design

A diagram and picture of a spherical deflector (SDA) type electrostatic analyzer, representative of ESAs in general, are shown in Figure 1. Particles enter the analyzer at the source plane and exit at the image plane. The analyzer geometry and applied voltages are chosen such that charged particles of a particular energy E_0/q, called the pass or transmission energy, curve along a prescribed path called the optic axis of the analyzer. The voltage difference between the plates ΔV, transmission energy, and geometry are related through equation (1), where C is the analzyer's geometrical constant.

$$\Delta V = (E_0/q)\, C \tag{1}$$

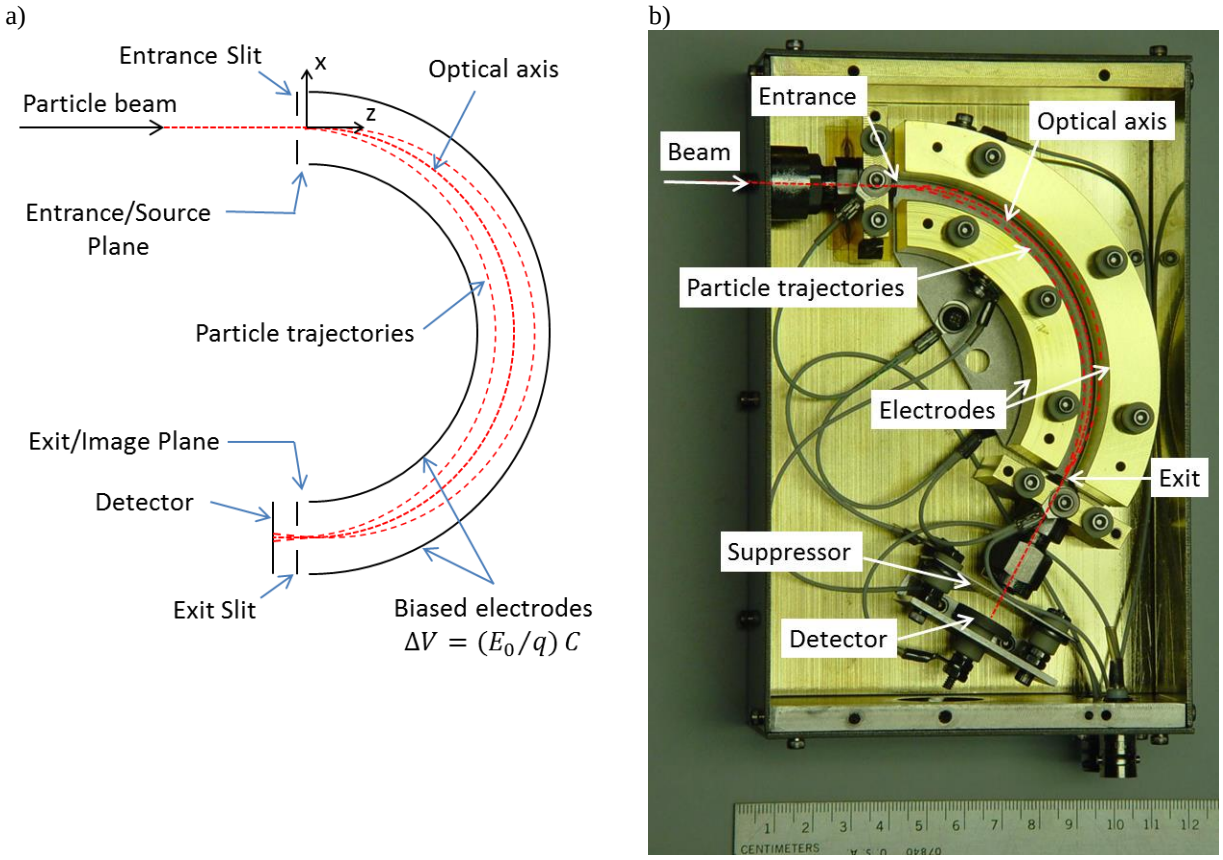

Figure 1. a) Diagram and b) photograph of an electrostatic analyzer made by Plasma Controls, LLC.

The function of the electrostatic analyzer is to separate charged particles according to their energy per charge. The main part of the ESA is a set of one or more electrodes, either flat or curved, that are biased to produce an electric field to curve the particles. The amount of deflection depends on each particle's initial energy to charge ratio, therefore enabling positional separation of particles based on energy.

The geometric size of the analyzer is chosen based on consideration of the desired energy resolving power as well as practicalities of overall dimensions, weight, and machinability. For analyzers designed to be flown in space as well as maneuvered in vacuum chambers with motion equipment, the volumetric size is typically on the order of 100's of cm^3 to 1000's of cm^3, and the mass is in the low kg range. Smaller designs have been manufactured that occupy as little volume as 1.5 cm^3 (C. Enloe 2003).

Figure 2 shows examples of particle trajectories passing through a spherical deflector analyzer. The x-z plane is the deflection, or dispersion, plane. A local coordinate system follows the particle along the optic axis, with x and y describing the particle position relative to the axis. The entrance is position 1 and the exit is position 2.

At the entrance, particles can deviate directionally through the half angles $\pm\alpha$ in the dispersion (x-z) plane and $\pm\beta$ in the perpendicular (y-z) plane, defined in equation (2). The analyzer geometry determines *where* the particles are refocused in the (α) deflection plane (at a particular φ about the y-axis), and *if* they are refocused in the (β) y-z plane.

$$\tan\alpha = \frac{v_x}{v_z}$$
$$\tan\beta = \frac{v_y}{v_z} \qquad (2)$$
$$v^2 = {v_x}^2 + {v_y}^2 + {v_z}^2 = {v_z}^2[(\tan\alpha)^2 + (\tan\beta)^2 + 1]$$

Particles that start on axis ($x_1 = 0$, $\alpha = 0°$) but have energy $E < E_0$ end up with $x_2 < 0$ as they don't have enough energy to stay on axis given the strength of the electric field. Conversely, particles with energy $E > E_0$ have too much energy to stay on axis. This is the basis of positional energy separation.

Particles typically enter and exit through slits of (generally equal) width w in the x direction and thin height in the y direction. Particles of energy $E = E_0$ and angle $\alpha = 0°$ entering at $x_1 = \pm\frac{w}{2}$ crossover the optic axis and exit at $x_2 = \mp\frac{w}{2}$. By optical analogy, all of the analyzers discussed herein are said to have a linear magnification coefficient $M_x = -1$, where the image of the object at the image plane is the same size but inverted.

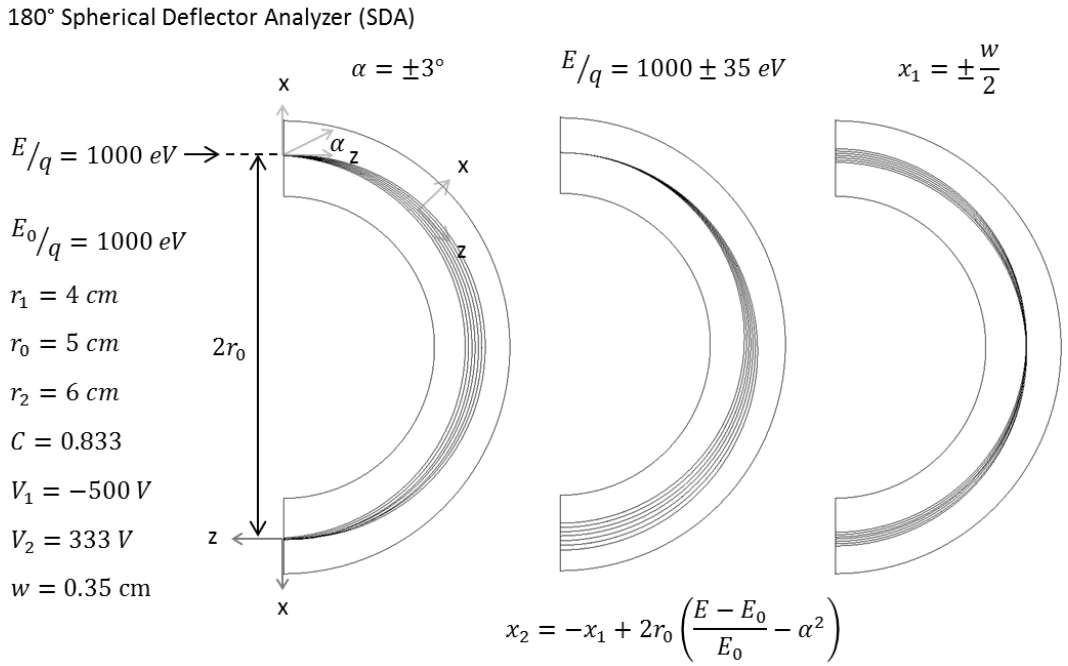

Figure 2. Particle trajectories through a 180° spherical deflector analyzer with angular, energy, and positional variation.

A detector can be placed at the downstream end of the exit slit to record the current of charged particles that exit the analyzer section. In the laboratory setting with an electric propulsion plasma device, the y-axis of the distribution function would typically be a current in the low microamp (μA) to picoamp (pA) range, scaling closely with the current density at the entrance slit. In general, entrance and exit slits help increase the resolving power and mitigate fringing electrostatic fields.

The analyzer can be operated as either a spectrometer (spectrometric mode) or a spectrograph (spectrographic mode) (Young, Space Plasma Particle Instrumentation and the New Paradigm: Faster, Cheaper, Better 1998). In a spectrometric mode, the energy E/q of the particle beam is analyzed by varying the electric field (thereby sweeping the pass energy E_0/q) and measuring the fraction of transmitted particles at a detector. The resulting current versus energy plot is called an energy transmission function, or an energy distribution function. Specifically, it is called an electron energy distribution function (EEDF) for electrons and an ion energy distribution function (IEDF) for ions. In a spectrographic mode, a range of energies are measured simultaneously by position sensitive detectors or a combination of detectors.

Desirable qualities of an analyzer include a small energy passband, large transmission, and accurate focusing. Two common terms that measure the quality of the analyzer are the energy dispersion, D_k, and the trace width, t_w (Rudd, Low Energy Electron Spectrometry 1972). The energy dispersion is the displacement of the image point per unit fractional change in (particle or analysis) energy. The trace width is the spread in the image for a monoenergetic point source due to the divergence half angles α and β of the particle beam. A large dispersion and small trace width increase analyzer resolving power.

The equation that describes the particle position at the imaging plane involves $B\alpha^n$ and $C\beta^n$ terms, which describe aberrations (imperfections) to the image. An analyzer that perfectly focuses a particle beam would have no aberration effects ($B = C = 0$). The order of focusing is $(n - 1)$ in each direction. Higher order focusing is desired for less dependence on the divergence angles, and will give higher transmission current at the detector (Rudd, Low Energy Electron Spectrometry 1972). For the analyzers described in this standard, focusing is either first or second order in α and β.

A list of particularly good review articles and references that provide information concerning the design of the most widely used analyzers is given in Appendix A: Additional References for ESAs.

A. Particle Energy

In electric propulsion applications, the kinetic energy of a particle comes from thermal energy plus energy gained through acceleration in electric and/or magnetic fields. The thermal velocity is typically small compared to the velocity gained due to electromagnetic forces.

Consider, for instance, an ion thruster with plasma potential V_p with respect to ground potential (vacuum chamber ground or spacecraft ground), as shown in Figure 3. An ESA can be used to measure the energy of particles originating from the plasma source. In this case, according to time invariant energy conservation, an ion from the plasma source with charge $q = ze$ will pass from a region at potential V_p to the analyzer entrance at potential V_s. The kinetic energy gain $E_p = q(V_p - V_s) = ze(V_p - V_s)$ is equal to the particle's potential energy loss. The velocity of the particle upon entering the optic axis of the analyzer is then given by equation (3), where, in classical mechanics, we consider the particle velocity to be much less than the speed of light.

$$E_p = q(V_p - V_s) = \frac{1}{2}mv^2 \;\; or \;\; v = \sqrt{\frac{2(E_p/q)ze}{m}} = \sqrt{\frac{2ze(V_p - V_s)}{m}} \tag{3}$$

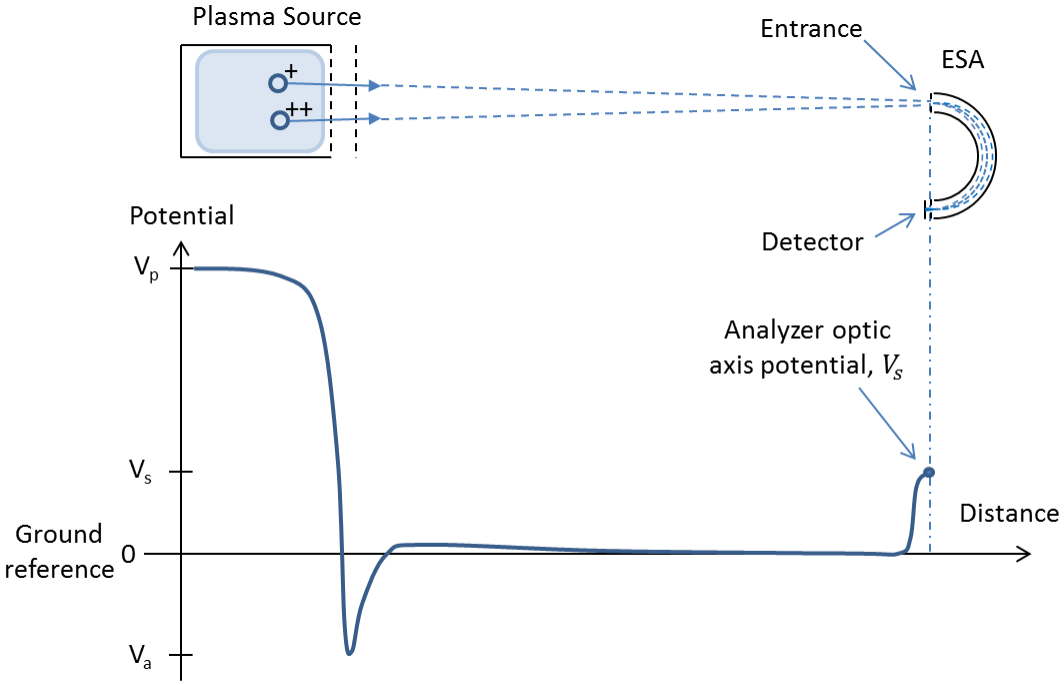

Figure 3. Illustration of how an ESA might be used in electric propulsion applications to measure the energy per charge of charged particles. A plasma source is shown that produces energetic ions due to the accelerating potential V_p. Singly charged ions and doubly charged ions will have different energies but the same energy to charge ratio, E/q.

The basis for charged particle analysis using electric and/or magnetic fields is given by the simplified Lorentz force relation of equation (4), that a particle with charge q will experience a force $\vec{F}$ due to an electric field $\vec{E}$. The particle velocity v does not figure into the equation since the magnetic field strength $\vec{B}$ is zero in an ESA. The analyzers discussed herein use electric fields to change a particle's direction, and may also change its velocity magnitude along the analysis path. The charge q on the particle is equal to the charge state z (integer number of charge units) multiplied by the elementary charge unit e, where z can be ≥ 1 for ions, ≤ -1 for negatively charged particles, or -1 for electrons).

$$\vec{F} = q\left(\vec{E} + v \times \vec{B}\right)$$
$$\vec{F} = q\vec{E} \quad \text{for} \quad \vec{B} = 0 \tag{4}$$

Particles with the same energy to charge ratio will follow the same trajectory due to the influence of the electric field. This means that ions with equivalent E/q values but of different mass to charge state m/q ratio cannot be distinguished using only electrostatic deflection (M. Yavor 2009). To distinguish mass and/or charge state, other instruments such as time-of-flight analyzers, electromagnetic analyzers (magnetic filters, ExB filters), or oscillating electric field analyzers (quadrupole) must be used.

B. Mirror-Type Electrostatic Analyzers

Mirror-type analyzers are designed based on fields in which particles are retarded, then re-accelerated. Mirror analyzers typically have a smaller dispersion to magnification ratio at the same path length compared with curved plate analyzers, but can have attractive features such as higher order of focusing or larger spatial acceptance (M. Yavor 2009). In this section we consider conventional parallel mirror analyzers and cylindrical mirror analyzers. Spherical mirror analyzers exist, proposed by Sar-El (Sar-El, More on the spherical condenser as an analyzer I. Nonrelativistic Part 1966), but are not widely used and therefore not discussed.

1. Parallel Plate/Plane Mirror Analyzer (PMA)

A parallel plate electrostatic analyzer creates a uniform field by placing a potential difference across a pair of plane parallel plates, as shown in Figure 4. This analyzer is also called a plane mirror analyzer (PMA). The particles enter the probe at an angle φ with respect to the (horizontal) entrance electrode and follow a parabolic trajectory through the analyzer due to the electric field. The pass energy of the analyzer E_0/q is determined by the voltage difference between the electrodes divided by the analyzer's geometrical constant C.

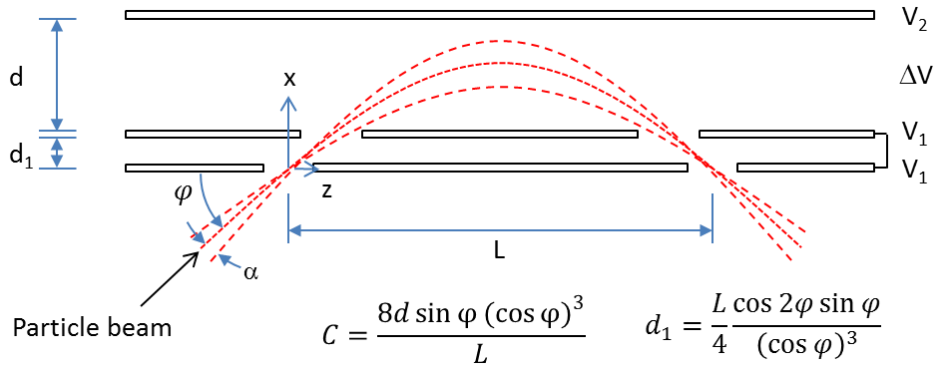

Figure 4. Parallel plate analyzer.

First order focusing, with respect to α, in the deflection plane is obtained when the entrance angle of entering particles is $\varphi = 45°$ as in Figure 5a (Moore, et al. 2009) (Harrower 1955) (M. Yavor 2009) (Roy and Carette, Electron Spectroscopy for Surface Analysis 1977). In that case, the distance $d_1 = 0$, and the entrance and exit slits are located in the single entrance plate.

A more favorable second order focusing in the plane of deflection occurs for an entrance angle of $\varphi = 30°$ instead of $\varphi = 45°$ (Green, T.S. and Proca 1970). In that case, $d_1 \neq 0$ and the energy resolving slits are placed in a field free region, shown in Figure 5b, where both the bottom plate and entrance and exit slits are held at potential V_1.

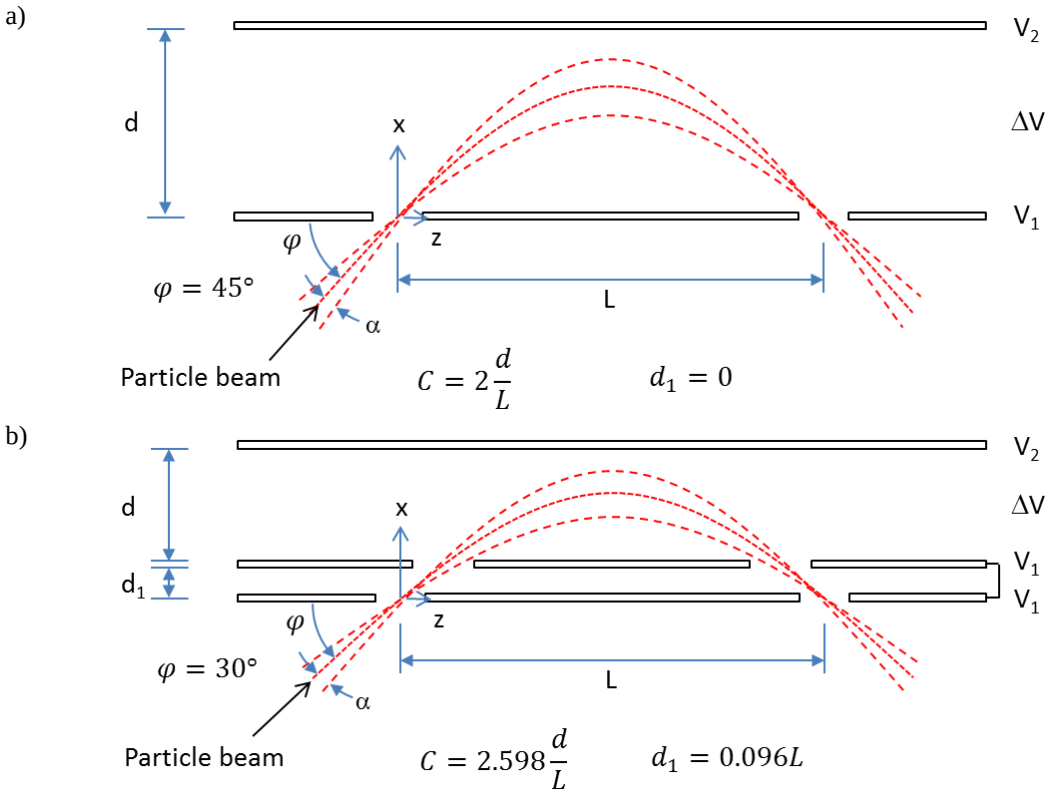

Figure 5. Diagrams of parallel plate analyzers where focusing occurs at either a) $\varphi = 45°$ or b) $\varphi = 30°$.

One drawback of a PMA is that angular focusing only occurs in the plane of deflection (x-z plane of Figure 5) and not in the perpendicular (y) direction. For the $\varphi = 45°$ analyzer, a point at the entrance slit is imaged as a line (in the y-direction) of length $2\sqrt{2}L\tan(\beta)$ at the exit slit (Moore, et al. 2009), as shown in Figure 6. For the $\varphi = 30°$ analyzer, the line length is $2.3L\tan(\beta)$ at the exit slit.

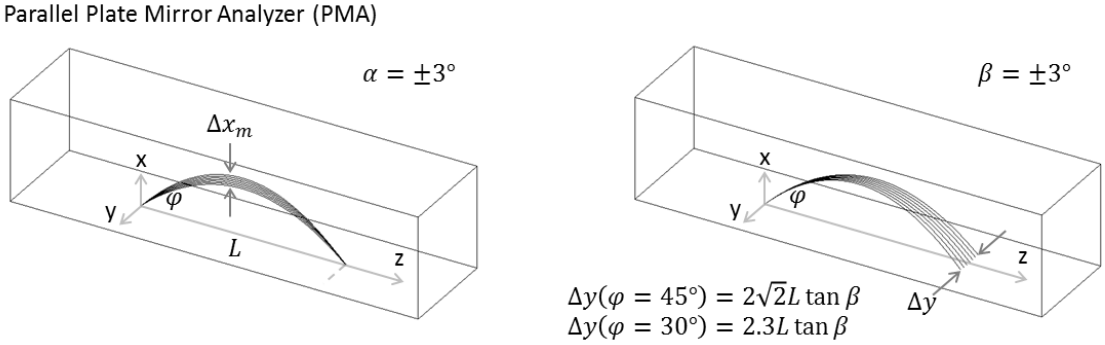

Figure 6. Parallel plate analyzers focus in the dispersion plane (x-z plane) but do not focus in the plane perpendicular to the dispersion plane (x-y plane).

Parameters for the PMA, including the analyzer constant, dispersion, and trace width, are summarized in Table 2. The energy dispersion, D_k, is a measure of the displacement of the image point per unit fractional change in energy in the plane of the particle beam (perpendicular to the optic axis). In the case of the mirror type analyzers, a more useful measure of the dispersion is in the direction along the length of the plates (z). This value, called the axial energy dispersion, is given as $\widetilde{D} = D_k/\sin\varphi$. D_k is commonly reported for the curved plate analyzers whereas $\widetilde{D}$ is reported for the mirror type analyzers.

For a PMA, the analyzer constant C can be calculated given the entrance angle φ and focusing distance L. Some texts use the calibration factor k, which is the reciprocal of the analyzer constant ($k = 1/C$).

$$C = \frac{1}{k} = \frac{8d \sin\varphi \, (\cos\varphi)^3}{L}$$
$$C = 2d/L \text{ (for } \varphi = 45°)$$
$$C = 2.598d/L \text{ (for } \varphi = 30°) \quad (5)$$

Next we consider the distance d_1 of the field free region to be the same at the entrance and exit. Other arrangements with the source and exit positions having different distances from the electrodes are possible; see for example, Green and Proca (Green, T.S. and Proca 1970) and Roy and Tremblay (Roy and Tremblay, Design of electron spectrometers 1990). Equation (6) gives the required thickness of the field free region as a function of L and φ. (Roy and Tremblay, Design of electron spectrometers 1990). $d_1 = 0$ for $\varphi = 45°$ which is why in that case there is no field free region and there is a single entrance electrode as shown in Figure 5a.

$$d_1 = \frac{2d}{C}\cos 2\varphi \, (\sin\varphi)^2 = \frac{L}{4}\frac{\cos 2\varphi \sin\varphi}{(\cos\varphi)^3}$$
$$d_1 = 0 \text{ (for } \varphi{=}45°)$$
$$d_1 = 0.096L \text{ (for } \varphi{=}30°) \quad (6)$$

The maximum distance, x_m, that the beam enters the analyzer (in the x-direction) is given by equation (7). This value is calculated to make sure that the beam does not hit the outer electrode. For $\varphi = 45°$ and $\alpha = 0°$, the maximum height is $x_m = L/4$. Therefore, a plate separation of $d > L/2$ should be adequate (Roy and Tremblay, Design of electron spectrometers 1990).

$$x_m = d_1 + \frac{L \sin(\varphi + \alpha)}{8\,(\cos(\varphi + \alpha))^3} \quad (7)$$

The voltage applied across the segments is equal to the transmission energy multiplied by the analyzer constant.

$$\Delta V = (E_0/q)\, C$$
$$\Delta V = (E_0/q)\,\tfrac{2d}{L} \text{ (for } \varphi{=}45°)$$
$$\Delta V = (E_0/q)\,\tfrac{2.598d}{L} \text{ (for } \varphi{=}30°) \quad (8)$$

Particle trajectories are shown passing through 45° and 30° parallel plate mirror analyzers in Figure 7 and Figure 8, respectively. These figures exhibit the angular refocusing, energy separation, and linear magnification characteristics of the 45° and 30° PMAs. Note that the energy dispersion of the 30° analyzer is two-thirds that of the 45° analyzer ($\widetilde{D}_{30°} = \frac{2}{3}\widetilde{D}_{45°}$), so that there is less spatial separation of the particles of variable energy ($\pm 35\ eV$) in the 30° PMA of Figure 8 than in the 45° PMA of Figure 7.

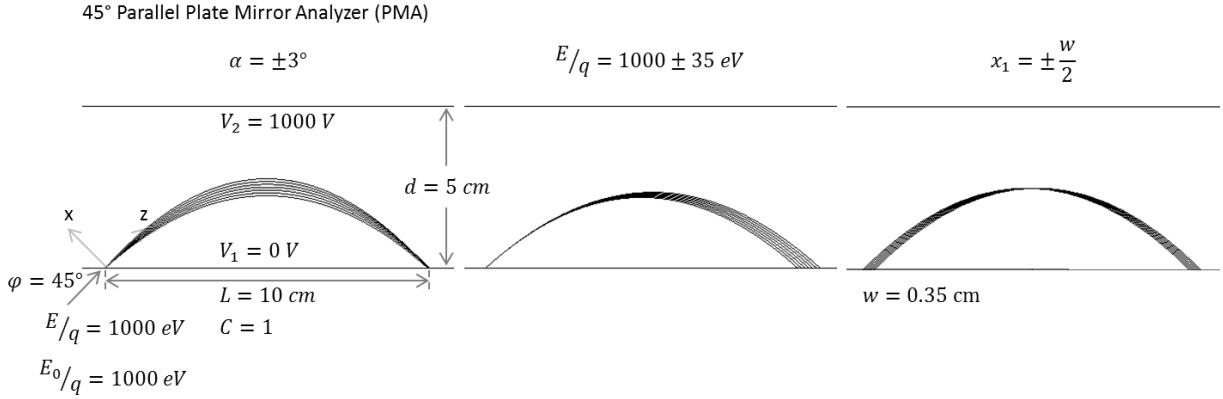

Figure 7. Particle trajectories through a 45° parallel plate mirror analyzer with angular, energy, and positional variation.

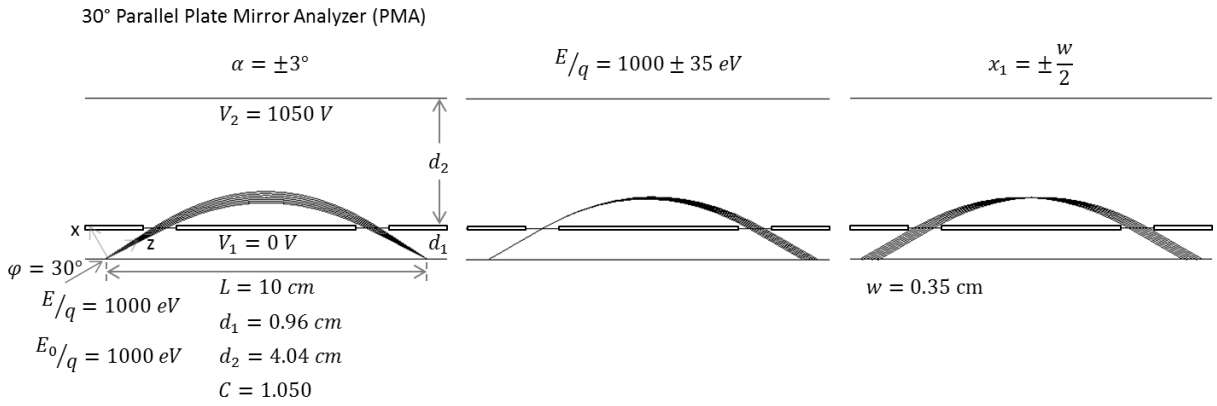

Figure 8. Particle trajectories through a 30° parallel plate mirror analyzer with angular, energy, and positional variation.

Though the concept of a parallel plate ESA is straightforward, there are design challenges to consider. The entrance and exit slits in the front plate act as lenses due to the electric fields, producing unwanted aberrations. This problem can be addressed by placing a fine wire mesh over the apertures to help create uniform electric fields. Also, fringing fields can arise due to the large gap between the plates. These fringing fields can be mitigated by extending the edges of the plate well beyond the deflection region, or by placing compensating electrodes at the edges of the gap (Moore, et al. 2009).

2. Cylindrical Mirror Analyzer (CMA)

A cylindrical mirror analyzer (CMA) uses coaxial cylinders as the deflection plates instead of parallel plates as in the PMA. This enables added focusing in the direction perpendicular to the deflection plane. The PMA can be considered a special case of the CMA with large radii. As described herein, the source and exit focusing points are located on the symmetry axis of the CMA, though other positions are possible (Aksela, Karras, et al. 1970).

Particles enter the analyzer at an angle φ through a slit of width w on the symmetry axis, and are deflected back to the symmetry axis as shown in Figure 9. Pass-through slits are located in the inner cylinder at radius r_1.

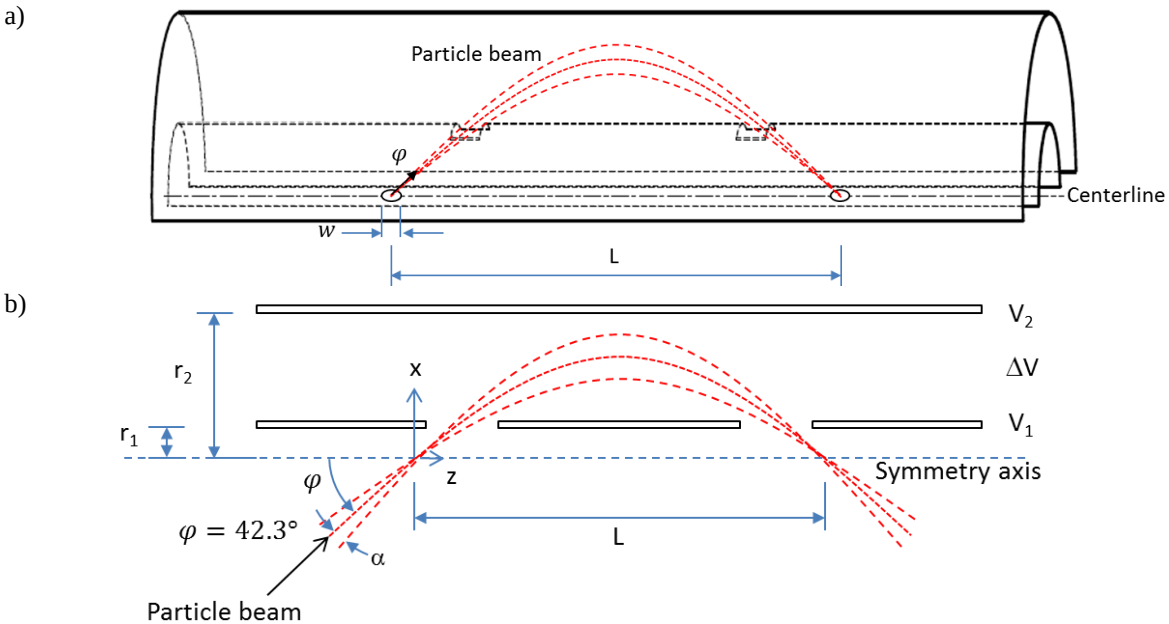

Figure 9. a) Diagram of an axial focusing cylindrical-mirror analyzer with the source and image located on the axis. b) Cross section of a CMA showing the axis of symmetry and radii of the electrodes.

The cylindrical mirror is double-focusing (focusing occurs in both the (α) deflection plane and the (β) perpendicular plane) so that the image of a point at the source appears as a point at the detector (Moore, et al. 2009). The cylindrical analyzer has the advantageous properties over the PMA in that particles coming from a wide range of azimuthal (β) angles can be refocused and collected at the exit.

With the source and image located on the centerline axis, the distance L from the entrance focus point to the detection point is given by equation (9). See Aksela et al. (Aksela, Karras, et al. 1970) and Risley (Risley, Design Parameters for the Cylindrical Mirror Energy Analyzer 1972) for variations on the source and image locations with respect to the symmetry axis. The CMA is second order focusing for a beam entrance angle of $\varphi = 42.3°$ and $K = 1.311$; giving $L = 6.13r_1$. There is no aberration term due to β. Parameters for the CMA are found in Table 2.

$$L = r_1\left(2\cot\varphi + 2\sqrt{K\pi}\cos(\varphi)\, exp(K(\sin\varphi)^2) erf\left(\sqrt{K}\sin\varphi\right)\right)$$
$$K = \frac{(E_0/q)}{\Delta V} ln(r_2/r_1) \tag{9}$$

$$L = 6.13r_1 \text{ (for } \varphi = 42.3° \text{ and } K = 1.311)$$

The inner cylindrical plate is held at the same potential as the source (the symmetry axis at V_1) to produce a field free region. The potential difference between voltages V_1 and V_2 is given by equation (10).

$$\Delta V = (E_0/q)\, C$$
$$\Delta V = (E_0/q)\left(0.763\, ln(r_2/r_1)\right) \tag{10}$$

The maximum extent that the beam will enter the CMA is $r_m = 1.8r_1$ for $\alpha = 42.3°$ (Steckelmacher 1973), so a value of $r_2 \geq 2.5r_1$ is recommended to ensure beam particles do not hit the outer cylindrical electrode (Moore, et al. 2009).

When the entrance and exit slots in electrode 1 are used to define the resolution, as in the case when the source is not small, the CMA is first order focusing instead of second order focusing. The CMA provides for high transmission, which makes it popular for use as a mirror spectrometer (M. Yavor 2009).

Figure 10 shows example particle trajectories moving through a 42.3° cylindrical mirror analyzer, with variations in particle angle, energy, and position.

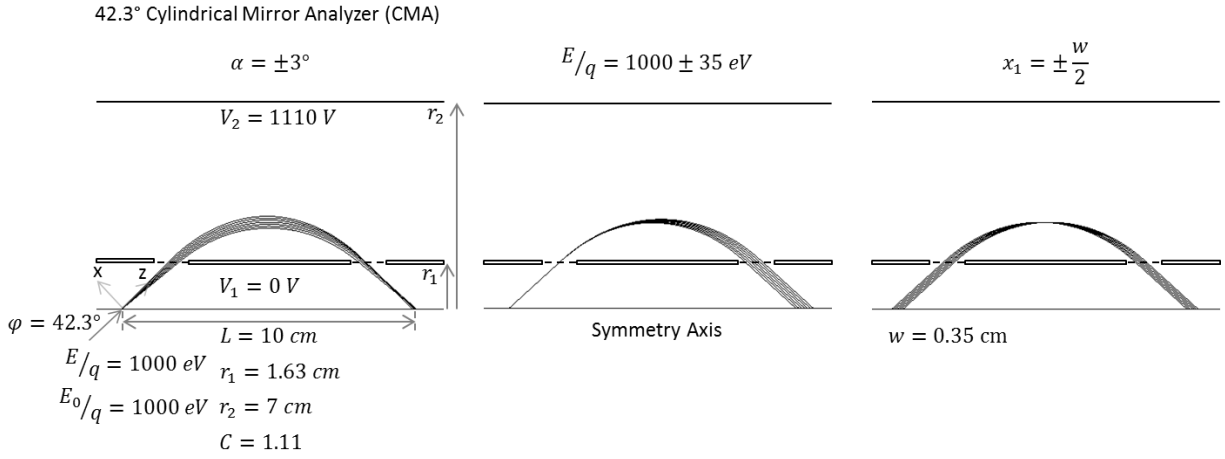

Figure 10. Particle trajectories through a 42.3° cylindrical mirror analyzer with angular, energy, and positional variation.

3. Spherical Mirror Analyzer (SMA)

The spherical mirror analyzer (SMA) is analogous to the CMA. Because it is not popularly used, it is not discussed here, though references are provided in the appendix. A good starting reference is Roy and Tremblay (Roy and Tremblay, Design of electron spectrometers 1990).

C. Curved Plate Analyzer (CPA) – Toroidal Geometry

Curved plate analyzers are also called deflector or sector field analyzers. First, a general toroidal geometry is described. Special cases of the toroidal geometry are the spherical and cylindrical configurations.

A toroidal electrostatic field is created when the equipotential surfaces are curved in both the dispersion plane (x-z) and in the plane perpendicular to the dispersion plane (x-y). This field is created by coaxial curved electrodes, which are usually circular arcs. Ewald and Liebl first proposed the toroidal design (Ewald and Liebl 1955). For a toroidal geometry, the location of the center of curvature of the circular arcs typically coincides. When the centers coincide, the radii $R_1 = R_0 - g_0$, and $R_2 = R_0 + g_0$, where g_0 is half of the gap between the electrodes. The center radius $R_0 = (R_1 + R_2)/2$. Note that here, upper case R's are used to denote curvature in the x-y plane, and lower case r's denote toroidal curvature in the x-z plane.

One particular centralized equipotential curve is given the radius $R(0)$. A coefficient called the toroidal factor c_t is the ratio of the radius r_0 to the radius $R(0)$, equation (11). The radius r_0 is the deflection radius of the optical axis in the x-z plane and the radius $R(0)$ is a deflection radius in the x-y plane. The equipotential curvature radius $R(0)$ can be approximated as $R_0 = (R_1 + R_2)/2$ (M. Yavor 2009).

$$c_t = \frac{r_0}{R(0)}$$
$$R(0) \cong R_0 = \frac{R_1 + R_2}{2} \tag{11}$$

A special case of the toroidal sector analyzer is the spherical deflector analyzer (SDA), where the electrode surfaces are concentric spheres. For the SDA, $R_1 = r_1 = r_0 - g_0$, $R_2 = r_2 = r_0 + g_0$, $R_0 = r_0$, and $c_t = 1$. Another special case is the cylindrical deflector analyzer (CDA), where the electrode surfaces are concentric cylinders, curved only in the deflection plane. For the CDA, $R_1 = R_2 = \infty$, and $c_t = 0$. The toroidal factor is given in Table 1 for the toroidal analyzer, CDA, and SDA.

Table 1 – Toroidal factors, c, for the toroidal, cylindrical, and spherical deflectors.

Analyzer	Focusing condition	Toroidal Factor, c_t
Toroidal Deflector	No analytical solution.	$\approx c_0 = \frac{r_0}{R_0}$ (ratio of radial main path radius to axial main path radius)
Cylindrical Deflector	$\varphi = \frac{\pi}{\sqrt{2}} = 127.3°$	0
Spherical Deflector	$\varphi = \pi = 180°$	1

1. *Cylindrical Deflector Analyzer (CDA) / Radial Cylindrical Analyzer*

The cylindrical deflector analyzer (CDA), also called the radial cylindrical analyzer, is shown in Figure 11. An electric field is produced by a potential difference ΔV placed across the cylindrical electrodes of radius r_1 (inner electrode) and r_2 (outer electrode). A logarithmic electric field distribution is created between the cylindrical surfaces (M. Yavor 2009). Beam particles usually enter the analyzer midway between the electrodes in a direction tangent to the arc radius, at $r_0 = (r_1 + r_2)/2$. The CDA becomes first order focusing (in α) at a deflection angle $\varphi = \pi/\sqrt{2} = 127.3°$. Additional parameters for the CDA are collected in Table 2.

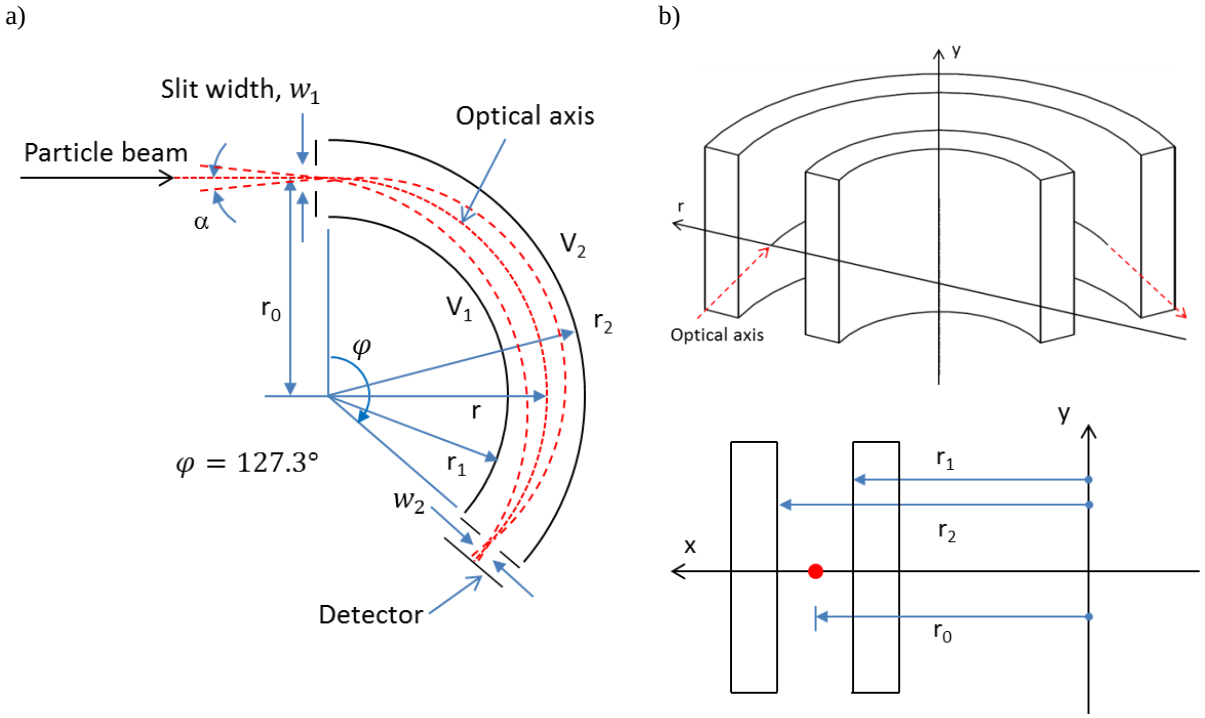

Figure 11. Diagram of the cylindrical deflector analyzer (CDA).

The CDA was first proposed for analyzing the kinetic energy of electrons (Hughes and Rojansky, On the Analysis of Electronic Velocities by Electrostatic Means 1929) (Hughes and McMillen, Re-Focussing of Electron Paths in a Radial Electrostatic Field 1929). Generally, slits of width w (in the local x-direction) are placed at the entrance and exit of the radial plates. The CDA can also be designed with deflecting angles smaller than 127.3° where the source and image plane are located outside of the analyzer in the field-free space (M. Yavor 2009).

With beam particles entering at a radius r_0, the voltages on the inner (V_1) and outer (V_2) electrodes are set as a function of the probe geometry, the selected transmission energy E_0/q (in eV), and the entrance/exit slit voltage V_s according to equations (12)-(14). In this case the optic axis at r_0 is at potential V_s.

$$V_1 = V_s + (E_0/q)\big(2ln(r_1/r_0)\big) \tag{12}$$

$$V_2 = V_s + (E_0/q)\big(2ln(r_2/r_0)\big) \tag{13}$$

$$\begin{aligned} \Delta V &= (E_0/q)\, C \\ \Delta V &= (E_0/q)\big(2ln(r_2/r_1)\big) \end{aligned} \tag{14}$$

The analyzer can alternatively be operated with equal and opposite voltages applied to the plates, with $V_2 = -V_1$. In that case the electrical center of the CDA is located at $r_0 = \sqrt{r_1 r_2}$ (Bryce, Dalglish and Kelly 1973), and the particle beam would be designed to enter the analyzer at this radius instead of at half the gap width.

Moore et al. (Moore, et al. 2009) recommends limiting the angle of divergence in the plane of deflection in order to keep the filling factor below 50%, according to equation (15).

$$\alpha < \frac{2\sqrt{2}}{\pi}\frac{(r_2 - r_1)}{r_0} \tag{15}$$

One drawback is that the CDA focuses only in the plane of deflection (x-z plane of Figure 11, with no y-direction focusing). A point at the entrance slit is imaged as a line (y-direction) of length $\sqrt{2}\pi r_0 \tan(\beta)$ at the exit slit (Moore, et al. 2009), similar to that shown for parallel plate analyzers in Figure 6.

Example particle trajectories passing through a cylindrical deflector analyzer are shown in Figure 12.

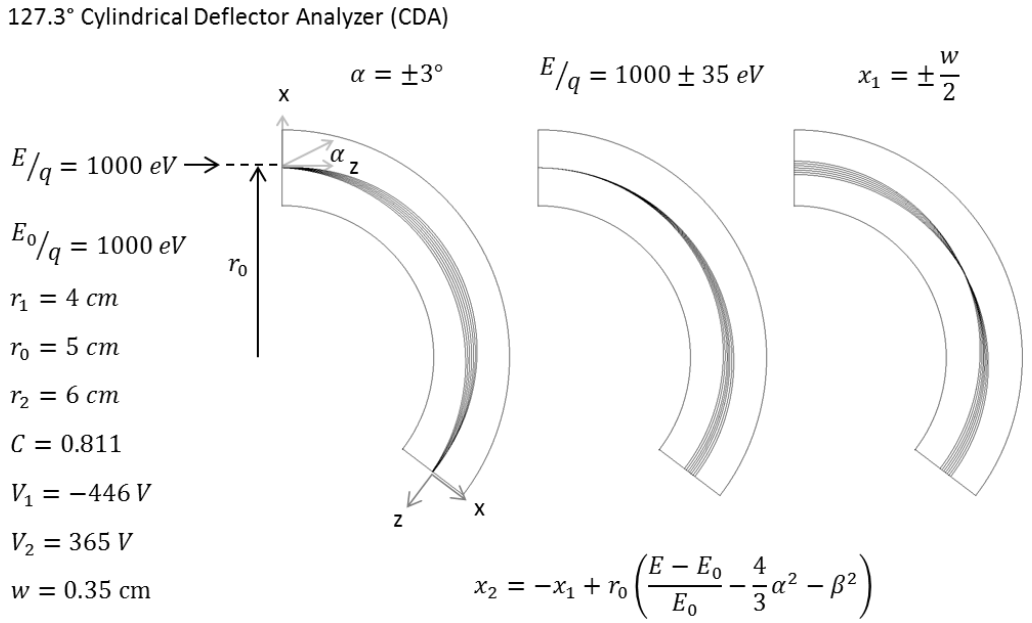

Figure 12. Particle trajectories through a 127.3° CDA with angular, energy, and positional variation.

2. Spherical Deflector Analyzer (SDA)

The spherical deflector analyzer (SDA), also called the spherical analyzer, is created by placing a voltage ΔV across a pair of spherical electrodes of radius r_1 (inner electrode) and r_2 (outer electrode). This creates a double focusing electric field, both in the deflection plane and the perpendicular plane. Focusing in both the x and y directions occurs for the special case of $\varphi = 180°$ deflection. A diagram of the SDA is shown in Figure 13. The hemispherical (180° spherical) energy analyzer was first proposed by Purcell (Purcell 1938).

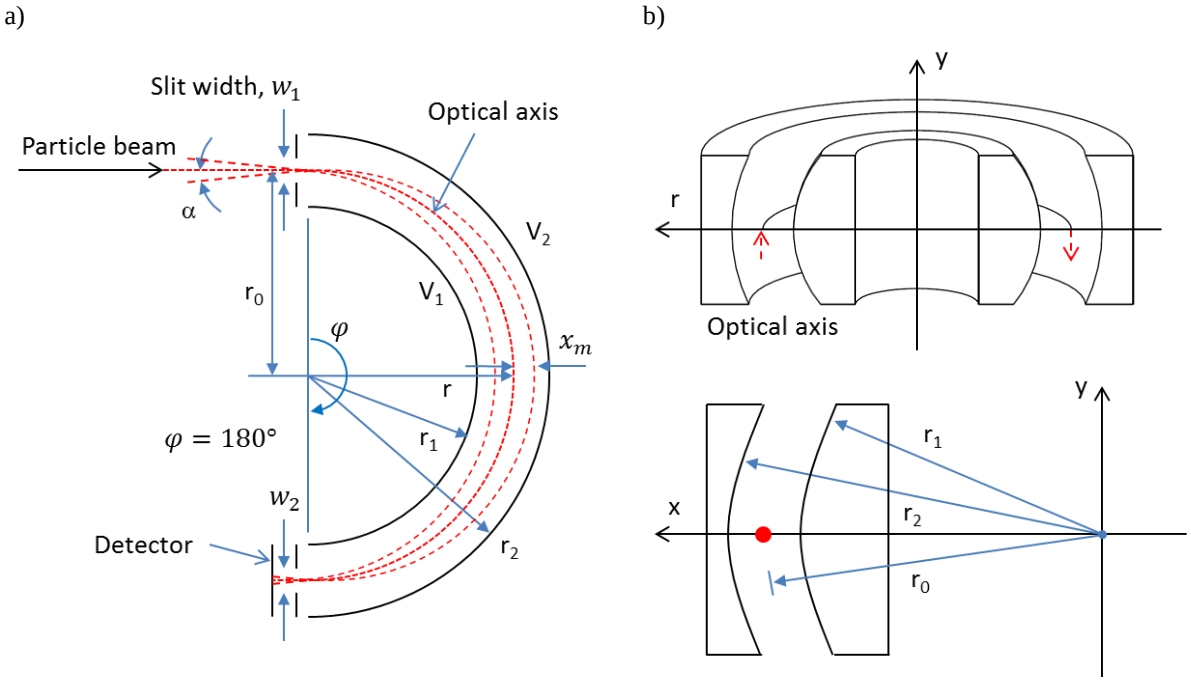

Figure 13. Diagram of the 180° (hemispherical) SDA showing example particle trajectories on the a) x-z plane and b) on the x-y plane.

Toroidal deflector analyzers can also be designed with the object and image positions in field free space outside the sector field (M. Yavor 2009). An example of a field free focusing analyzer is Osterwalder et al. (Osterwalder 1989) where a 145° spherical deflecting angle was used.

The voltages on the inner (V_1) and outer (V_2) electrodes are set as a function of the selected transmission energy E_0/q (in eV), the entrance/exit slit voltage V_s, and the geometry of the ESA, according to equations (16)-(18). Additional parameters for the SDA can be found in Table 2.

$$V_1 = V_s + 2(E_0/q)\left(1 - \frac{r_0}{r_1}\right) \tag{16}$$

$$V_2 = V_s + 2(E_0/q)\left(1 - \frac{r_0}{r_2}\right) \tag{17}$$

$$\Delta V = (E_0/q)\,C$$
$$\Delta V = (E_0/q)\left(\frac{r_2}{r_1} - \frac{r_1}{r_2}\right) \tag{18}$$

The maximum deviation, x_m, of a particle trajectory from the central path is given by equation (19) (Moore, et al. 2009). This value would be used to select the analyzer's required inner and outer radii to avoid having particles of maximum angular deviation α strike the segment surfaces.

$$\frac{x_m}{r_0} = \frac{w}{2r_0} + \alpha + \frac{\alpha^2}{2} + \frac{1}{2\alpha}\left(\frac{w}{r_0} + \frac{\alpha^2}{2}\right)^2 \tag{19}$$

The SDA has the advantage over the PMA and CMA analyzers in that lower electrode potentials are required to achieve higher transmission energies through the analyzer. Also, the close spacing of the electrodes helps to mitigate fringing fields (Moore, et al. 2009). The main drawback is that it is more difficult to manufacture and align the spherical sectors.

Sample particle trajectories through a spherical deflector analyzer are shown in Figure 14.

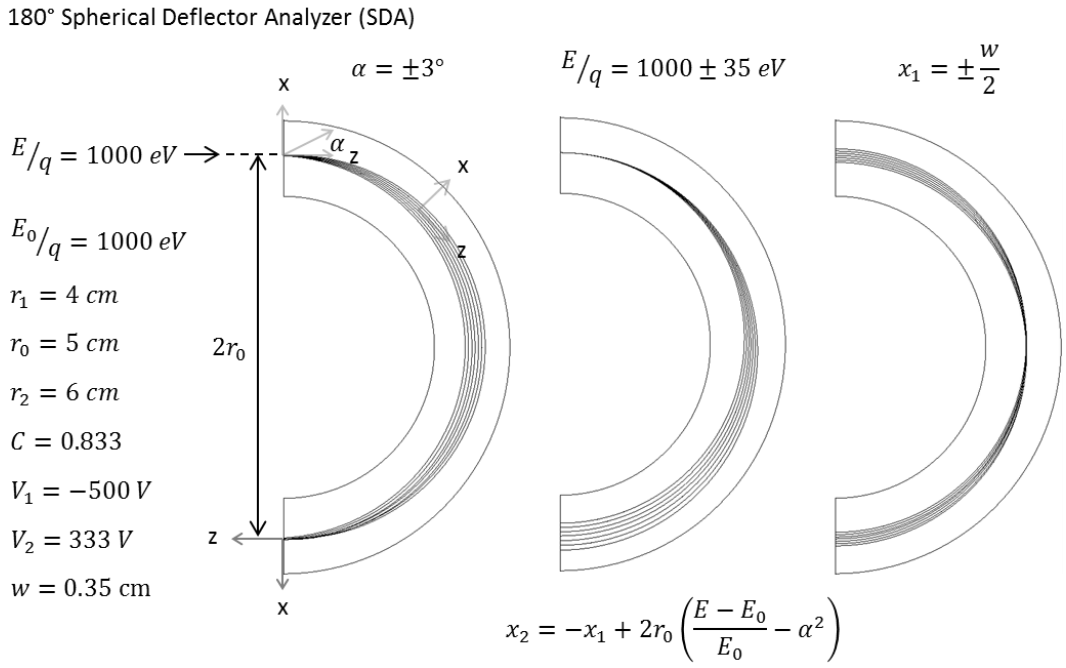

Figure 14. Particle trajectories through a 180° SDA with angular, energy, and positional variation.

D. Parameters for selected types of electrostatic analyzers.

Useful parameters for all types of electrostatic analyzers discussed in this guide are collected in Table 2.

Table 2 – Parameters for selected types of electrostatic analyzers.

Symbol	Parallel-plate mirror, PMA (45°)	Ref	Parallel-plate mirror, PMA (30°)	Ref	Cylindrical Mirror, CMA (42.3°)	Ref
Electric Field						
$\vec{E}$	$\vec{E}_x = -\Delta V/d$ $\vec{E}_y = \vec{E}_z = 0$	d	$\vec{E}_x = -\Delta V/d$ $\vec{E}_y = \vec{E}_z = 0$	d	$\vec{E}_r(r) = -\Delta V/(r\ln(r_2/r_1))$ $\vec{E}_\theta = \vec{E}_z = 0$	g
Energy of the Central Ray						
E_0	$q\Delta VL/(2d)$	c,d	$q\Delta VL/(2.598d)$	e	$q\Delta V/(0.763\ln(r_2/r_1))$	a,b
Analyzer Constant						
C	$2d/L$	c,d	$2.598d/L$	e	$0.763\ln(r_2/r_1)$	a,b
Focusing Condition						
φ	$\varphi = \pi/4$	d	$\varphi = \pi/6$	d	$\varphi = 42.308°$	d
Potential						
V	$\Delta V = (E_0/q)\frac{2d}{L}$	b,d	$\Delta V = (E_0/q)\frac{2.598d}{L}$ (V_1 is at the slit potential)	b	$\Delta V = 0.763(E_0/q)\ln\left(\frac{r_2}{r_1}\right)$ (V_1 is at the slit potential)	a,b
Axial Dispersion, $\widetilde{D} = D_k/\sin\varphi$						
$\widetilde{D}$	L	d,f,h	$\frac{2L}{3}$	f,h	L $0.914L$	d f,h
Trace Width, $\widetilde{D}(\alpha+\beta\ terms)$						
t_w	$L(2\alpha^2+\beta^2)$	d	$\frac{2L}{3}(9.33\alpha^3+2\beta^2)$	h	$2.85L_0\alpha^3$ $5.06L_0\alpha^3$	d h
Path Length of Central Ray						
	$\approx 1.148L$	d	$\approx 1.087L$	h	$\approx 1.20L$	h
Image Width Due to β for a Point Source						
	$\sqrt{2}L\tan(\beta)$	b	$2.3L\tan(\beta)$	h	$0\ (focusing\ in\ \beta)$	e

Symbol	Cylindrical Deflector, 127.3° CDA	Ref	Spherical Deflector, 180° SDA	Ref
Electric Field				
$\vec{E}$	$\vec{E}_r = -\Delta V/(r_0\ln(r_2/r_1))$ $\vec{E}_\theta = \vec{E}_z = 0$	d	$\vec{E}_r = -\Delta V r_1 r_2/\left({r_0}^2(r_2-r_1)\right)$ $\vec{E}_\theta = \vec{E}_z = 0$	d
Energy of the Central Ray				
E_0	$q\Delta V/(2\ln(r_2/r_1))$	c,d	$q\Delta V/(r_2/r_1 - r_1/r_2)$	c,d
Analyzer Constant				
C	$2\ln(r_2/r_1)$	d	$r_2/r_1 - r_1/r_2$	d
Focusing Condition				
φ	$\varphi = \frac{\pi}{\sqrt{2}} = 127.3°$	d	$\varphi = \pi = 180°$	d
Potential				
V	$V(r) = (2E_0/q)\ln(r/r_0)$ if $V = 0$ at $r = r_0$	d	$V(r) = (2E_0r_0/q)(1/r_0 - 1/r)$ if $V = 0$ at $r = r_0$	d
Energy Dispersion				
D_k	r_0	d	$2r_0$	d
Trace Width, $D_k(\alpha+\beta\ terms)$				
t_w	$r_0(4\alpha^2/3+\beta^2)$	d	$2r_0\alpha^2$	d
Path Length of Central Ray				
	$\frac{\pi}{\sqrt{2}}r_0$	d	πr_0	d
Image Width Due to β for a Point Source				
	$\sqrt{2}\pi r_0\tan(\beta)$	b	$0\ (focusing\ in\ \beta)$	e

[a]Steckelmacher (Steckelmacher 1973)
[b]Moore, et al. (Moore, et al. 2009)
[c]Roy and Carette (Roy and Carette, Electron Spectroscopy for Surface Analysis 1977)
[d]Rudd (Rudd, Low Energy Electron Spectrometry 1972)
[e]Roy and Tremblay, Dube and Roy (Roy and Tremblay, Design of electron spectrometers 1990) (Dube and Roy, A Generalized Approach for the Determination of Transmission Functions of Charged-Particle Energy Analyzers 1982)
[f]Yavor (M. Yavor 2009)
[g]Aksela (Aksela, Instrument Function of a Cylindrical Electron Energy Analyzer 1972)
[h]Calculated from energy resolution equations in Table 3, or calculated.

E. Noteworthy Analyzer Designs and Modifications

1. *Top Hat Analyzer*

A top hat type analyzer is a special case of a spherical deflector analyzer. In a top hat analyzer, the particles to be analyzed enter at the midpoint of two hemispherical sectors, as shown in Figure 15. A third nested hemispherical electrode, called the top hat (or top cap) is positioned above the entrance apertures (Collinson and Kataria, On variable geometric factor systems for top-hat electrostatic space plasma analyzers 2010). Advantages over other designs are that the top hat analyzer has a very wide field of view (up to 360°) and can incorporate position sensitive detectors at the downstream end of the sectors. Because of their wide field of view and resolution, top hat analyzers are popular for space missions (see Table 6).

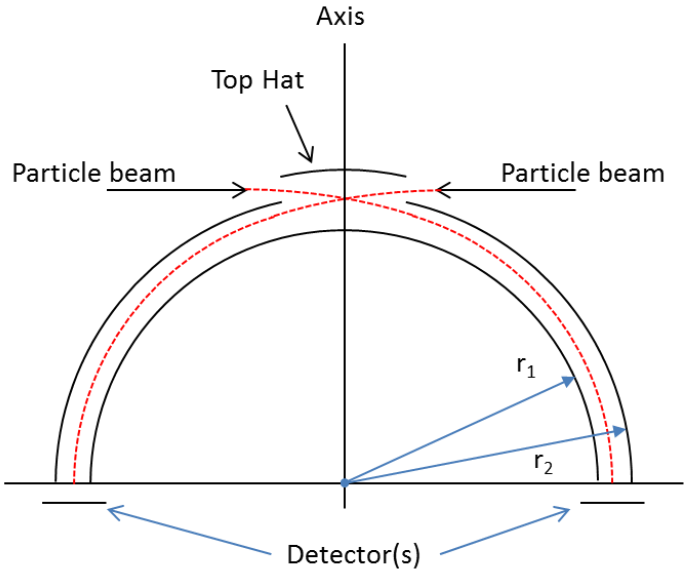

Figure 15. Cross sectional illustration of a top hat analyzer. The geometry of the analyzer is rotated about the central axis.

2. *Matsuda Plate Cylindrical Analyzer*

A modification to the CDA can be made to make the analyzer perform like an SDA. This is done by applying potentials V_T to flat plates placed above and below the cylindrical electrodes. These additional plates were described by Matsuda in 1961 (Matsuda, Electrostatic Analyzer with Variable Focal Length 1961) and are called Matsuda plates. The plates have the effect of forming a toroidal deflecting field within the region of the particle beam. The cylindrical deflector analyzer with Matsuda plates is shown in Figure 16. A discussion of improvements and drawbacks to the design of toroidal analyzers formed with Matsuda plates is given in Yavor (M. Yavor 2009). Matsuda plates create an effective field distribution when the distance from the plates to the optic axis is 2 to 3 times the value of half of the gap between the inner and outer cylindrical segments ($y_T \approx k_T g_0,\ k_T = 2\ to\ 3,\ g_0 = \frac{1}{2}(r_2 - r_1)$). One drawback is the inclusion of large third-order geometric aberrations.

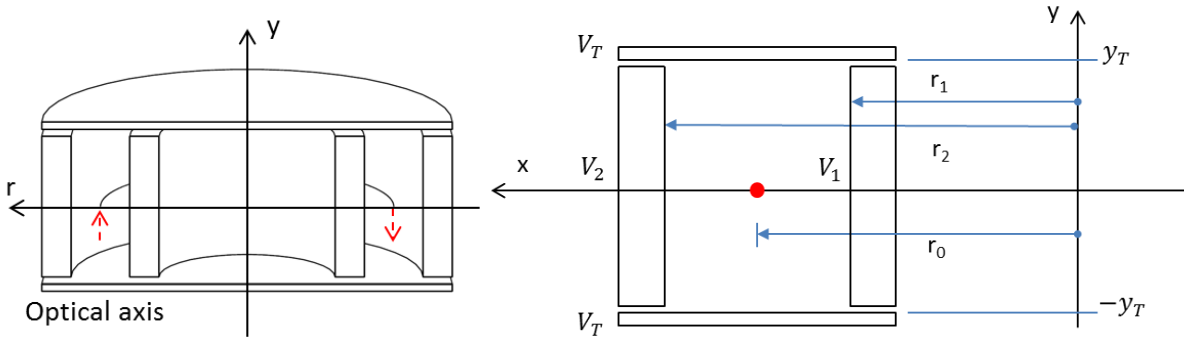

Figure 16. A CDA with Matsuda plates on the top and bottom to create a spherical electric field in the region where the particle beam travels inside the analyzer.

The toroidal factor of the Matsuda plate CDA can be calculated for given electrode voltages and geometries (Leventhal and North 1971) (Fishkova and Ovsyannikova 1995). Equation (20) from Yavor (M. Yavor 2009) gives an approximate analytical expression for the toroidal factor.

$$c_t \approx \frac{2\pi r_0}{g_0}\left[\frac{2V_T - V_1 - V_2}{V_2 - V_1}\right] exp\left(-\frac{\pi}{2}\frac{y_T}{g_0}\right) \tag{20}$$

3. Analyzer Modifications

Other analyzer types include elliptical mirror, hyperbolic field, box type, ideal focusing, rotationally symmetric mirror, quasi-conical, toroidal mirror, polar toroidal, angle and energy resolving mirror, conical, and cusp type (M. Yavor 2009). These designs are modifications of the simpler mirror and deflector designs, aimed at improving the accuracy, resolution, field-of-view, or other capabilities of electrostatic analyzers. A list of references for these analyzer types is given in this guide under the heading Analyzer Modification References.

III. Energy Resolution

An electrostatic analyzer can be used to obtain the energy distribution of a particle beam by plotting transmitted current versus selected energy. For an ideal monochromatic beam the transmission function is triangular, but for a real beam and analyzer it resembles a Gaussian, an example of which is shown in Figure 17.

The energy *passband* ΔE of the analyzer may be defined as the full width at half maximum (FWHM) of the energy distribution that appears in measuring a monochromatic beam (Moore, et al. 2009). The pass energy through the analyzer is defined as E_0. The energy resolution of analyzers is usually defined as the ratio $\Delta E/E_0$ (Roy and Carette, Electron Spectroscopy for Surface Analysis 1977).

The full width of the transmission function, called the base resolution (FBW), can be calculated and is defined as ΔE_B (Roy and Carette, Improvement of the Resolving Power and Transmission of Electrostatic Spectrometers 1971) (Roy and Carette, Electron Spectroscopy for Surface Analysis 1977) (Roy and Tremblay, Design of electron spectrometers 1990). We shall define ΔE_h (HBW) to be half of the full width of the base resolution, ΔE_B. The resolution $\Delta E_h/E_0$ is commonly calculated in the literature as a close approximation of $\Delta E/E_0$. Since ΔE_h is slightly greater than the FWHM, ΔE, this approximation of $\Delta E_h/E_0$ overestimates the passband of a real analyzer (Moore, et al. 2009) (Rudd, Low Energy Electron Spectrometry 1972). However, for a well-designed analyzer, $\Delta E \approx \Delta E_{B/2}$. The resolving power ρ is the reciprocal of the energy resolution: $\rho = E_0/\Delta E$ (or sometimes calculated using the HBW as $\rho_h = E_0/\Delta E_h$) (Roy and Carette, Electron Spectroscopy for Surface Analysis 1977).

To first order, the entrance and exit slits (also called apertures), usually of equal width w, establish the passband. For unequal widths, w should be replaced by $(w_1 + w_2)/2$ (Roy and Carette, Electron Spectroscopy for Surface Analysis 1977). The transmission function also depends upon the maximum angular extent to which particles deviate from the central path leading from the entrance to the exit slit. This angular deviation is defined by the angles $\pm\alpha$ in the deflection plane and $\pm\beta$ in the perpendicular plane.

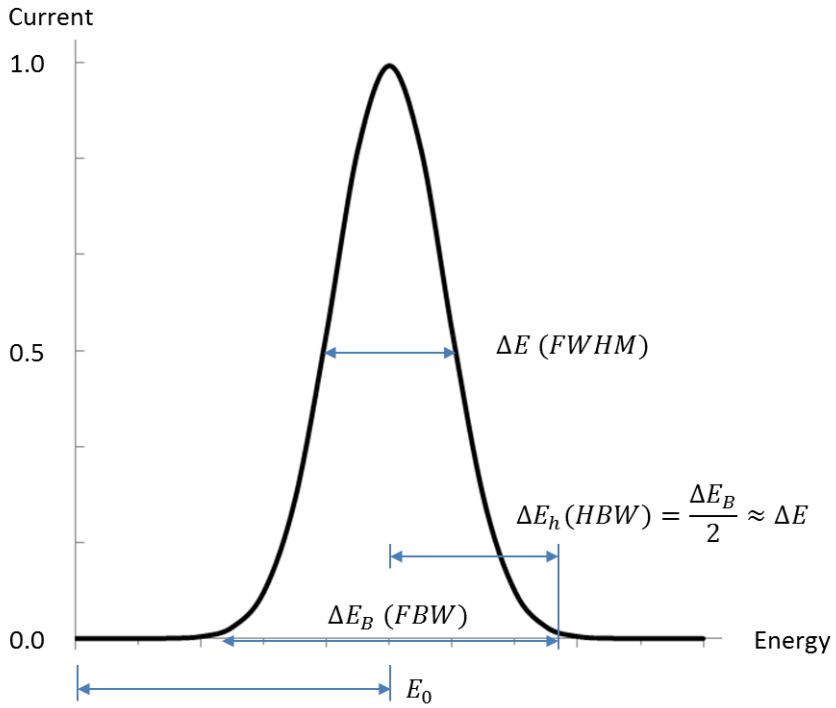

Figure 17. Energy resolution terms with an example measured Gaussian curve. If the particle beam were monoenergetic and measured with a perfectly designed analyzer, the shape of the curve would be triangular.

The base resolution $\Delta E_B/E_0$ is described by equation (21), using the constants from Table 3. The HBW resolution is calculated as $\Delta E_h/E_0 = \Delta E_B/2E_0$ (equation (22)).

$$\frac{\Delta E_B}{E_0} = Aw + B\alpha^n + C\beta^2 \quad (21)$$

(Roy and Carette, Electron Spectroscopy for Surface Analysis 1977).
(note upper case constants used for ΔE_B.)

$$\frac{\Delta E_h}{E_0} = \frac{1}{2}\frac{\Delta E_B}{E_0} \quad (22)$$

(Noting that for a well-designed analyzer, $\Delta E \approx \Delta E_h$).

Table 3 – $\Delta E_B/E_0$ constants for selected electrostatic analyzers. Use in equations (21) and (22).

Analyzer	$A\ (2/D_k)$	B	C	n
Parallel Mirror - 45°	$2/L$	2	1 [b,c,d]	2
Parallel Mirror - 30°	$3/L$	9.2 [a,b,c] 9.33 [d]	1 [c] 1.5 [b] 2 [d]	3 [a,c,d] 2 [b**]
Cylindrical Mirror - 42°	$2.18/L$ [a,b] $2.2/L$ [c] $2.19/L$ [d]	5.55 [c] 5.54 [d]	0 [c,d]	3 [c,d]
Cylindrical Deflector - 127°	$2/r_0$	4/3	1	2
Spherical Deflector - 180°	$1/r_0$	1	0 [c,d]	2

[*] If no superscript is given, the value is found in references a, b, c, and d.
[a] Steckelmacher (Steckelmacher 1973)
[b] Moore, et al. (Moore, et al. 2009) **May be misprint.
[c] Roy and Carette (Roy and Carette, Electron Spectroscopy for Surface Analysis 1977)
[d] Dube and Roy (Dube and Roy, A Generalized Approach for the Determination of Transmission Functions of Charged-Particle Energy Analyzers 1982)

A. Entrance and Exit Particle Positions

Equation (21), which describes the base energy resolution for a monochromatic beam, originates from analysis of particle trajectories through the analyzer to the focusing plane (Rudd, Low Energy Electron Spectrometry 1972). A more basic form of equation (21) can be used to describe the initial and final positions, x_1 and x_2, of particles in the dispersion direction from the source plane to the focused image plane. x_1 and x_2 are measured relative to a local coordinate system that follows the optic axis. For the CDA and SDA with the center of the beam at radius r_0 for instance, $x_1 = r_i - r_0$ (position at the source plane) and $x_2 = r_f - r_0$ (position at the exit focused plane). Substituting $(x_1 + x_2)/2$ in place of the slit width w and $\Delta E_p = E_p - E_0$ in place of ΔE_B, yields equation (23). E_p is the particle energy and ΔE_p is the particle energy relative to the pass energy.

$$\frac{\Delta E_p}{E_0} = A\frac{(x_1 + x_2)}{2} + B\alpha^n + C\beta^2 \tag{23}$$

For example, equation (24) gives the position function for the 45° PMA. This describes how the exit position of a particle is a function of its entrance position, energy deviation, and angular deviations α and β.

$$\frac{\Delta E_p}{E_0} = \frac{(x_1 + x_2)}{L} + 2\alpha^2 + \beta^2 \implies x_2 = -x_1 + \frac{L\Delta E_p}{E_0} - 2L\alpha^2 - L\beta^2 \tag{24}$$

B. Effective Energy Resolution

Roy and Carette and Dube and Roy have further given equations to calculate the effective energy resolution for a monochromatic beam, $\Delta E/E_0$, directly when particular conditions are met (Roy and Carette, Electron Spectroscopy for Surface Analysis 1977) (Dube and Roy, A Generalized Approach for the Determination of Transmission Functions of Charged-Particle Energy Analyzers 1982) (Roy and Tremblay, Design of electron spectrometers 1990). The energy resolution can be approximated from equation (25) using the constants found in Table 4. For the most part, these constants are the same as the constants in Table 3. These values only differ slightly for the 30° PMA and the CMA. The coefficients a, b, c, and n are constants that are characteristic of the particular analyzer. The energy dispersion coefficient D_k is equal to $2/a$ (M. Yavor 2009).

$$\frac{\Delta E}{E_0} = \frac{1}{2}aw + \frac{1}{4}b\alpha^n + \frac{1}{4}c\beta^2 \tag{25}$$

Approximate relationship from (Roy and Carette, Electron Spectroscopy for Surface Analysis 1977), (Rudd, Low Energy Electron Spectrometry 1972).

Table 4 – $\Delta E/E_0$ values for selected electrostatic analyzers. Use in equation (25).

Analyzer	a $(2/D_k)$	b	c	n
Parallel Mirror - 45°	$2/L$ [c,d]	2 [c,d]	1 [c]	2 [c]
Parallel Mirror - 30°	$3/L$ [c,d]	9.2 [c] 4.67 [d]	1 [c]	3 [c]
Cylindrical Mirror - 42°	$2.2/L$ [c] $2.18/L$ [d]	5.55 [c] 2.77 [d]	0 [c]	3 [c]
Cylindrical Deflector - 127°	$2/r_0$ [c,d]	4/3 [c,d]	1 [c]	2 [c]
Spherical Deflector - 180°	$1/(r_0)$ [c,d]	1 [c,d]	0 [c]	2 [c]

[c]Roy and Carette (Roy and Carette, Electron Spectroscopy for Surface Analysis 1977)

[d]Terms calculated from Dube and Roy (Dube and Roy, A Generalized Approach for the Determination of Transmission Functions of Charged-Particle Energy Analyzers 1982) (Roy and Tremblay, Design of electron spectrometers 1990).

From Roy and Carette, equation (25) is valid if the terms are nearly equal ($\frac{1}{2}Aw = B\alpha^n = C\beta^2$) (Roy and Carette, Electron Spectroscopy for Surface Analysis 1977).

The coefficients a, b, c, and n in Table 4 were calculated from the work of Dube and Roy (Dube and Roy, A Generalized Approach for the Determination of Transmission Functions of Charged-Particle Energy Analyzers 1982) (Roy and Tremblay, Design of electron spectrometers 1990). The authors used different notation but the values of a, b, c, and n could be calculated. Dube and Roy used equations (26)-(31) with constants from Table 5. In Table 5, $|M|$ is the absolute value of the linear magnification coefficient, which is the ratio of the width of the

focused image at the exit to the width of the focused image at the entrance. For the five analyzers discussed herein, the magnification is $M_x = -1$ in the deflection plane (i.e. $x_2 = -x_1$). In the perpendicular plane, $M_y = 1$ for the PMA and the CDA (which do not focus in the perpendicular plane), and $M_y = -1$ for the CMA and SDA. The quantity $D^* l_n$ is the energy dispersion D_k. The coefficient c (relating to the angle β) is less discussed, defined, or derived in the literature compared to the coefficients a and b. However, the resolution of the analyzer is less dependent on β than on α and the geometrical terms (w, r_0, and L).

$$\frac{\Delta E_B}{E_0} = \frac{2(\mathrm{a}^* + \mathrm{c}^*) + (\omega + 1)\mathrm{b}^*}{D^*} \tag{26}$$

Where:

$$a^* = \frac{1}{2}\frac{w_2}{l_n}|M| \tag{27}$$

$$b^* = C^*(\Delta\alpha) \tag{28}$$

$$c^* = \frac{1}{2}\frac{w_2}{l_n} \tag{29}$$

$$\omega = \begin{cases} 0 & if\ n\ is\ even \\ 1 & if\ n\ is\ odd \end{cases} \tag{30}$$

The effective energy resolution (based on the FWHM), $\Delta E/E_0$, can be approximated by equation (31) if $w_2 = M w_1$ and $\frac{b^*}{a^*} \leq 2^{3-n}$ is satisfied:

$$\frac{\Delta E}{E_0} = \frac{2a^* + b^*/4}{D^*} \tag{31}$$

Table 5 – Coefficients for equations (26)-(31) for determining the base energy resolution and effective energy resolution (FWHM).

Analyzer	$\lvert M\rvert$	D^*	C^*	n	l_n
Parallel Mirror - 45°	1	1	2	2	L
Parallel Mirror - 30°	1	0.66	3.08	3	L
Cylindrical Mirror - 42°	1	0.914	2.53	3	L
Cylindrical Deflector - 127°	1	1	1.33	2	r_0
Spherical Deflector - 180°	1	2	2	2	r_0

In general, a smaller resolution (higher resolving power) can be achieved by decreasing the slit widths, decreasing the beam acceptance angle, and increasing the analyzer dimensions (to decrease the constant A [and a]) (Steckelmacher 1973). However, this will also decrease the transmission through the analyzer.

Other metrics that can be used to quantify analyzer performance include the transmission, etendue, luminosity, energy dispersion (D_k), trace width (t_w), and effective resolution (Roy and Carette, Electron Spectroscopy for Surface Analysis 1977) (Steckelmacher 1973) (H. Wollnik 1967).

IV. Selected Missions with Electrostatic Analyzers

Many missions have been flown with ESAs as part of the instrument suite. These analyzers have been flown independently or as part of combined energy per charge and mass per charge analyzers. Table 6 provides a description of some selected missions. Also, a compilation of articles in the book Measurement Techniques in Space Plasmas – Particles, edited by Pfaff, Borovsky and Young (Pfaff, Borovsky and Young 1998) provides a good overview of space missions and measurement techniques using electrostatic analyzers and other diagnostics.

Table 6 – Selected History of Missions that Utilized Electrostatic Analyzers.

Year Launched	Mission Name – Instrument Name	Type of Electrostatic Analyzer	Example Reference for Mission
1961	Ranger 1 and Ranger 2	Deflector	(JPL 1961)
1962	Mariner 2	CDA	(Bame, et al. 1986) (Young, Space Plasma Particle Instrumentation and the New Paradigm: Faster, Cheaper, Better 1998)
1965-1967	Pioneer 6, 7, and 8 - ARC	Quadrispherical	(Smith and Day 1971) (Sablik, et al. 1988)
1966	OGO-3	CDA	(L. A. Frank 1967)
1973	Mariner 10	SDA	(Bridge 1974)
1973	Nike-Tomahawk Flights / ATS-F	-	(Arnoldy, et al. 1973)
1984	AMPTE	Deflector	(Gloeckler, The Charge-Energy-Mass Spectrometer for 0.3-300 keV/e Ions on the AMPTE CCE 1985)
1985	Giotto - FIS	SDA	(Johnstone, Coates, et al. 1985)
1985	SUISEI/Planet-A	SDA	(Mukai and Miyake 1986)
1989	Galileo	SDA	(Frank, et al. 1992)
1990	CRRES - LEPA	Quadrispherical	(Hardy 1993)
1990	Ulysses - SWICS	Deflector	(Gloeckler, The Solar Wind Ion Compostion Spectrometer 1992)
1992	GEOTAIL	Spherical	(Hirahara and Mukai 1993)
1994	WIND – SWICS/MASS, VEIS	Deflector, CDA	(Gloeckler, The Solar Wind Ion Compostion Spectrometer 1992) (Ogilvie, et al. 1995)
1996	FAST	Top Hat (Spherical)	(Carlson, McFadden, et al. 2001) (Klumpar 2001)
1996	Interball Auroral	SDA	(Dubouloz 1998)
1996	POLAR – TIDE	Electrostatic mirror section	(T. Moore 1995)
1997	EQUATOR-S – 3DA	Top Hat (Spherical)	Derivative of WIND
1997	Cassini-Huygens - CAPS	Top Hat (Spherical)	(Vilppola, Tanskanen and Huomo, et al. 1996) (Vilppola, Tanskanen and Barraclough, et al. 2001)
1998	Deep Space 1 – PEPE	Top Hat (Spherical)	(Bolton 1997)
2000	Cluster – CIS-1, PEACE	Quadrispherical, Top Hat	(Reme 2001) (McFadden and Carlson 1998) (Johnstone, Alsop, et al. 1997)
2004	MESSENGER	Deflector	(Andrews, et al. 2007)
2005	Venus Express, ASPERA-4, Mars Express	Top Hat (Spherical)	(Collinson, Kataria and Coates, et al. 2009)
2006	New Horizons - SWAP	RPA/Top Hat (Spherical)	(McComas, D., et al. 2007)
2006	STEREO	Top Hat (Spherical)	(Sauvaud, et al. 2008)
2007	THEMIS	Top Hat (Spherical)	(J. McFadden 2008)
2008	Interstellar Boundary Explorer – IBEX-Hi/IBEX-Lo	Focusing SDA	(Funsten, Harper and McComas 2005) (McComas 2009)
TBD	LATTES – EQUARS	CDA	(Dallaqua, et al. 2003)
(2014)	Magnetospheric Multiscale (MMS) - DES	Top Hat (Spherical)	(Collinson, Dorelli, et al. 2012)

V. Improving Measurements Using Pre-retardation

The sensitivity of spectrometers can be increased by preliminarily retarding the particle beam prior to entering the analyzer (Roy and Carette, Electron Spectroscopy for Surface Analysis 1977) (M. Yavor 2009). The utility of this technique can be seen in the calculation of the analyzer energy resolution $\Delta E/E_0$. By pre-retarding the beam, the pass energy E_0 can be reduced which allows for a narrower energy spread ΔE through the analyzer given that the ratio $\Delta E/E_0$ is a constant.

VI. Calibration

Calibration of ESAs can be done using a combination of theory and experiment. As will be discussed in the error and uncertainty section, there are many factors than can lead to erroneous energy measurement including fringing fields (Herzog and Jost), electrode alignment, surface contamination, secondary electron emission, stray electric and magnetic fields, sweep speed, space charge effects, and charge exchange. These sources of error affect both the true energy measurement of the beam as well as the magnitude of the current.

In calibrating an ESA, a term called the geometric factor (GF) can be used to convert the number of particles detected during an integration time to the ambient plasma differential energy flux (Theodoridis and Paolini, The Angular Response of Spherical Plate Electrostatic Analyzers 1969) (Wuest, Evans and Steiger 2007) (Collinson, Kataria and Coates, et al. 2009) (Collinson, Dorelli, et al. 2012). The geometric factor can be used to determine the particle flux and the distribution function of incoming particles.

The most common method to calibrate an ESA is by experimental means of measuring the ESA transmission using a particle beam of known energy, angle, energy spread, and magnitude. With the characteristics of the ion or electron beam already known, the transmission function of the ESA can be used to determine the FWHM of the analyzer and whether any aberrations are caused by the ESA. Additionally, multiple ESAs or other energy analyzers (i.e. RPA, time-of-flight) can be used for comparison among one another. The ESA can also be checked repeatedly over time to determine if the performance is changing, due for instance to surface contamination. A comprehensive overview of calibration on space instruments is given in chapters 3-5 of ISSI Scientific Report SR-007, edited by Wuest, Evans, and Steiger (Wuest, Evans and Steiger 2007). Appendix C of this report lists some facilities that have capabilities to calibrate space physics particle instruments.

Numerical investigations can also be performed to simulate the response of the analyzer. These software packages are designed to calculate electric fields and charged particle trajectories given initial electrode geometries, voltage biases, and particle positions and velocities. An overview of the required components for instrument and particle beam simulation can be found in Appendix A and B of ISSI Scientific Report SR-007, edited by Wuest, Evans, and Steiger (Wuest, Evans and Steiger 2007). This reference also lists commercially available raytracing software packages. A commonly used commercially available program is called SIMION® (Dahl 2000).

VII. Methodology of Data Collection

There are two main sweeping modes used to collect current in electrostatic analyzers. The first is known as the constant acceleration mode, constant-relative-resolution mode, sector field sweeping mode, or the variable transmission energy mode (VTE). The second is known as the constant energy mode, constant-absolute-resolution mode, or the constant transmission energy mode (CTE) (Rudd, Low Energy Electron Spectrometry 1972) (Roy and Carette, Electron Spectroscopy for Surface Analysis 1977) (Roy and Tremblay, Design of electron spectrometers 1990).

In the constant acceleration mode, the particles to be analyzed enter the probe either with their own energy, or an energy increased/decreased by a constant amount of pre-acceleration/deceleration. The pass energy E_0 of the analyzer is swept over the range of interest. In contrast, in the constant energy mode the pass energy of the analyzer is held constant and the particles to be analyzed are accelerated/decelerated by a variable sweeping voltage.

The accelerating/decelerating voltage V_s is usually applied to the entrance and exit slit electrodes. The voltages applied to the analyzer's surfaces are then biased relative to the voltage V_s.

Table 7 summarizes the features of each mode with associated advantages and drawbacks. The CTE mode is generally preferred due to the constant resolution over the energy range. Figure 18 shows a biasing schematic for both modes.

Table 7 – Sweeping Modes for Energy Analysis.

Mode Names	Constant acceleration mode Constant-relative-resolution mode Variable transmission energy mode (VTE) Sector field sweep mode	Constant energy mode Constant-absolute-resolution mode Constant transmission energy mode (CTE)
Resolution mode	$\Delta E/E_0 = constant$	$\Delta E = constant$
Slit Voltage, V_s	Constant (ground potential, or can be set to accelerate/decelerate particles).	Variable (swept over range of interest). Can be set to accelerate/decelerate particles into the analyzer section.
Transmission/Pass Energy, E_0	Variable (swept over range of interest).	Constant.
Advantages	Easy to design lenses.	Absolute resolution ΔE is constant. Better for qualitative analysis.
Drawbacks	Absolute resolution ΔE is not constant.	Hard to design focusing optics.

a) Constant acceleration mode. CDA/SDA.

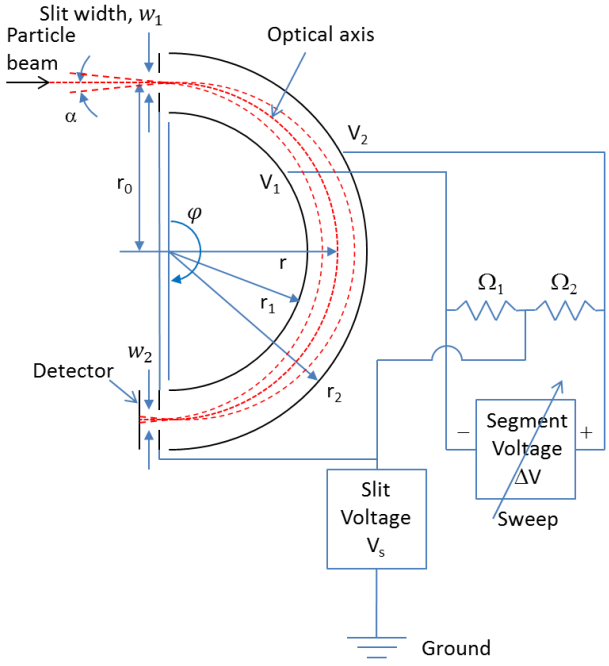

b) Constant energy mode. CDA/SDA.

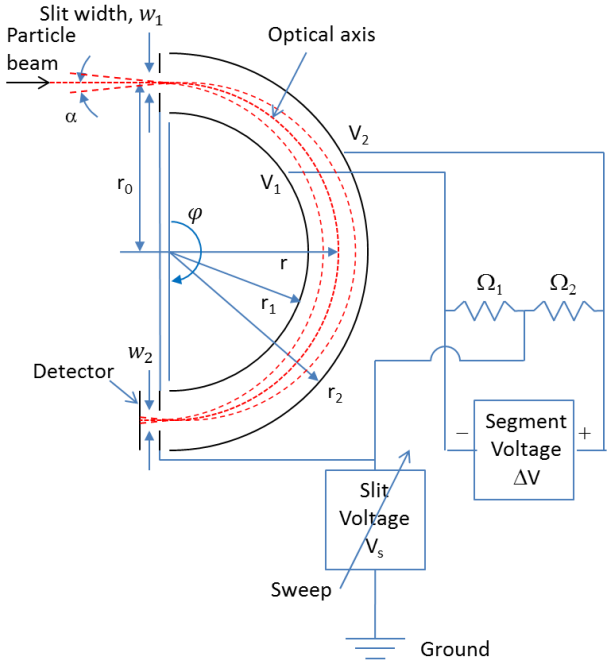

c) Constant acceleration mode. 30° PMA.

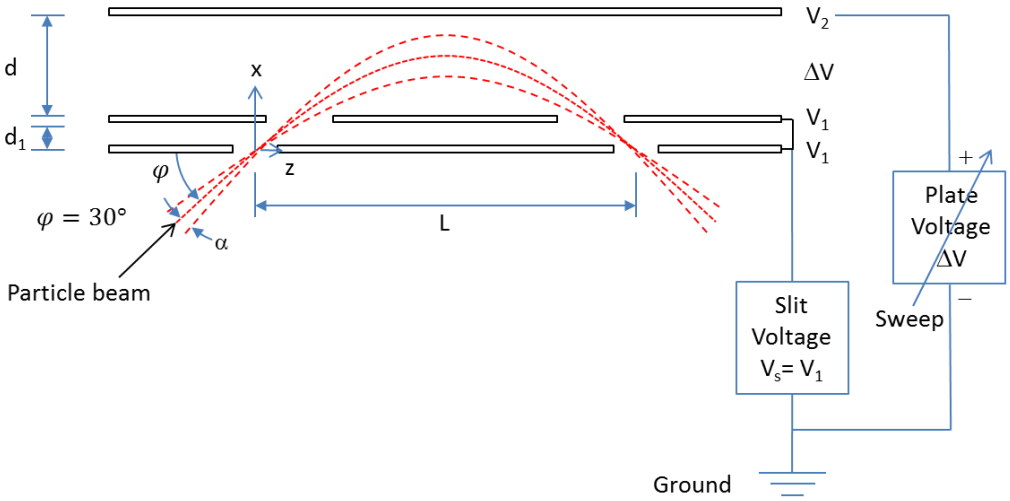

d) Constant energy mode. 30° PMA.

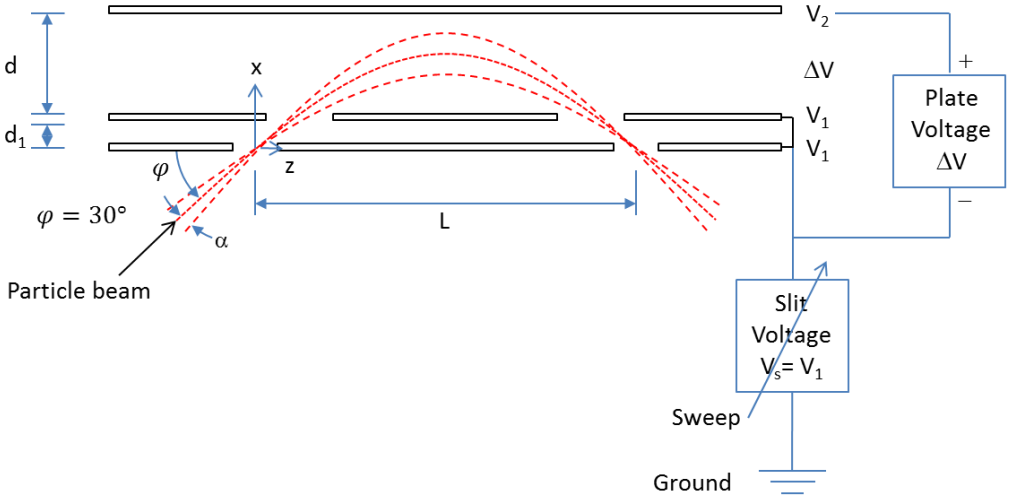

Figure 18. – Electrical biasing setup using modes 1 and 2 for ion analysis using a) and b) CPAs and c) and d) mirror analyzers. Entrance and exit slits are at the same potential. For electron analysis, the plate voltage, ΔV, is reversed.

VIII. Example Data and Data Reduction

As an example, we describe a procedure to use a spherical deflector analyzer (SDA) to measure the ion energy distribution from an ion thruster. With the ion thruster operating at a beam voltage of 900 V, we will use the SDA to look for ions (z = 1, 2, etc.) with E/q ratios near 900 eV. We will choose the transmission energy of the analyzer to be $E_0/q = 1000\ eV$.

The analyzer will selectively pass ions of energy E/q based on the applied slit voltage and transmission energy according to equation (32).

$$E/_q = V_s + {}^{E_0}/_q = V_s + {}^{\Delta V}/_C \tag{32}$$

We can use this equation to calculate a baseline slit voltage that we need to apply to select for ions near the beam voltage (i.e. when $E/q = 900\ eV$) as $V_s = 900 - E_0/q = 900 - 1000 = -100\ V$. The slit voltage, in general, serves to accelerate or decelerate the beam ions as they enter the analyzer. In this case, a slit bias of -100 V accelerates the 900 eV beam ions to the 1000 eV pass energy of the ESA.

The geometry of the SDA is $r_1 = 4\ cm$, $r_2 = 6\ cm$, $r_0 = 5\ cm$, and $\varphi = 180°$. From this, the analyzer constant C is calculated using the equation found in Table 2 for a SDA.

$$C = r_2/r_1 - r_1/r_2 = 6/4 - 4/6 = 0.833$$

The voltage applied across the segments is then equal to the transmission energy multiplied by the analyzer constant:

$$\Delta V = (E_0/q)\, C$$
$$\Delta V = 1000 * 0.833 = 833\ V \qquad \text{(equation (1))}$$

The particular outer and inner segment voltages are biased relative to the slit voltage, and are a function of the transmission energy E_0/q and probe radii:

$$V_1 = V_s + 2\frac{E_0}{q}\left(1 - \frac{r_0}{r_1}\right) = -100 + 2 * 1000\left(1 - \frac{5}{4}\right) = -600\ V \qquad \text{(equation (16))}$$

$$V_2 = V_s + 2\frac{E_0}{q}\left(1 - \frac{r_0}{r_2}\right) = -100 + 2 * 1000\left(1 - \frac{5}{6}\right) = 233\ V \qquad \text{(equation (17))}$$

The voltages V_1 and V_2 calculated above are relative to ground potential (or the "ground" potential from which the potential of the particle beam is measured). In practice, one power supply could supply the voltage ΔV which floats relative to a second power supply that sets V_s (see Figure 18). Also note that the voltage magnitudes could be made smaller by reducing the difference in segment radii $r_2 - r_1$.

With the basic settings, a data collection mode can be chosen for the analyzer: either the constant acceleration mode or the constant energy mode. In constant energy mode, the slit voltage is swept to measure the transmission function. For example, the slit voltage V_s could be swept from -150 V to -50 V in order to measure ions with energies from 850 eV to 950 eV. In constant acceleration mode, the slit voltage is held constant (not necessarily at 0 V) while the segment voltage difference ΔV is swept. With $V_s = -100\ V$ held constant, sweeping ΔV from 792 to 875 V would allow ions from 850 to 950 eV to pass through the ESA. In either case, the selected ion energy is found for the geometry in question from equation (32):

$$E/q = V_s + 1.20\Delta V \qquad \text{(equation (32))}$$

Here, we will choose to use the constant energy mode, varying the slit voltage V_s while keeping the potential difference ΔV and transmission energy E_0/q constant. We will assume that there are no focusing effects due to the nonzero V_s.

The trajectories of monoenergetic 900 eV ions are shown passing through the ESA for three slit voltages in Figure 19. These particle paths were calculated using ANSYS® Multiphysics software.

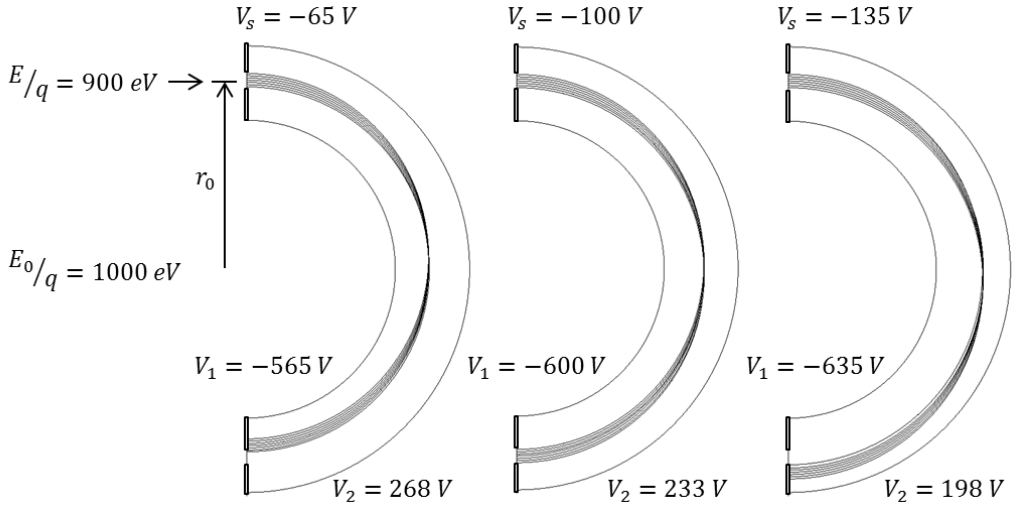

Figure 19. Ion trajectories in a spherical analyzer during data collection for three selected slit voltages.

In Figure 19, the entrance and exit slit widths are both $w = 0.35\ cm$ in the plane of the paper, and are thin in the perpendicular plane. The entrance slit is uniformly covered with incoming (ion) particles. As V_s is varied positive and negative of $V_s = -100\ V$, the ion beam spot sweeps across the exit plane. No ions pass through the second slit when the selected energy is below 865 or above 935 eV, whereas all ions pass through the second slit for a selected energy of 900 eV.

A. Numerical Particle Tracking

Equation (23) for an SDA is an approximation to the solution of the differential equation that describes a particle's trajectory in a $1/r^2$ electric field. The solution to the differential equation that includes the deflection angle, φ, is given in equation (33), where r is the particle's radius from the center of the analyzer and E is the incoming particle's energy before it reaches the analyzer.

$$r = \frac{r_i}{\frac{r_0 E_0}{r_i\left(E - 2E_0\left(1 - {}^{r_0}/_{r_i}\right)\right)\cos^2\alpha}(1 - \cos\varphi) + \cos\varphi - \tan\alpha\sin\varphi} \tag{33}$$

B. ESA Simulation Using Particle Tracking Software

Energy distributions can also be calculated using particle tracking software such as SIMION. A hemispherical SDA with dimensions $r_1 = 4\ cm$, $r_2 = 6\ cm$, $r_0 = 5\ cm$, and $\varphi = 180°$ was drawn in SIMION 8.1 for comparison to the numerical calculations using equation (33). A partial view of the hemisphere is shown in Figure 20 with example particle trajectories.

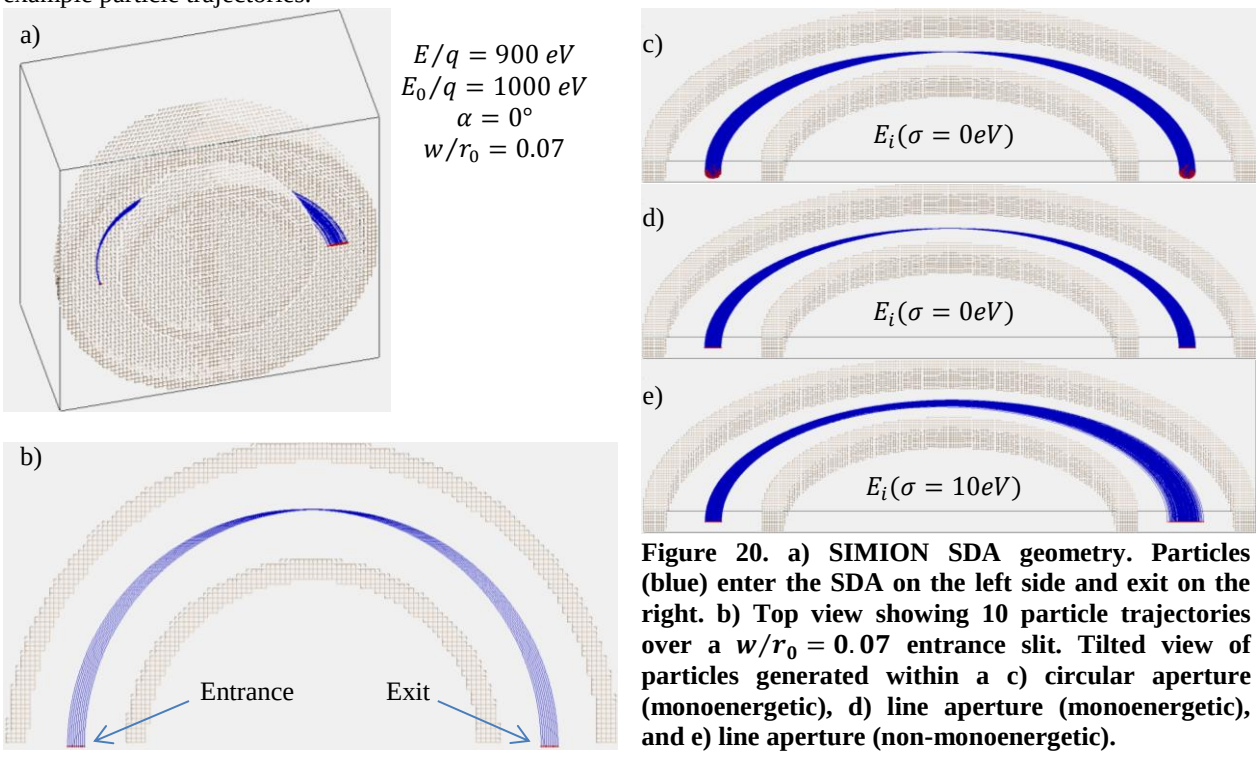

Figure 20. a) SIMION SDA geometry. Particles (blue) enter the SDA on the left side and exit on the right. b) Top view showing 10 particle trajectories over a $w/r_0 = 0.07$ entrance slit. Tilted view of particles generated within a c) circular aperture (monoenergetic), d) line aperture (monoenergetic), and e) line aperture (non-monoenergetic).

By continuously varying V_s and measuring the current to the analyzer collector downstream of the second slit, a distribution of the form shown in Figure 21 is obtained. The distributions are calculated numerically using equation (33) and in SIMION by determining if each particle would pass through the exit aperture for the given energy, pass energy, initial position, deflection angle, and particle angle. In most cases, the numerical calculation and SIMION simulation agreed to high degree, with small errors in the solution of electric potential (typically less than a few volts) occurring in SIMION due to the mesh-approximated geometry. The transmission f is the fraction of particles passed through the exit slit to the number of particles that enter the entrance slit. For a monoenergetic source with no angular deviations, the transmission reaches unity when the selected energy equals the particle energy. Because the

aperture widths are finite, a linear decrease in the transmission is seen as the beam spot sweeps away from the second slit in both directions.

If the slits are made thinner ($\frac{w}{r_0} = 0.07 \rightarrow 0.035 \rightarrow 0.0175$), the transmission drops to zero faster with equal changes in selection energy, and the resolving power of the analyzer improves. However, the magnitude of particle current to the collector decreases as well. At the limit $w = 0$, the transmission function would be a vertical line at ${}^{E}/_{q} = 900\ eV$.

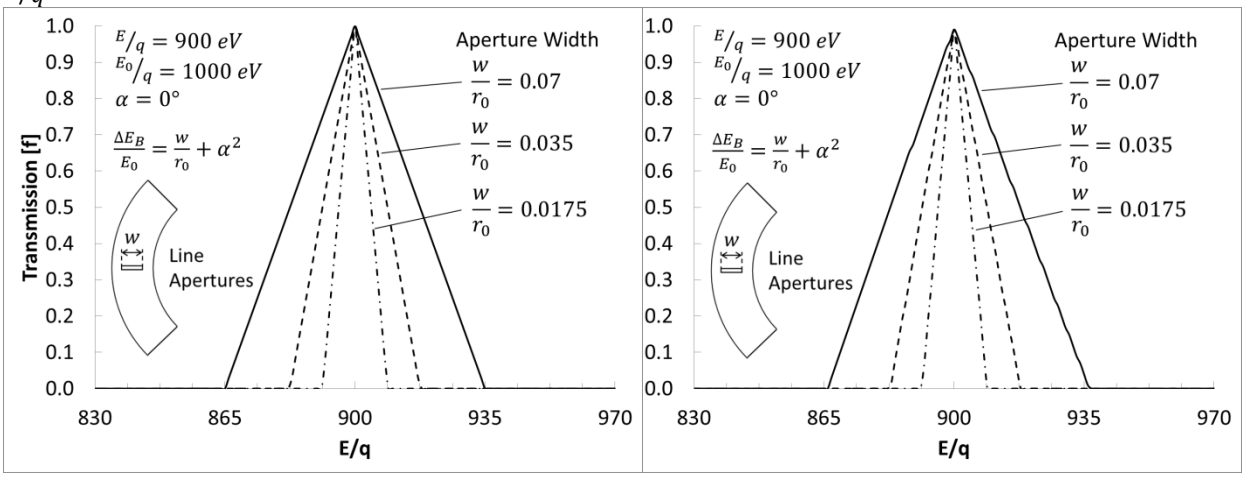

Numerical Calculation, Equation (33) *SIMION Simulation*

Figure 21. Spherical deflector data collection as a function of slit voltage for a monoenergetic beam. Left shows numerically predicted transmission and right shows the SIMION simulation (with good agreement). The resolving power of the ESA increases with decreasing slit width.

The full base width of the distribution for the SDA is predicted by equation (21): $\frac{\Delta E_B}{E_0} = \frac{w}{r_0} + \alpha^2$. For $\frac{w}{r_0} = 0.07$ and $\alpha = 0°$, the base with is expected to be $\Delta E_B = 70\ eV$, which agrees with that shown in Figure 21.

Next, we consider what the transmission function looks like for the case of a non-monoenergetic particle source, shown in Figure 22. Here, we model the entrance particle beam as having a Gaussian shape centered around $900\ eV$. A standard deviation $\sigma = 10\ eV$ in this case would indicate that 68% of ions entering the analyzer would have energies in the range of 890 to 910 eV (within $\pm\sigma$). The non-monoenergetic source has a smoothing effect on the resulting distribution from the low and high energy outliers.

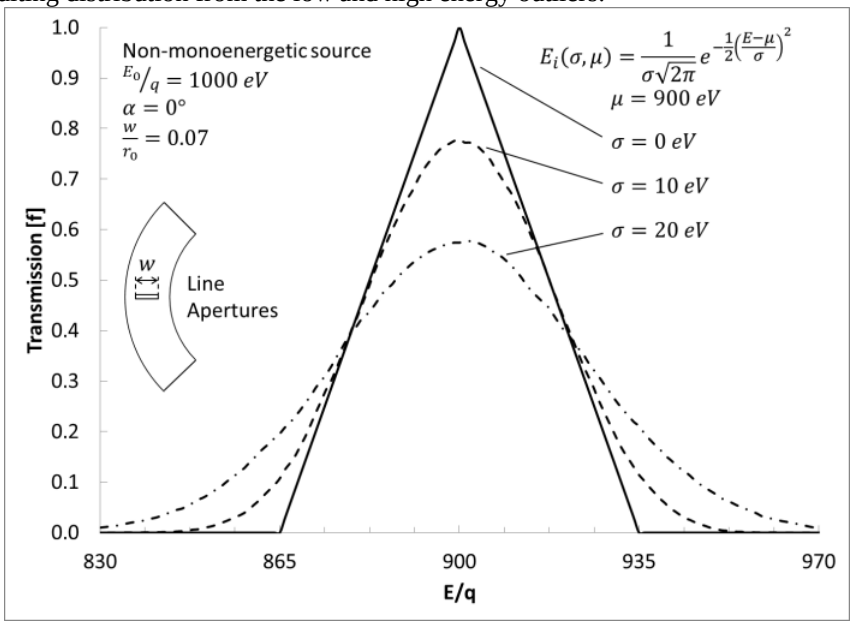

Figure 22. Example SDA output data of non-monoenergetic input source beams.

We can improve the resolving power in the non-monoenergetic case by decreasing the aperture size, as shown in Figure 23 for the $\sigma = 10\ eV$ standard deviation case. Figure 24 shows the same data normalized to each curve's peak value along with the shape of the input non-monoenergetic beam (also normalized to unity). In contrast to the case where the aperture size is decreased in the monoenergetic case, the peak transmission does not reach unity and decreases with decreasing aperture width, on top of the intensity decrease due to the reduced entrance/exit aperture area. Increasing the resolving power, though, makes the measured distribution more closely resemble the distribution of the source particles.

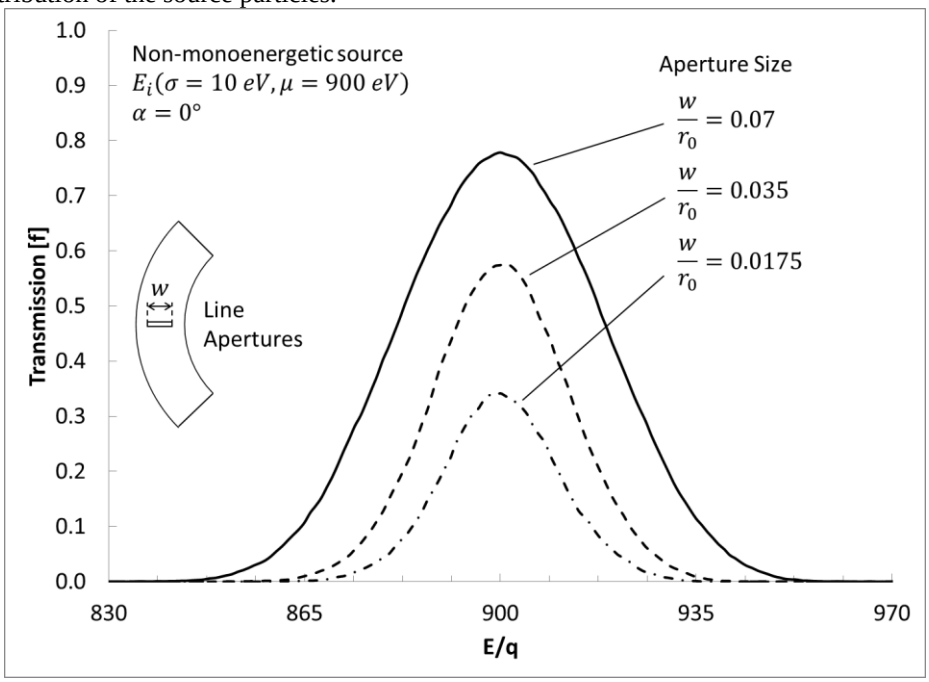

Figure 23. Improving the resolving power of an SDA by reducing the slit diameter.

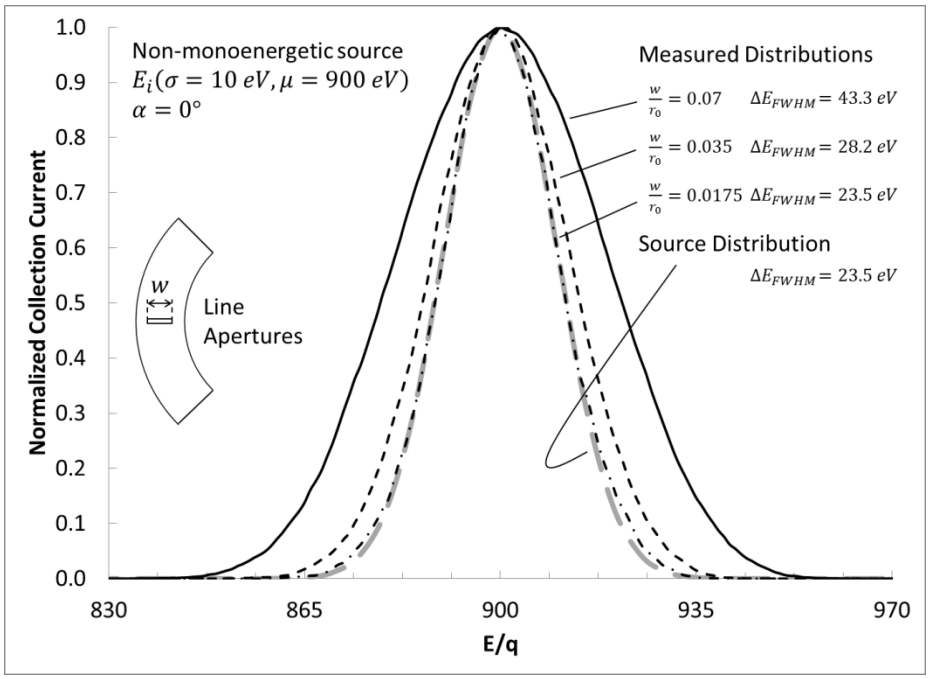

Figure 24. Improving the resolving power of an SDA by reducing the slit diameter. The data of Figure 23 is normalized and shown with the input source distribution.

The angular distribution of the incoming particle beam affects the shape of the transmission function, even in the case of a monoenergetic particle beam, as shown in Figure 25. Here, the incoming particles have uniform and random half angles among the range $[-\alpha, +\alpha]$. Choosing $\alpha = 7.58°$ in this case suggests that the angular aberration term is one-quarter of the size of the slit width term in determining the base width of the energy distribution function. Similarly, choosing $\alpha = 10.72°$ for this geometry makes the angular aberration term half the size of the slit width term, causing the base width to be 50% wider than for $\alpha = 0°$. Notice however, that the full width at half maximum is not increased as much as the base width in either case. This is predicted from equation (25), the full width at half maximum resolution, compared to equation (21), the base width resolution, where the full width at half maximum increases one-quarter as fast as the base width due to the α term.

Base width $$\frac{\Delta E_B}{E_0} = \frac{1}{r_0} w + \alpha^2 \qquad \text{(equation (21))}$$

Full width at half maximum $$\frac{\Delta E}{E_0} = \frac{1}{2r_0} w + \frac{1}{4} \alpha^2 \qquad \text{(equation (25))}$$

Figure 25 shows data from both the numerical calculation and SIMION simulation. The results nearly match except for lower transmission energies for the $\alpha = 10.72°$ angular source aberration. The difference is due to a small fraction of ions being lost in the SMION simulation from hitting the electrode walls before they reach the exit of the SDA. Note that most of these highly angled ions would not be transmitted even if not intercepted by the walls. On the other hand, particles are not lost in calculating the final position using equation (33), giving the erroneously high transmission.

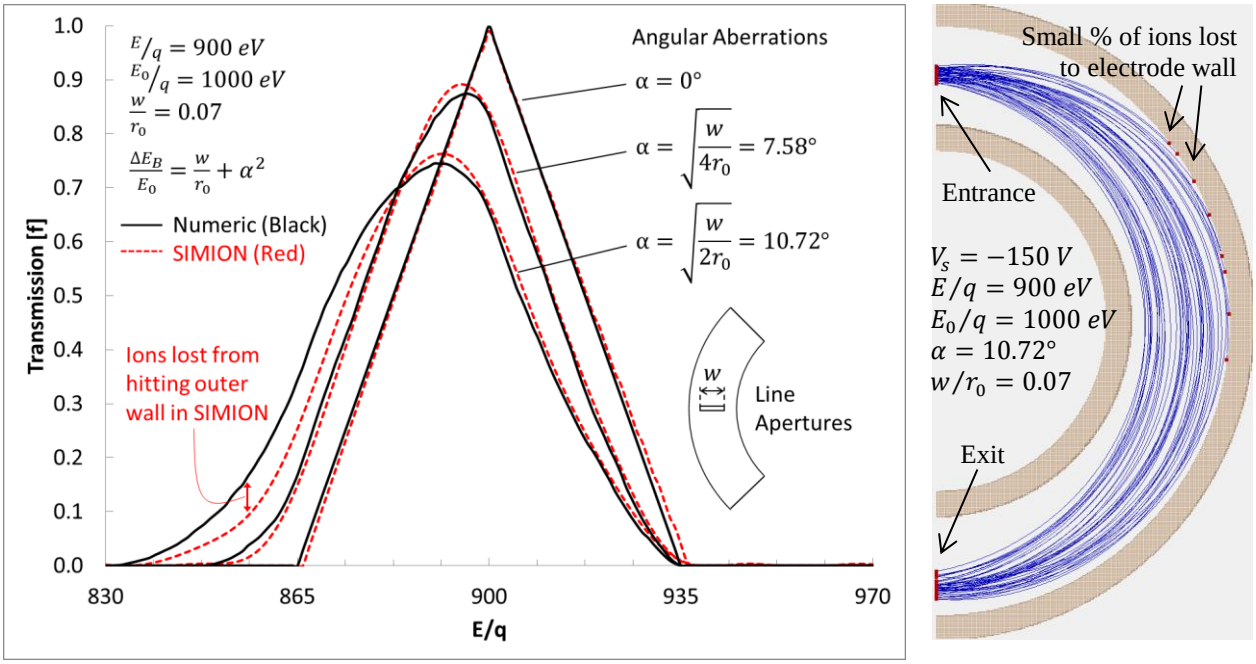

Figure 25. Shape of measured distribution function with angular source aberrations. The numerical calculation differed from the SIMION result for $\alpha = 10.72°$ due to some ions hitting the outer electrode wall at low E/q. Picture at right shows a small fraction of particles that are lost to the wall (red dot marker) at a selected energy of 850 V, one or two of which would otherwise follow trajectories to pass through the exit aperture.

The reason for shift in the peak energy location in Figure 25 is illustrated in Figure 26. Here, a point source of monoenergetic particles ($\Delta E/E_0 = 0$) is located at the entrance of the ESA along the optical axis, with local coordinate $x_1 = 0$. The local exit x-coordinate for these particles is then $x_2 = -2r_0\alpha^2$ [equation (23)], where any particle with non-zero α is shifted slightly toward the center of the analyzer regardless of initial sign. The net effect is that particles with nonzero α appear to have less energy.

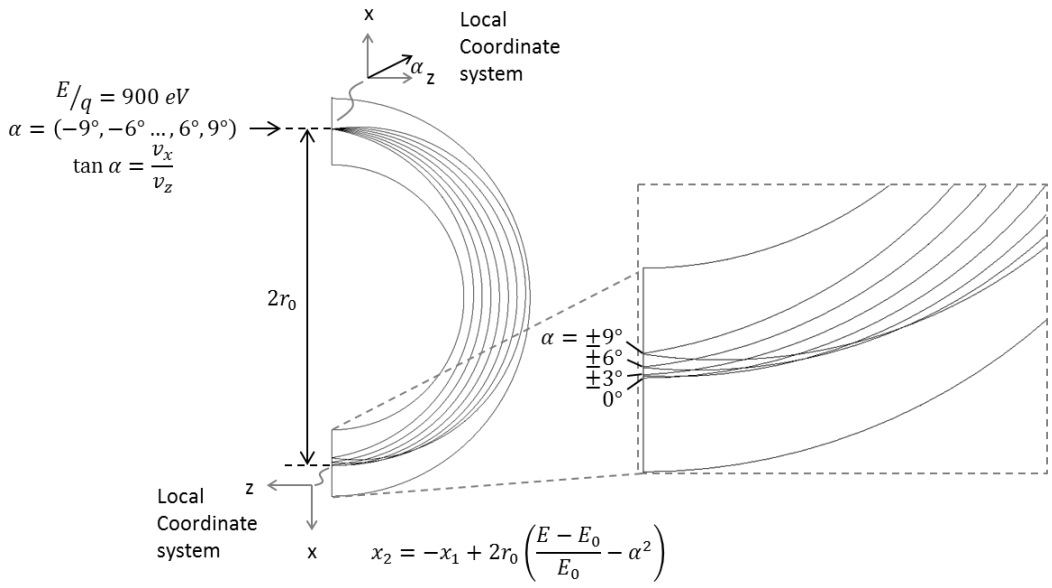

Figure 26. Ion trajectories from a monoenergetic point source with angular deviations.

Now suppose that we have a particle source with both energy and angular aberrations, and that several data sets are taken with different entrance and exit slit widths as in Figure 27. Here, each curve has been normalized to its maximum value. The source distribution is shown as a dashed light gray line, and has a full width at half maximum energy spread of 23.5 eV. The FWHM of the measured distribution approaches this value using successively smaller aperture widths. Notice additionally that the measured curves are consistently shifted toward lower energies due to the angular deviations of the source beam, and that the shift remains regardless of slit width.

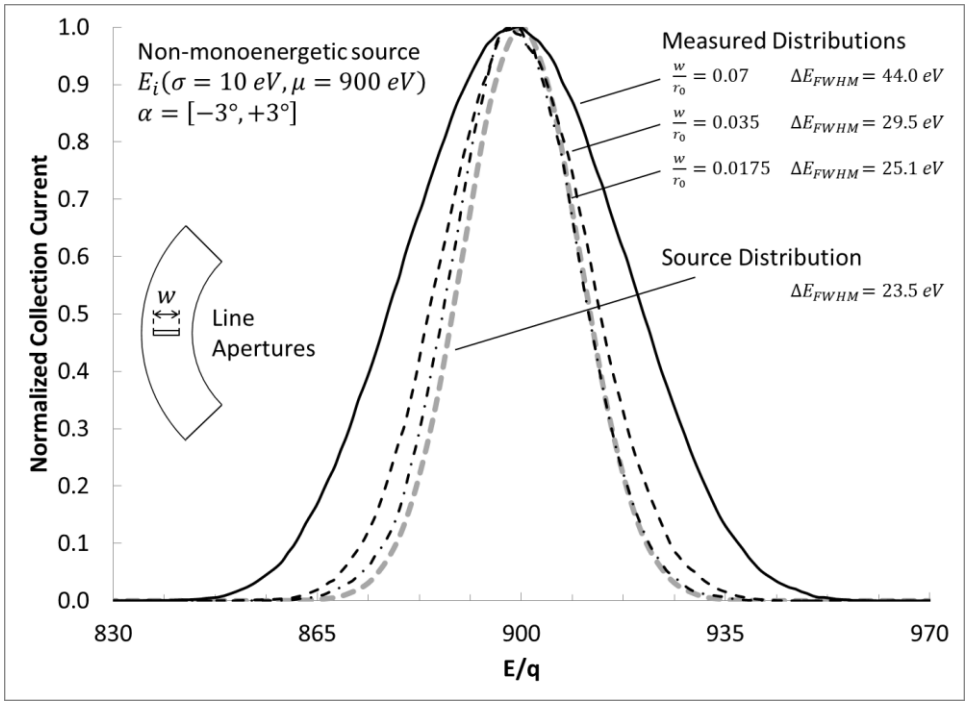

Figure 27. Normalized measured energy distributions approaching the source distribution with smaller slit width. The measured distribution is shifted toward lower energy due to angular deviations of the input beam.

Thus far, the entrance and exit apertures have been thin horizontal lines. If instead the apertures are circular, the transmission function of a monoenergetic source is shown in Figure 28. The shape of the transmission function is influenced a small amount by the area overlap of the circular beam sweeping across the circular exit aperture.

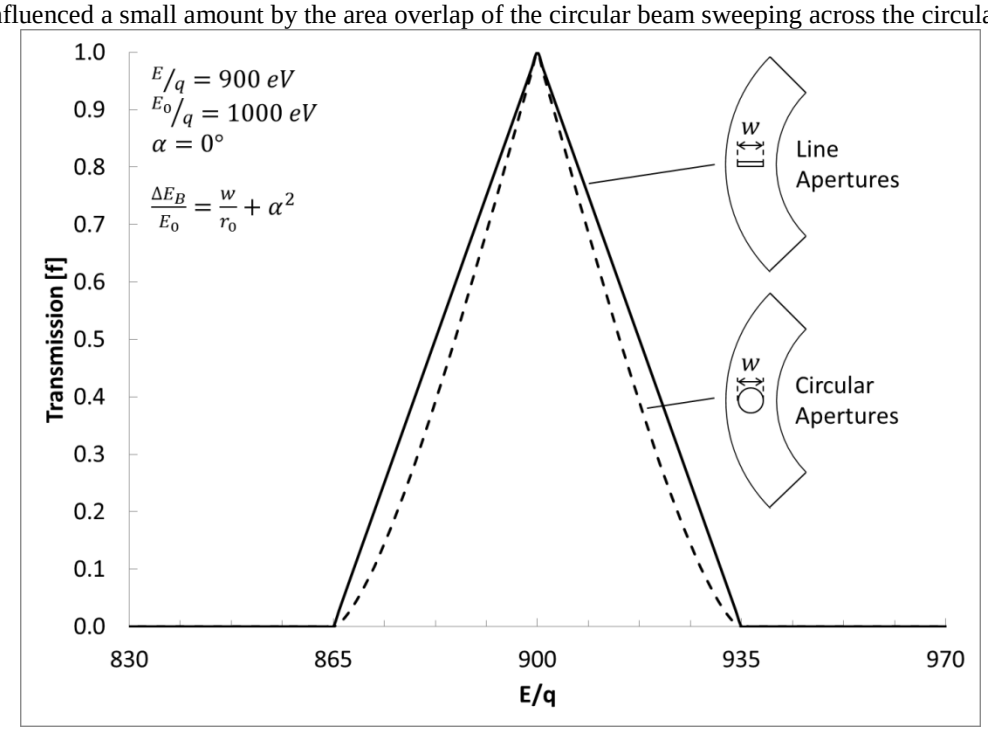

Figure 28. Monoenergetic distribution for horizontal and circular entrance and exit apertures.

IX. Error Analysis and Uncertainty

There are a wide variety of sources that affect charged particle beam energy analysis. These sources of error affect both the true energy measurement of the beam as well as the magnitude of the current. Sources of error include: fringing fields (Herzog and Jost), electrode alignment, surface contamination, secondary electron emission, stray electric and magnetic fields, sweep speed, space charge effects, and charge exchange.

A. Fringing Field Effects in ESAs

1. Effective boundaries and Herzog shunts

The true angular deflection φ of beam particles is determined by the effective electric field boundaries, which do not necessarily coincide with the physical dimensional boundaries of the analyzer (Roy and Carette, Electron Spectroscopy for Surface Analysis 1977). These fringing fields can be mitigated and corrected with proper design of the inlet and outlet apertures using fringing field shunts. In this way, the effective deflection angle of the beam can be made equal to the mechanically designed deflection angle of the sectors. Herzog first defined a set of parameters in 1935 to enable slit apertures to act as fringing field shunts (M. Yavor 2009). A set of parameters were defined to provide a desired fringing field (Hu, Matsuo and Matsuda 1982) as shown in Figure 29: $b = w/2$ and d, which is the separation distance between the slit and the deflection plates. The distance between the ideal field boundary and the end of the electrodes is denoted by h. In practice, the most widely used shunt dimensions are $b = 0.5g_0$, and $d \approx 0.4g_0$ (M. Yavor 2009). Information is also provided in Roy and Carette to calculate the beam deflection angle with fringing fields (Roy and Carette, Electron Spectroscopy for Surface Analysis 1977).

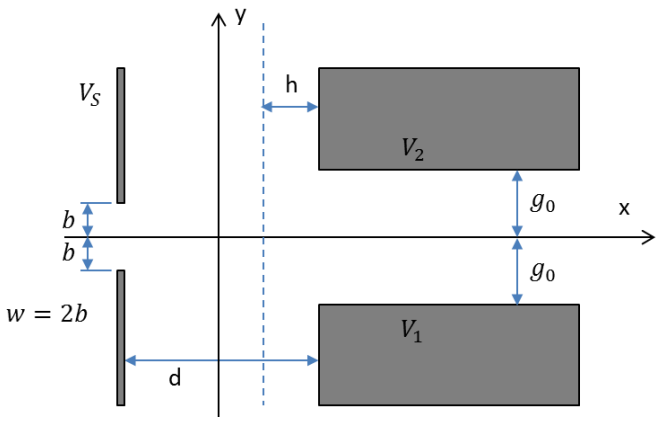

Figure 29. Design of entrance and exit apertures to make the ideal field boundary coincide with the end of the condenser electrodes (from (Hu, Matsuo and Matsuda 1982)).

2. Jost fringing field shunts

Fringing field shunts are also used when the effective boundary position of the electrostatic field lies within the condenser electrodes. This occurs in both the SDA and the CDA when there are narrow source and exit slits. In this case, the real deflection angle of the analyzer becomes smaller than the mechanical sector angle. Ways to correct for the effective boundary position include changing the mechanical sector angle, tilting the entrance angle of the beam, or moving the position of the entrance and exit slits relative to the centerline (M. Yavor 2009). Sise et al. gives a comparison of these methods (Sise, et al. 2007).

One correction method is called a Jost fringing field shunt, which adjusts the position of the effective boundary to the position of the mechanical sectors (Jost, Fringing field correction for 127° and 180° electron spectrometers 1979). This is an "almost-closed" fringing field shunt (M. Yavor 2009). In this case, the edges of the electrodes are moved inward near the slits, which causes a small region near the optic axis to be at a higher potential than the pass energy. This idea is shown in Figure 30. To adjust the position of the effective boundary to the position of the mechanical sectors, the width of the central part of the shunt should be made to be approximately one-third of the gap width between the electrodes. Baraldi, et al. used this boundary shift method when they combined two hemispherical deflector analyzers (Baraldi, Dhanak and King 1992).

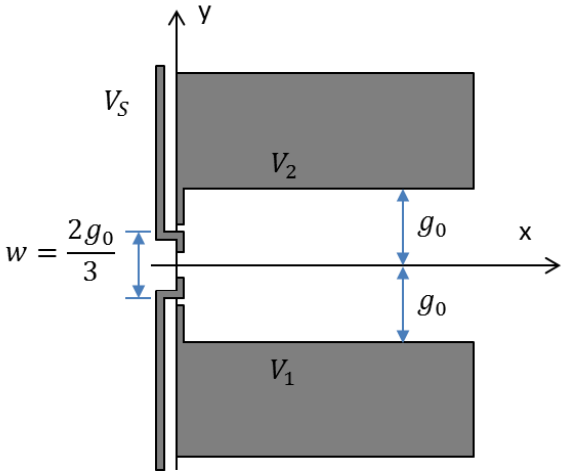

Figure 30. Diagram of a Jost fringing field shunt. The Jost shunt is designed to make the effective electric field boundary equal to the mechanical sector boundary. This type of shunt is used in CDAs and SDAs when the fringing field causes the effective field boundary to be within the mechanical sectors.

3. Defocusing Action of Fringing Fields

In addition to affecting the angle of deflection, fringing fields also create lenses to defocus the particle beam (M. Yavor 2009) (Matsuda, The influence of a toroidal electric fringing field on the trajectories of charged particles in a third order approximation 1971). The fringing fields act to defocus the beam in the dispersion plane. This effect is small for sector field analyzers but may be important to consider in imaging energy filters.

4. Second Order Angular Aberrations in ESAs

Second order focusing aberrations occur in sector field analyzers but can be corrected with design of the entrance and/or exit of the analyzer. One correction is to curve the entrance and exit electrode boundaries. Another correction can be done by accelerating the particles at the entrance and/or decelerating the particles at the exit (M. Yavor 2009).

B. Probe Alignment

Errors in energy analysis can be caused by misalignment of the entrance and exit apertures and non-uniform gap widths in the plates and sectors (H. Wollnik 1967). These problems are similar to fringing field effects in causing variations in the electric fields that accelerate and shift the particle beams. When this occurs, the probe theory and analyzer constants no longer match experiment. These effects would likely need to be investigated on an individual analyzer-by-analyzer basis using either computer simulation tools or experiment. Experiments could include performance comparisons with other ESAs or purposeful misalignment of the ESA geometry to determine changes in energy and resolution. An example can be seen in Vilppola et al. of misalignment of hemispherical sectors in an ion beam spectrometer (Vilppola, Keisala, et al. 1993).

In the case of aperture misalignment in the dispersion plane, an offset of either the entrance or exit aperture by a distance d will shift the apparent energy of the measured distribution by $\frac{d}{D_k}E_0$, as illustrated by the example SDA in Figure 31. The center of the entrance aperture is at r_0 and the center of the exit aperture is at $r_0 + \frac{1}{2}w$. In this case, the transmission is 100 % for ${E_0}/{q} = 982.5\ eV$ instead of the ideal ${E_0}/{q} = 1000\ eV$. If the slits are moved farther apart the measured distribution will shift lower in energy. Conversely, moving the slits closer together shifts the measured distribution higher in energy. The shape of the distribution would not change for reasonably small misalignment.

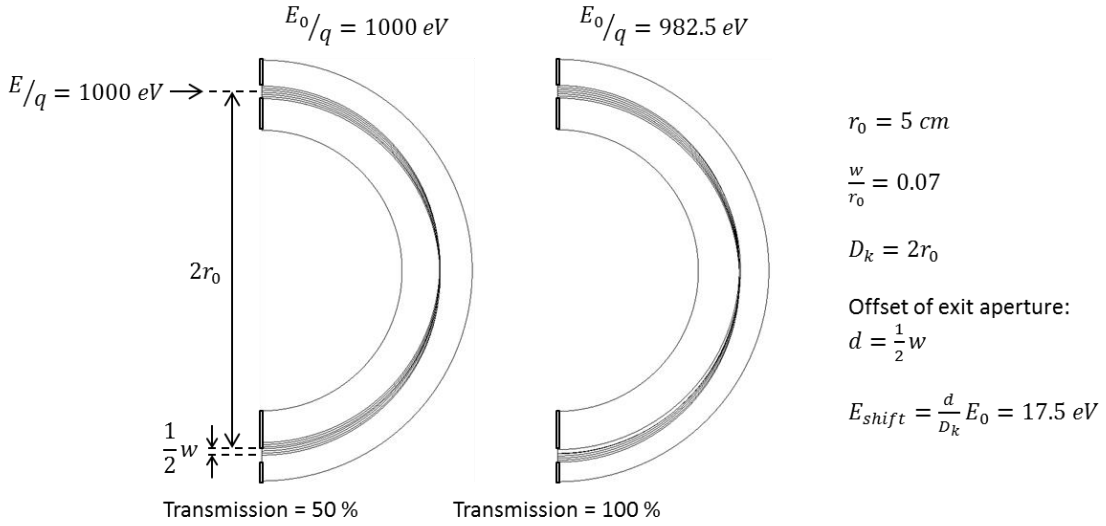

Figure 31. Example of aperture misalignment showing a shift in transmission for a SDA. The ESA indicates lower energy ions at 100% transmission due to the exit aperture being located at $r_0 + \frac{1}{2}w$ instead of r_0.

C. Contamination

Probe surface contamination can present a problem by charging portions of the electrodes to non-uniform potentials or creating insulating surfaces. Contamination can be from films or adsorbates adhering to the electrode surfaces that cause non-uniform surface potentials. These insulating films can be caused by bombarding ion or electron beams (Roy and Carette, Electron Spectroscopy for Surface Analysis 1977) (Petit-Clerc and Carette 1968). Non-uniform surface potentials can also be caused by a non-uniform polycrystalline structure of the electrode material and from unevenness of an applied surface coating (Amatucci, W.E., et al. 2001). These contaminations can affect the work function and secondary electron emission coefficients from the electrodes.

A common solution to reduce probe contamination is to heat (bake-out) the analyzer in vacuum. This is commonly done for other plasma probes such as Langmuir probes. A bake-out can be done by indirect heating of the surfaces using heaters, or by biasing the electrodes positive and/or negative to collect plasma species. The surfaces can be biased positive to collect electron current to heat the electrodes as well as negative for ion sputter cleaning (Thomas and Battle 1970). Hysteresis and repeatability tests are often performed to check for contamination, and pulsing and other cleaning methods are employed to prevent contamination buildup and probe charging while recording data (Szuszczewicz and Holmes 1975) (Oyama and Hirao 1976). Similar techniques can be employed for ESAs when contamination effects are suspected.

D. Secondary Electron Emission and Detectors

Another consideration is reflected and secondary electron (or Auger) emission from the electrons and ions striking the metal electrodes of the analyzer (Wuest, Evans and Steiger 2007). Roy and Carette (Roy and Carette, Electron Spectroscopy for Surface Analysis 1977) illustrate that a good electrode material will minimize the secondary electron emission yield, surface potential variation, surface property changes due to gas adsorption and baking, and residual magnetic fields. For electron spectrometers, they suggest molybdenum as a good electrode material. Other common materials are gold, stainless steel, steel, and copper. Electrode coatings are platinum black, soot, graphite, and electron velvet (Marmet and Kerwin 1960).

When using an electrode plate or Faraday cup style detector, the elimination of reflected and secondary electron loss is especially desired at the collector surface of the analyzer. Loss of reflected and secondary electrons is a problem because electrons that leave the collector will reduce the indicated electron current or increase the indicated ion current, depending on whether electrons or ions are being measured. When measuring ions, secondary electron emission increases the measured current because an electron leaving the collector appears like an ion arriving.

In addition to choosing materials with low secondary electron yields, the analyzer can be designed with a biased suppressor plate in front of the collector. For example, the combination of the negative bias on the body and the positive bias on the Faraday collector disk serves to eliminate secondary (or Auger) electron emission from the collector. The secondary electrons that are generated from ions striking the collector disk will return back to the collector due to the adverse potential gradient created between the body and the collector disk. However, in this example, some secondary electron current generated at the suppressor plate would be directed toward the collector.

Other detectors that are used to measure low fluxes of ions and electrons include channel electron multipliers, microchannel plates, and solid-state or scintillation detectors. A review report edited by Wuest, Evans, and Steiger, provides a comprehensive overview of different types of detectors and their associated advantages, drawbacks, and sources of error and uncertainty (Wuest, Evans and Steiger 2007). The detection efficiency can depend on the incidence angle, energy, and mass of the incoming particle and the response of the detectors change with time and contamination. For space instruments, the effects of ultraviolet radiation are also considered for possible errors and changes with exposure over time.

E. Stray electric and magnetic fields

For best measurement accuracy, it is desirable to shield out unwanted electric and magnetic fields. To shield out magnetic fields that may be present near the experiment, two methods are used. The first is to place the analyzer inside a set of Helmholtz coils; the second is to enclose the analyzer within a high-permeability magnetic shield (Roy and Carette, Electron Spectroscopy for Surface Analysis 1977). The high-permeability metal is often called Mu-metal (Wadey 1956). To shield out stray electric fields, the analyzer is placed within a metal box. The electrodes are also shielded from insulators which can build up charges on their surfaces.

In addition to shielding of the ESA, effective shielding of the detection equipment and electrical lines is recommended. This includes ensuring a proper ground reference in a laboratory setting for voltage references and reducing electrical noise (Wuest, Evans and Steiger 2007).

F. Effect of Sweep Speed

If the voltage is continuously swept over a voltage range while measuring the collected current, the transmission function may be affected by the detection system time constant (Rudd, Low Energy Electron Spectrometry 1972). In this case, if the time constant of the detection system is known, it is possible to correct for changes in the transmission function height, shift in energy, and the increase in FWHM. A practical solution is to reduce either the time constant or the voltage sweep speed until the transmission function reaches steady state.

G. Space Charge Effects

An unneutralized charged particle beam which consists of positively or negatively charged particles creates its own electric field that pushes the beam both in the axial direction (z direction) and outward in the radial direction (x-y plane). The self-induced force on the particles within the beam is called space charge repulsion. Since the charged particle beam also affects the local potential, the beam shape and density may need to be accounted for along with the electrode potentials if the current density is high. Significant ion beam spreading can lead to overestimation of the energy spread of the ion beam (Green 1970).

The effect of space charge can be approximated for the simplified case of a circular beam with uniform current density over the entire cross section (Hutter 1967). The radial velocity of any charged particle is proportional to its distance from the central axis. A laminar beam is assumed wherein particle trajectories don't cross and particles at the outer radius of the beam determine the beam edge. This simplified beam is shown in Figure 32.

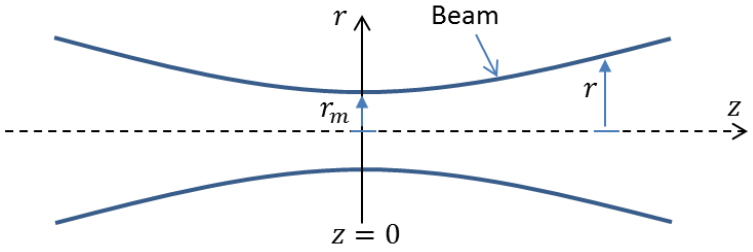

Figure 32. Illustration of beam expansion due to space charge. A converging, laminar, circular, and uniform current density beam is shown that reaches a minimum radius r_m at $z = 0$.

Generally, the radial force due to space charge is greater than the axial force, although both forces can be taken into account. If the axial force is neglected, as when the beam passes through a drift region, the size of the beam radius is described by equation (34), the universal beam spreading curve (Hutter 1967) (Wilson and Brewer 1973). Non-relativistic velocities are assumed. The minimum beam radius is r_m and occurs at position $z = 0$. R_B is the ratio of the beam radius at a distance z to the minimum beam radius r_m. A factor called the perveance P is defined as the beam current J divided by the voltage of the beam to the 3/2 power. The mass m is the mass of either an electron or an ion.

$$\int_1^{R_B} \frac{dR_B}{\sqrt{\ln R_B}} = \frac{z}{r_m}\left(\frac{1}{2^{3/2}\pi\varepsilon_0}\sqrt{\frac{m}{e}}P\right)^{1/2} \tag{34}$$

$$R_B = \frac{r}{r_m} \tag{35}$$

$$P = \frac{J}{V^{3/2}} \tag{36}$$

This equation relates the change in the radius of the beam with distance z for given values of beam current and beam voltage. For an ESA, this equation can be used as a rough approximation to how a beam might spread as it travels through the probe, noting that inside the ESA the optic axis is actually curved and the beam is not laminar as in the idealized case of equation (34).

As an example, consider a circular entrance slit illuminated by a $1000\,eV$ xenon ion beam ($m_{xenon} = 2.18x10^{-25}\,kg$) at a current density of $0.1\ mA/cm^2$. For an ESA orifice radius of $0.5\,mm$ and beam path length $z = 15\ cm$, equation (34) can be solved for $R_B = 6.1$. The beam would expand from a 1 mm diameter beam to a 6.1 mm diameter beam over a 15 cm distance. Since the analyzer path length is constant, the expansion of the beam could be reduced by decreasing the current density or increasing the beam voltage. For an electron beam at the same conditions ($m_e = 9.11x10^{-31}\,kg$), $R_B = 1.02$ meaning the beam has nearly the same entrance and exit diameter.

H. CEX Facility effects on measurements

The total flux of charged particles passing to the analyzer collector is affected by scattering and charge exchange collisions with background particles. These processes occur in the regions between the plasma plume and the analyzer as well as within the analyzer itself. A detailed description of scattering and charge exchange is beyond the scope of this guide but an overview can be found in Goebel and Katz for electric propulsion applications (Goebel and Katz 2008).

An initial current J_0 of charged particles will be attenuated as a function of the distance travelled (z) and the mean free path (λ) according to equation (37). The mean free path (λ) is the average distance travelled by a moving particle between successive impacts.

$$J(x) = J_0 e^{\left(\frac{-z}{\lambda}\right)} \tag{37}$$

Equation (38) gives the collisional mean free path for a fast moving particle relative to a stationary (or very slow moving) group of particles of density (n) and cross section (σ). The particle density can be calculated from the pressure inside the vacuum chamber or the pressure inside the ESA for instance. The cross section depends on the type of background particles and the collisional process (scattering, charge exchange, ionization, excitation, or a combination).

$$\lambda = \frac{1}{n\sigma} \tag{38}$$

A mean free path equal to the distance travelled ($\lambda = z$) would attenuate the charged particle beam to 37% of its initial value. A mean free path equal to three times the distance ($\lambda = 3z$) would allow 72% of the initial beam to be undisturbed by the background particles. From this, we can see that lower background pressures are desired.

As an example, consider scattering collisions between fast moving xenon ions and background xenon atoms. The atomic radius of the xenon atom $r_a = 0.108\,nm$ gives a collisional cross section of $1.47x10^{-19}\,m^2$ according to equation (39) for the same colliding atoms.

$$\begin{aligned} \sigma &= \pi(2r_a)^2 \quad \text{(same atoms)} \\ \sigma &= \pi(r_a + r_b)^2 \quad \text{(different atoms)} \end{aligned} \tag{39}$$

Assuming a uniform vacuum chamber pressure of $P = 1.0x10^{-4}\,torr$ and neutral xenon atom temperature of $T = 300\,K$ gives a particle density of $n = 3.2x10^{18}\,\frac{particles}{m^3}$ according to equation (40) (Goebel and Katz 2008).

$$\begin{aligned} n &= \frac{P}{k_B T} \quad (P\ in\ Pascal, T\ in\ Kelvin) \\ n &= 9.65x10^{24}\frac{P}{T} \quad (P\ in\ torr, T\ in\ Kelvin) \end{aligned} \tag{40}$$

The result is a collisional mean free path of $\lambda = 2.1\,m$, which is likely on the order of the total path length distance between the plasma source and the analyzer detector. Decreasing the pressure to $P = 1.0x10^{-5}\,torr$ would increase the mean free path to $\lambda = 21\,m$. For a path length $z = 2\,m$, 91% of the beam current would be transmitted.

X. Conclusion

ESAs are one type of diagnostic used to measure the energy per unit charge E/q distribution of ion and electron beams. A discussion of the fundamental types of electrostatic analyzers was presented, including mirror-type and deflector-type analyzers. The pass energy (transmission energy) of an ESA is determined by the voltage potentials applied to the electrodes and the analyzer constant, which depends on its geometry. The procedure for energy resolution calculations of ESAs was described, which is a common way of comparing analyzers. A follow on guide is planned that will describe recommended practices for the use of ESAs.

The commonly used spherical deflector (SDA) analyzer was addressed in detail. Example data was given for simple ion beams with ideal analyzer properties. Ion beam trajectories and distributions modeled using SIMION and ANSYS Multiphysics software compared closely with those given by energy resolution equations. ESAs used in the laboratory and on space missions can be similarly modeled to make comparisons between predicted and experimentally observed resolutions.

Appendix A: Additional References for ESAs

This section lists references in addition to those of the main text. Many papers are categorized according to their specificity to a particular topic or analyzer, though they may have broader applicability.

References on All Analyzer Types and Transmission Functions

The following are particularly good general references for the most widely used analyzers.

- Wollnik – Focusing of Charged Particles (H. Wollnik 1967) Curved plate analyzer designs.
- Rudd – Low Energy Electron Spectroscopy (Rudd, Low Energy Electron Spectrometry 1972) Curved plate and mirror-type analyzers, including electrical biasing setup.
- Steckelmacher – "Energy analysers for charged particle beams" (Steckelmacher 1973) Curved plate and mirror-type analyzers.
- Roy and Carette – Electron Spectroscopy for Surface Analysis (Roy and Carette, Electron Spectroscopy for Surface Analysis 1977) Curved plate and mirror-type analyzers with energy resolution equations.
- Roy and Tremblay – "Design of electron spectrometers" (Roy and Tremblay, Design of electron spectrometers 1990) Curved plate and mirror-type analyzers with energy resolution equations.
- Pfaff, Borovsky and Young, Editors – Measurement Techniques in Space Plasmas – Particles (Pfaff, Borovsky and Young 1998) Space measurement techniques with example electrostatic analyzers.
- Wuest, Evans and Steiger, Editors – "Calibration of Particle Instruments in Space Physics" (Wuest, Evans and Steiger 2007) Curved plate analyzers, geometrical factors, detectors, and calibration.
- Moore, et al.: Building Scientific Apparatus (Moore, et al. 2009) Curved plate and mirror-type analyzers with energy resolution equations.
- Yavor – Advances in Imaging and Electron Physics (M. Yavor 2009) Especially chapters 2 and 6. Curved plate and mirror-type analyzers with energy resolution equations.

See also: (SarEl, Criterion for Comparing Analyzers 1970), (Roy and Carette, Improvement of the Resolving Power and Transmission of Electrostatic Spectrometers 1971), (Roy and Carette, Spectrometres Electrostatiques. Partie III 1971), (Dube and Roy, A Generalized Approach for the Determination of Transmission Functions of Charged-Particle Energy Analyzers 1982), (Leckey 1987)

Parallel Plate Analyzer (PMA) References

More information on parallel plate analyzers, especially for entrance angles other than $\alpha = 30°, 45°$ can be found in:

(Yarnold and Bolton 1949), (Harrower 1955), (Hutchison 1956), (Rudd, Analog Plotting System for Recording Energy Spectra of Low Energy Charged Particles 1966), (Green, T.S. and Proca 1970), (Proca and Green 1970), (Risley, Magnetic Field Measurements Using an Electron Beam and an Electrostatic Analyzer 1971), (Schmitz and Melhorn 1972), (Roy and Carette, Electron Spectroscopy for Surface Analysis 1977), (Kuypers and Hopman 1988), (de Zeeuw, et al. 1991), (Hamada, et al. 1994), (Gaus, et al. 1994), (King 1998), (Hofer, Haas and Gallimore 1999), (Beal and Gallimore, Energy Analysis of a Hall Thruster Cluster 2003), (C. Enloe 2003), (Beal, Clustering of Hall effect thrusters for high-power electric propulsion applications 2004)

Cylindrical Mirror Analyzer (CMA) References

(Blauth 1957), (Sar-El, Cylindrical Capacitor as an Analyzer I. Nonrelativistic Part 1967), (Hafner, Simpson and Kuyatt 1968), (Aksela, Karras, et al. 1970), (SarEl, Cylindrical Mirror Analyzer with Surface Entrance and Exit Slots. I. Nonrelativistic Part 1971), (Aksela, Instrument Function of a Cylindrical Electron Energy Analyzer 1972), (Risley, Design Parameters for the Cylindrical Mirror Energy Analyzer 1972), (Wang 1972), (Renfro and Fischbeck 1975), (L. Frank 1976), (McIlroy, et al. 1995), (Grzelakowski, Man and Altman 2001), (Read, The parallel cylindrical mirror electron energy analyzer 2002), (Ilyin, New class ofelectrostatic energy analyzers with a cylindrical face-field 2003), (Read, Cubric, et al. 2004), (Ilyin and Ilyina, New electrostatic energy analysers with a bounded cylindrical field 2005), (Ilyin and Ilyina, An electrostatic face-field energy analyser for space and plasma measurements 2007), (Rubio-Zuazo, Escher, et al. 2010), (Rubio-Zuazo and Castro, First principle study of the properties of a Cylindrical Sector Analyzer: Complete calculation of the electron trajectory 2011)

Spherical Mirror Analyzer (SMA) References

(Ritchie, Cheka and Birkhoff 1960), (Sar-El, More on the spherical condenser as an analyzer I. Nonrelativistic Part 1966), (Daimon 1988)

Curved Plate Analyzer (CPA) / Toroidal Geometry References

(Ewald and Liebl 1955), (Matsuo, Matsuda and Wollnik 1972), (Wollnik, Matsuo and Matsuda 1972), (Decreau, Prange and Berthelier 1975), (Young, Ghielmetti, et al. 1987), (Young, Bame, et al. 1988), (Liebl 1990), (E. Mobius 1998), (Siggel-King, et al. 2004)

Cylindrical Deflector Analyzer (CDA) References

(Hughes and McMillen, Re-Focussing of Electron Paths in a Radial Electrostatic Field 1929), (Hughes and Rojansky, On the Analysis of Electronic Velocities by Electrostatic Means 1929), (Warren, Powell and Herb 1947), (Matsuda, Electrostatic Analyzer with Variable Focal Length 1961), (Theodoridis and Paolini, Charged Particle Transmission through Cylindrical Plate Electrostatic Analyzers 1968), (Roy and Carette, Optimum Deflection Angle for Cylindrical and Spherical Electrostatic Spectrometer 1970), (Leventhal and North 1971), (Roy and Carette, Methods of Measuring the Performance of an Electrostatic Spectrometer 1971), (Bolduc, De Celles and Baril 1972), (Johnstone, The Geometric Factor of a Cylindrical Plate Electrostatic Analyzer 1972), (Bryce, Dalglish and Kelly 1973), (Arnow 1976), (Dube, Roy and Ballu, New approach to improve performances of electron spectrometers 1981), (Oshima, Franchy and Ibach, Numerical calculations of electron trajectories in the 127° analyzer using a position-sensitive detector under conditions of fringing fields 1983), (Oshima, Souda, et al. 1985), (Stroscio and Ho 1986), (O'Connor 1987), (Fishkova and Ovsyannikova 1995), (Dallaqua, et al. 2003), (Kreckel, et al. 2010)

Spherical Deflector Analyzer (SDA) References

(Purcell 1938), (Browne, Craig and Williamson 1951), (Rogers 1951), (Simpson, Design of Retarding Field Energy Analyzers 1961), (Simpson, High Resolution, Low Energy Electron Spectrometer 1964), (Kuyatt and Simpson 1967), (Paolini and Theodoridis 1967), (Hafner, Simpson and Kuyatt 1968), (Theodoridis and Paolini, The Angular Response of Spherical Plate Electrostatic Analyzers 1969), (Roy and Carette, Optimum Deflection Angle for Cylindrical and Spherical Electrostatic Spectrometer 1970), (Smith and Day 1971), (Chase 1973), (Moestue 1973), (Basto, Raitt and Sojka 1976), (Imhof, Adams and King 1976), (Polaschegg 1976), (Gosling, et al. 1978), (Poulin and Roy 1978), (Warmack, Stockdale and Compton, Apparatus for Energy, Angle, and Mass Analysis of Products from Alkali-Molecule Reactions 1978), (Warmack, Stockdale and Compton, Ionizing collisions of cesium and potassium atoms with water 1978), (Jost, Novel design of a 'spherical' electron spectrometer 1979), (Compton, et al. 1980), (Gloeckler, The Charge-Energy-Mass Spectrometer for 0.3-300 keV/e Ions on the AMPTE CCE 1985), (Mukai and Miyake 1986), (Nishigaki and Kanai 1986), (DeSerio 1989), (Osterwalder 1989), (Coxon, et al. 1990), (Gelius 1990), (Holber and Forster 1990), (Gloeckler, The Solar Wind Ion Compostion Spectrometer 1992), (McGarity, et al. 1992), (Hirahara and Mukai 1993), (Vilppola, Tanskanen and Huomo, et al. 1996), (Gruntman 1997), (Ruan, Nguyen and Fink 1999), (Vilppola, Tanskanen and Barraclough, et al. 2001), (Zouros and Benis 2005), (Belov and Yavor, High-resolution energy analyzer for photoelectron diffraction studies 2007), (Mankey, et al. 2007), (Farnell, et al. 2009), (McComas, IBEX—Interstellar Boundary Explorer 2009), (Gershman and Zurbuchen 2010)

Top Hat-type Spherical Deflector Analyzer References

(Sablik, et al. 1988), (Carlson, McFadden, et al. 2001), (Klumpar 2001), (Victor, Zurbuchen and Gallimore, Top hat electrostatic analyzer for far-field electric propulsion plume diagnostics 2006), (Victor, Design and Utilization of a Top Hat Analyzer for Hall Thruster Plume Diagnostics 2006), (J. McFadden 2008), (Collinson, Kataria and Coates, et al. 2009) (Collinson and Kataria, On variable geometric factor systems for top-hat electrostatic space plasma analyzers 2010)

Analyzer Modification References

(Gough 1970), (Mariani 1970), (Allen, Jr., Wolfe and Schweitzer 1972), (Brewer, Newell and Smith 1980), (Smeenk, et al. 1982), (Carlson, Curtis, et al. 1983), (Hellings, et al. 1985), (Mobius, et al. 1990), (Yavor and Baranova 1990), (Yavor, et al. 1992), (Bratschi, et al. 1993), (Tokesi, Kover and Varga 1994), (Davydov, Kudinov, et al. 1995), (Downie, Reynolds and Powis 1995), (Krasnova, et al. 1995), (Trubitsyn 1995), (Varga, Tokesi and Rajta 1995), (Chornay, Hunsaker and Keller 1997), (Enloe, Agnew and Cifuentes, Novel bandpass electrostatic analyzer 1997), (Siegbahn, Kholine and Golikov 1997), (Davydov, Golikov, et al. 1998), (Belov and Yavor, Two-stage systems with intermediate beam retarding for energy and spatial analysis of photoelectrons 1999), (Belov and Yavor, New type of high-resolution high-transmission energy analyzers based on toroidal mirrors 1999), (Jacka, et al. 1999), (Belov and Yavor, High-resolution energy analyzer with a large angular acceptance for photoelectron spectromicroscopy applications 2000), (Belov and Yavor, Design of a versatile energy analyzer for photoelectron spectroscopy studies at synchrotron radiation sources 2001), (Offi, et al. 2005), (Kasahara, et al. 2006)

Fringing Field References

(Matsuda, The influence of a toroidal electric fringing field on the trajectories of charged particles in a third order approximation 1971), (Bosi 1972), (Jost, Fringing field correction for 127° and 180° electron spectrometers 1979), (Hu, Matsuo and Matsuda 1982), (Nishigaki and Kanai 1986), (Baraldi, Dhanak and King 1992), (Hu and Leung 1995), (Benis and Zouros 2000), (Sagara, et al. 2000), (Dogan, Sise and Ulu 2007), (Sise, et al. 2007)

Acknowledgments

The authors thank John Dankanich for providing financial support for travel to present this paper and direction from the AIAA Committee on Standards for Electric Propulsion Testing.

Bibliography

Aksela, S. "Instrument Function of a Cylindrical Electron Energy Analyzer." *Rev. Sci. Instrum.* 43, no. 9 (1972): 1350-1356.

Aksela, S., M. Karras, M. Pessa, and E. Suoninen. "Study of the Electron Optical Properties of an Electron Spectrograph with Coaxial Cylindrical Electrodes." *Rev. Sci. Instrum.* 41, no. 3 (1970): 351-355.

Allen, Jr., J.D., J.P. Wolfe, and G.K. Schweitzer. "A new electron spectrometer design." *International Journal of Mass Spectrometry and Ion Physics* 8, no. 1 (1972): 81-83.

Amatucci, W.E., et al. "Contamination-free sounding rocket Langmuir probe." *Rev. Sci. Instr.* 72, no. 4 (2001): 2052-2057.

Andrews, G.B., et al. "The Energetic Particle and Plasma Spectrometer Instrument on the MESSENGER Spacecraft." *Space Science Reviews* 131, no. 1-4 (2007): 523-556.

Arnoldy, R.L., P.O. Isaacson, D.F. Gats, and L.W. Choy. "The Calibration of Electrostatic Analyzers and Channel Electron Multipliers Using Laboratory Simulated Omnidirectional Electron Beams." *Rev. Sci. Instrum.* 44, no. 2 (1973): 172-177.

Arnow, M. "Electrostatic cylindrical spectrometers." *J. Phys. E: Sci. Instrum.* 9 (1976): 372-376.

Bame, S.J., D.J. McComas, D.T. Young, and R.D. Belian. "Diagnostics of space plasmas (invited)." *Rev. Sci. Instrum.* 57, no. 8 (1986): 1711-1716.

Baraldi, A., V.R. Dhanak, and G.C. King. "A fringing field corrector for the boundary between two electrostatic deflection analysers placed in tandem." *Meas. Sci. Technol.* 3 (1992): 778-779.

Basto, R.A., W.J. Raitt, and J.J. Sojka. "A High Resolution, Low Energy Electrostatic Analyser for Rocket Payloads." *Planet. Space Sci.* 24 (1976): 115–129.

Beal, B.E. "Clustering of Hall effect thrusters for high-power electric propulsion applications." *Ph.D. Dissertation.* University of Michigan, 2004.

Beal, B.E., and A.D. Gallimore. "Energy Analysis of a Hall Thruster Cluster." *28th International Electric Propulsion Conference.* Toulouse, France, 2003. IEPC-2003-035.

Belov, V.D., and M.I. Yavor. "Design of a versatile energy analyzer for photoelectron spectroscopy studies at synchrotron radiation sources." *Nuclear Instruments and Methods in Physics Research A* 470 (2001): 105-109.

Belov, V.D., and M.I. Yavor. "High-resolution energy analyzer for photoelectron diffraction studies." *Nuclear Instruments and Methods in Physics Research A* 575 (2007): 262-265.

Belov, V.D., and M.I. Yavor. "High-resolution energy analyzer with a large angular acceptance for photoelectron spectromicroscopy applications." *Rev. Sci. Instrum.* 71, no. 4 (2000): 1651-1655.

Belov, V.D., and M.I. Yavor. "New type of high-resolution high-transmission energy analyzers based on toroidal mirrors." *Journal of Electron Spectroscopy and Related Phenomena* 104 (1999): 47-54.

Belov, V.D., and M.I. Yavor. "Two-stage systems with intermediate beam retarding for energy and spatial analysis of photoelectrons." *Nuclear Instruments and Methods in Physics Research A* 427 (1999): 197-202.

Benis, E.P., and T.J.M. Zouros. "Improving the energy resolution of a hemispherical spectrograph using a paracentric entry at a non-zero potential." *Nuclear Instruments and Methods in Physics Research A* 440 (2000): 462-465.

Blauth, E. "Zur Energieverteilung der von Protonen in Gasen ausgelösten Sekundärelektronen." *Zeitschrift ftir Physik* 147, no. 2 (1957): 228-240.

Bolduc, L., M. De Celles, and M. Baril. "Motion of Charged Particles in the Normal Section of a Cylindrical Condenser." *J. Appl. Phys.* 43, no. 4 (1972): 1655-1661.

Bolton, S.J., et al. "Plasma Experiment for Planetary Exploration (PEPE)." *AIP Conf. Proc.* 387 (1997): 241-244.

Bosi, G. "Fringing Field of Electrostatic Analyzers." *Rev. Sci. Instrum.* 43, no. 3 (1972): 475-478.
Bratschi, O., A.G. Ghielmetti, E.G. Shelley, and H. Balsiger. "Experimental tests of a massangle spectrograph with poloidal ion optics." *Rev. Sci. Instrum.* 64, no. 1 (1993): 184-190.
Brewer, D.F.C., W.R. Newell, and A.C.H. Smith. "A coaxial cone electrostatic velocity analyser. I. Analysis of electron optical properties." *J. Phys. E: Sci. Instrum.* 13 (1980): 114-122.
Bridge, H.S., et al. "Observations at Venus Encounter by the Plasma Science Experiment on Mariner 10." *Science* 183, no. 4131 (1974): 1293-1296.
Browne, C.P., D.S. Craig, and R.M. Williamson. "Spherical Electrostatic Analyzer for Measurement of Nuclear Reaction Energies." *Rev. Sci. Instrum.* 22, no. 12 (1951): 952-965.
Bryce, P., R.L. Dalglish, and J.C. Kelly. "The 127° Electrostatic Analyzer: Performance as a Spectrometer." *Can. J. Phys.* 51, no. 5 (1973): 574-586.
Carlson, C.W., D.W. Curtis, G. Paschmann, and W. Michael. "An Instrument for Rapidly Measuring Plasma Distribution Functions with High Resolution." *Advances in Space Research* 2, no. 7 (1983): 67-70.
Carlson, C.W., J.P. McFadden, P. Turin, D.W. Curtis, and A. Magoncelli. "The Electron and Ion Plasma Experiment for FAST." *Space Science Reviews* (Kluwer Academic Publishers) 98 (2001): 33-66.
Chase, L.M. "The Geometrical Factor of Large Aperture Hemispherical Electrostatic Analyzers." *Rev. Sci. Instrum.* 44, no. 8 (1973): 998-1002.
Chornay, D.J., F.H. Hunsaker, and J.W. Keller. "Evaluation of an elliptical grid mirror electrostatic analyzer for space applications." *Rev. Sci. Instrum.* 68, no. 3 (1997): 1604-1608.
Collinson, G.A., and D.O. Kataria. "On variable geometric factor systems for top-hat electrostatic space plasma analyzers." *Meas. Sci. Technol.* 21 (2010): 105903.
Collinson, G.A., et al. "Electron optical study of the Venus Express ASPERA-4 Electron Spectrometer (ELS) top-hat electrostatic analyser." *Meas. Sci. Technol.* (IOP PUBLISHING), 2009: 1-8.
Collinson, G.A., et al. "The geometric factor of electrostatic plasma analyzers: A case study from the Fast Plasma Investigation for the Magnetospheric Multiscale mission." *Rev. Sci. Instr.* 83, no. 3 (2012): 03303.
Compton, R.N., J.C. Miller, A.E. Carter, and P. Kruit. "Resonantly Enchanced Multiphoton Ionization of Xenon: Photoelectron Energy Analysis." *Chemical Physics Letters* 71, no. 1 (1980): 87-90.
Coxon, P., J. Krizek, M. Humpherson, and I.R.M. Wardell. "Escascope - a new imaging photoelectron spectrometer." *Journal of Electron Spectroscopy and Related Phenomena* 52 (1990): 821-36.
Dahl, D.A. "SIMION for the personal computer in reflection." *International Journal of Mass Spectrometry* 200, no. 1-3 (2000): 3-25.
Daimon, H. "New displaytype analyzer for the energy and the angular distribution of charged particles." *Rev. Sci. Instrum.* 59, no. 4 (1988): 545-549.
Dallaqua, R.S., I.H. Tan, M.V. Alves, and E. del Bosco. "Development of an Electrostatic Energy Analyzer (ESA) for the EQUARS Scientific Satellite." *NASA STAR report INPE-9603-NTC352* 41, no. 10 (2003).
Davydov, S.N., Yu.A. Kudinov, Yu.K. Golikov, and V.V. Korablev. "High-resolution electron energy analyser for angle-resolved spectroscopy." *Journal of Electron Spectroscopy and Related Phenomena* 72 (1995): 317-321.
Davydov, S.N., Yu.K. Golikov, S.N. Romanov, and N.K. Krasnova. "Cone electrostatic energy analyser of high luminosity." *Journal of Electron Spectroscopy and Related Phenomena* 97 (1998): 209-214.
de Zeeuw, W.A., H.W. van der Ven, J.M.M. de Wit, and J.H. Donne. "An electrostatic timeofflight analyzer for simultaneous energy and mass determination of neutral particles." *Rev. Sci. Instrum.* 62, no. 1 (1991): 110-117.
Decreau, P., R. Prange, and J.J. Berthelier. "Optimization of toroidal electrostatic analyzers for measurements of low energy particles in space." *Rev. Sci. Instrum.* 46, no. 8 (1975): 995-1007.
DeSerio, R. "Spherical sector electrostatic analyzers for measurements of energy and angular distributions." *Rev. Sci. Instrum.* 60, no. 3 (1989): 381-388.
Dogan, M., O. Sise, and M. Ulu. "Design of electron energy analyzers for electron impact studies." *Radiation Physics and Chemistry* 76 (2007): 445-449.
Downie, P., D.J. Reynolds, and I. Powis. "Parallel, multichannel energy and angle resolving electrostatic electron analyzer." *Rev. Sci. Instrum.* 66, no. 7 (1995): 3807-3818.
Dube, D., and D. Roy. "A Generalized Approach for the Determination of Transmission Functions of Charged-Particle Energy Analyzers." *Nuclear Instruments and Methods* (North-Holland Publishing Company) 201 (1982): 291-301.

Dube, D., D. Roy, and Y. Ballu. "New approach to improve performances of electron spectrometers." *Rev. Sci. Instrum.* 52, no. 10 (1981): 1497-1500.
Dubouloz, N., et al. "Thermal ion measurements on board Interball Auroral Probe by the Hyperboloid experiment." *Ann. Geophysicae* 16 (1998): 1070-1085.
Enloe, C.L., and J.R. Shell. "Optimizing the energy resolution of planar retarding potential analyzers." *Rev. Sci. Instrum.* 63, no. 2 (1992): 1788-1791.
Enloe, C.L., et al. "Miniaturized electrostatic analyzer manufactured using photolithographic." *Rev. Sci. Instrum.* 74, no. 3 (2003): 1192-1195.
Enloe, C.L., K.A. Agnew, and A.F. Cifuentes. "Novel bandpass electrostatic analyzer." *Rev. Sci. Instrum.* 68, no. 5 (1997): 2023-2026.
Ewald, H., and H. Liebl. "Der Astigmatismus des Toroidkondensators." *Zeitschrift Naturforschung Teil A* 10 (1955): 872.
Farnell, C.C., D.L. Brown, G. Willis, R. Branam, and J.D. Williams. "Remote Diagnostic Measurements of Hall Thruster Plumes." *31st International Electric Propulsion Conference.* University of Michigan, USA, 2009. IEPC-2009-031.
Fishkova, T.Ya., and L.P. Ovsyannikova. "Cylindrical deflector focusing in two directions." *Nuclear Instruments and Methods in Physics Research A* 363 (1995): 494-496.
Frank, L. A. "On the Extraterrestrial Ring Current During Geomagnetic Storms." *J. Geophys. Res.* 72, no. 15 (1967): 3753-3767.
Frank, L. "Note on the design of the cylindrical mirror energy analyser." *J. Phys. E: Sci. Instrum.* 9 (1976): 670-672.
Frank, L.A., K.L. Ackerson, J.A. Lee, M.R. English, and G.L. Pickett. "The plasma instrumentation for the Galileo Mission." *Space Science Reviews* 60, no. 1-4 (1992): 283-304.
Funsten, H.O., R.W. Harper, and D.J. McComas. "Absolute detection efficiency of space-based ion mass spectrometers and neutral atom imagers." *Rev. Sci. Instrum.* 76 (2005): 053301.
Gaus, A.D., W.T. Htwe, J.A. Brand, T.J. Gay, and M. Schulz. "Energy spread and ion current measurements of several ion sources." *Rev. Sci. Instrum.* 65, no. 12 (1994): 3739-3745.
Gelius, U., et al. "A new ESCA instrument with improved surface sensitivity, fast imaging properties and excellent energy resolution." *Journal of Electron Spectroscopy and Related Phenomena* 52 (1990): 747-785.
Gershman, D.J., and T.H. Zurbuchen. "Modeling extreme ultraviolet suppression of electrostatic analyzers." *Rev. Sci. Instrum.* 81 (2010): 045111.
Gloeckler, G., et al. "The Charge-Energy-Mass Spectrometer for 0.3-300 keV/e Ions on the AMPTE CCE." *IEEE Transactions on Geoscience and Remote Sensing* GE-23, no. 3 (1985): 234-240.
Gloeckler, G., et al. "The Solar Wind Ion Compostion Spectrometer." *Astron. Astrophys. Suppl. Ser.* 92, no. 2 (1992): 267-289.
Goebel, D.M., and I. Katz. *Fundamentals of Electric Propulsion: Ion and Hall Thrusters.* Jet Propulsion Laboratory, California Institute of Technology: JPL Space Science and Technology Series, 2008.
Gosling, J.T., J.R. Asbridge, S.J. Bame, and W.C. Feldman. "Effects of a long entrance aperture upon the azimuthal response of spherical section electrostatic analyzers." *Rev. Sci. Instrum.* 49, no. 9 (1978): 1260-1268.
Gough, M.P. "An annular curved plate analyser with large geometrical factor and high resolution." *J. Phys. E: Sci. Instrum.* 3 (1970): 332-333.
Green, T.S. "Space charge effects in plasma particle analyzers." *Plasma Phys.* 12 (1970): 877-883.
Green, T.S., and G.A. Proca. "A Parallel Plate Electrostatic Spectrograph." *Rev. Sci. Instrum.* 41, no. 10 (1970): 1409-1414.
Gruntman, M. "Energetic neutral atom imaging of space plasmas." *Rev. Sci. Instrum.* 68, no. 10 (1997): 3617-3656.
Grzelakowski, K., K.L. Man, and M.S. Altman. "The miniature cylindrical mirror analyzer: A new tool for surface analysis." *Rev. Sci. Instrum.* 72, no. 8 (2001): 3362-3365.
Hafner, H., J.A. Simpson, and C.E. Kuyatt. "Comparison of the Spherical Deflector and the Cylindrical Mirror Analyzers." *Rev. Sci. Instrum.* 39, no. 1 (1968): 33-35.
Hamada, Y., Y. Kawasumi, H. Iguchi, A. Fujisawa, Y. Abe, and M. Takahashi. "Mesh effect in a parallelplate analyzer." *Rev. Sci. Instrum.* 65, no. 5 (1994): 1606-1612.
Hardy, D.A., et al. "Low Energy Plasma Analyzer." *IEEE Transactions on Nuclear Science* 40, no. 2 (1993): 246-251.
Harrower, G.A. "Measurement of Electron Energies by Deflection in a Uniform Electric Field." *Rev. Sci. Instrum.* 26, no. 9 (1955): 850-854.

Hellings, G.J.A., H. Ottevanger, S.W. Boelens, C.L.C.M. Knibbeler, and H.H. Brongersma. "A simultaneous energy and angle resolved ion scattering spectrometer." *Surface Science* 162 (1985): 913-920.

Hirahara, M., and T. Mukai. "Satellite borne energetic ion mass spectrometer for three-dimensional measurement of velocity distribution." *Rev. Sci. Instrum.* 64, no. 2 (1993): 406-419.

Hofer, R.R., J.M. Haas, and A.D. Gallimore. "Development of a 45-Degree Parallel-Plate Electrostatic Energy Analyzer for Hall Thruster Plume Studies: Preliminary Data." *26th International Electric Propulsion Conference.* Kitakyushu, Japan, 1999. IEPC 99-113.

Holber, W.M., and J. Forster. "Ion energetics in electron cyclotron resonance discharges." *J. Vac. Sci. Technol. A* 8, no. 5 (1990): 3720-3725.

Hu, D.Q., and K.T. Leung. "SIMION study of the fringing field effects in deflectortype electrostatic electron energy analyzers: A new flexible Jost-based correction scheme." *Rev. Sci. Instrum.* 66, no. 4 (1995): 2865-2870.

Hu, Z.H., T. Matsuo, and H. Matsuda. "Numerical calculation of fringing—field integrals for arbitrary electrode (magnetic pole) structures." *International Journal of Mass Spectrometry and Ion Physics* 42, no. 3 (1982): 145-155.

Hughes, A.Ll., and J.H. McMillen. "Re-Focussing of Electron Paths in a Radial Electrostatic Field." *Physical Review* 34, no. 2 (1929): 291-295.

Hughes, A.Ll., and V. Rojansky. "On the Analysis of Electronic Velocities by Electrostatic Means." *Physical Review* 34, no. 2 (1929): 284-290.

Hutchison, D.A. "Critical Ionization Potentials Using a ParallelPlate Energy Selector." *J. Chem. Phys.* 24 (1956): 628-629.

Hutter, Rudolf. "Chapter 3.1 Beams with Space-Charge." In *Focusing of Charged Particles*, edited by Albert Septier, 3-22. New York: Academic Press, 1967.

Ilyin, A.M. "New class ofelectrostatic energy analyzers with a cylindrical face-field." *Nuclear Instruments and Methods in Physics Research A* 500 (2003): 62-67.

Ilyin, A.M., and I.A. Ilyina. "An electrostatic face-field energy analyser for space and plasma measurements." *Meas. Sci. Technol.* 18 (2007): 724-726.

Ilyin, A.M., and I.A. Ilyina. "New electrostatic energy analysers with a bounded cylindrical field." *Meas. Sci. Technol.* 16 (2005): 1798-1801.

Imhof, R.E., A. Adams, and G.C. King. "Energy and time resolution of the 180° hemispherical electrostatic analyzer." *J. Phys. E: Sci. Instrum.* 9 (1976): 138-142.

Jacka, M., M. Kirk, M.M. El Gomati, and M. Prutton. "A fast, parallel acquisition, electron energy analyzer: The hyperbolic field analyzer." *Rev. Sci. Instrum.* 70, no. 5 (1999): 2282-2287.

Jahn, R.G., and E.Y. Choueiri. "Electric Propulsion." *Encyclopedia of Physical Science and Technology.* Vol. 5. Academic Press, 2002.

Johnstone, A.D. "The Geometric Factor of a Cylindrical Plate Electrostatic Analyzer." *Rev. Sci. Instrum.* 43, no. 7 (1972): 1030-1040.

Johnstone, A.D., et al. "PEACE: A Plasma Electron and Current Experiment." *Space Science Reviews* 79, no. 1-2 (1997): 351-398.

Johnstone, A.D., et al. "The Giotto three-dimensional positive ion analyser." *J. Phys. E: Sci. Instrum.* 20, no. 6 (1985): 795-805.

Jost, K. "Fringing field correction for 127° and 180° electron spectrometers." *J. Phys. E: Sci. Instrum.* 12 (1979): 1001-1005.

Jost, K. "Novel design of a 'spherical' electron spectrometer." *J. Phys. E: Sci. Instrum.* 12 (1979): 1006-1012.

JPL. *Scientific Experiments for Ranger 1 and 2.* NASA Technical Report 32-55, Pasadena, CA: JPL California Institute of Technology, 1961.

Kasahara, S., K. Asamura, Y. Saito, T. Takashima, and M. Hirahara. "Cusp type electrostatic analyzer for measurements of medium energy charged particles." *Rev. Sci. Instrum.* 77 (2006): 123303.

King, L.B. "Transport-Property and Mass Spectral Measurements in the Plasma Exhaust Plume of a Hall-Effect Space Propulsion System." *Ph.D. Dissertation.* University of Michigan, 1998.

Klumpar, D.M., et al. "The Time-of-Flight Energy, Angle, Mass Spectrograph (TEAMS) Experiment for FAST." *Space Science Reviews* (Kluwer Academic Publishers), 2001: 197-219.

Krasnova, N.K., S.N. Davydov, Yu.K. Golikov, V.V. Korablev, and Yu.A. Kudinov. "Cone electrostatic energy analyser, used for concurrent energy- and angle-resolved measurements." *Journal of Electron Spectroscopy and Related Phenomena* 72 (1995): 323-326.

Kreckel, H., et al. "A simple double-focusing electrostatic ion beam deflector." *Rev. Sci. Instrum.* 81 (2010): 063304.

Kuyatt, C.E., and J.A. Simpson. "Electron Monochromator Design." *Rev. Sci. Instrum.* 38, no. 1 (1967): 103-111.

Kuypers, A.D., and H.J. Hopman. "Ion energy measurement at the powered electrode in an rf discharge." *J. Appl. Phys.* 63, no. 6 (1988): 1894-1898.

Leckey, R.C.G. "Recent Developments in Electron Energy Analyzers." *Journal of Electron Spectroscopy and Related Phenomena* (Elsevier Science Publishers B.V., Amsterdam) 43, no. 3 (1987): 183-214.

Leventhal, J.J., and G.R. North. "Study of Calibration, Resolution, and Transmission of Electrostatic Velocity Selector." *Rev. Sci. Instrum.* 42, no. 1 (1971): 120-123.

Liebl, H. "Stigmatic sector-field energy analyzer without second-order angular image aberrations." *Nuclear Instruments and Methods in Physics Research A* 292, no. 3 (1990): 537-540.

Mankey, G.J., S.A. Morton, J.G. Tobin, S.W. Yu, and G.D. Waddill. "A spin- and angle-resolved photoelectron spectrometer." *Nuclear Instruments and Methods in Physics Research A* 582 (2007): 165-167.

Mariani, F. "An Electrostatic Analyzer with No Fringe Field for Measurements of Low Energy Particles on Space Vehicles." *Rev. Sci. Instrum.* 41, no. 6 (1970): 807-812.

Marmet, P., and L. Kerwin. "An Improved Electrostatic Electron Selector." *Can. J. Phys.* 38, no. 6 (1960): 787-796.

Matsuda, H. "Electrostatic Analyzer with Variable Focal Length." *Rev. Sci. Instrum.* 32, no. 7 (1961): 850-852.

Matsuda, H. "The influence of a toroidal electric fringing field on the trajectories of charged particles in a third order approximation." *Nuclear Instruments and Methods* 91 (1971): 637-647.

Matsuo, T., H. Matsuda, and H. Wollnik. "Particle trajectories in a toroidal condenser calculated in a third order approximation." *Nuclear Instruments and Methods* 103, no. 3 (1972): 515-532.

McComas, D., et al. "The Solar Wind Around Pluto (SWAP) Instrument Aboard New Horizons." *Space Sci.Rev.* 140 (2007): 261-313.

McComas, D.J., et al. "IBEX—Interstellar Boundary Explorer." *Space Sci Rev* 146 (2009): 11-33.

McFadden, J.P., and C.W. Carlson. "Computer Simulation in Designing Electrostatic Optics for Space Plasma Experiments." In *Measurement Techniques in Space Plasmas: Particles*, edited by R.F. Pfaff, J.E. Borovsky and D.T. Young, 249-255. Washington, D.C.: American Geophysical Union, 1998.

McFadden, J.P., et al. "The THEMIS ESA Plasma Instrument and In-flight Calibration." *Space Sci Rev* 141, no. 1-4 (2008): 277-302.

McGarity, J.O., A. Huber, J. Pantazis, M.R. Oberhardt, D.A. Hardy, and W.E. Slutter. "Compact ion/electron analyzer for spaceflight or laboratory use." *Rev. Sci. Instrum.* 63, no. 3 (1992): 1973-1977.

McIlroy, D.N., P.A. Dowben, A. Knoop, and E. Ruhl. "A novel design for a small retractable cylindrical mirror analyzer." *Journal of Vacuum Science and Technology B: Microelectronics and Nanometer Structures* 13, no. 5 (1995): 2142-2144.

Mobius, E., et al. "The 3-D plasma distribution function analyzers with time-of-flight mass discrimination for cluster, FAST, and Equator-S." In *Measurement Techniques in Space Plasmas: Particles*, edited by R.F. Pfaff, J.E. Borovsky and D.T. Young, 243-248. Washington, D.C.: American Geophysical Union, 1998.

Mobius, E., P. Bochsler, A.G. Ghielmetti, and D.C. Hamilton. "High mass resolution isochronous time-of-flight spectrograph for three dimensional space plasma measurements." *Rev. Sci. Instrum.* 61, no. 11 (1990): 3609-3612.

Moestue, H. "The electric field and geometrical factor of an annular curved plate electrostatic analyzer." *Rev. Sci. Instrum.* 44, no. 12 (1973): 1709-1713.

Moore, J.H., C.C. Davis, M.A. Coplan, and S.C Greer. *Building Scientific Apparatus.* 4th Edition. Cambridge Univeristy Press, 2009.

Moore, T.E., et al. "The Thermal Ion Dynamics Experiment and Plasma Source Instrument." *Space Science Reviews* (Kluwer Academic Publishers) 71, no. 1-4 (1995): 409-458.

Mukai, T., and W. Miyake. "Transmission characteristics and fringing field effect of a 270° spherical electrostatic analyzer." *Rev. Sci. Instrum.* 57, no. 1 (1986): 49-55.

Nishigaki, S., and S. Kanai. "Optimization of the Herzog correction in the hemispherical deflector analyzer." *Rev. Sci. Instrum.* 57, no. 2 (1986): 225-228.

O'Connor, D.J. "Compact medium-energy electrostatic analyser." *J. Phys. E: Sci. Instrum.* 20 (1987): 437-439.

Offi, F., A. Fondacaro, G. Paolicelli, A.De. De Luisa, and G. Stefani. "Design and test ofa lens system for a high energy and high resolution electron spectrometer." *Nuclear Instruments and Methods in Physics Research A* 550 (2005): 454-466.

Ogilvie, K.W., et al. "SWE, a comprehensive plasma instrument for the WIND spacecraft." *Space Science Reviews* 71, no. 1-4 (1995): 55-77.
Oshima, C., R. Franchy, and H. Ibach. "Numerical calculations of electron trajectories in the 127° analyzer using a position-sensitive detector under conditions of fringing fields." *Rev. Sci. Instrum.* 54, no. 8 (1983): 1042-1046.
Oshima, C., R. Souda, M. Aono, and Y. Ishizawa. "Optimum angle of deflection electrodes of a cylindrical electrostatic analyzer." *Rev. Sci. Instrum.* 56, no. 2 (1985): 227-230.
Osterwalder, J., et al. "Electron trajectory analysis of the spherical-sector electrostatic spectrometer: focussing properties and multichannel detection capability." *Journal of Electron Spectroscopy and Related Phenomena* 48, no. 1 (1989): 55-99.
Oyama, K., and K. Hirao. "Inaccuracies in electron density estimates due to surface contamination of Langmuir probes." *Planet. Space Sci.* 24 (1976): 87-89.
Paolini, F.R., and C.G. Theodoridis. "Charged Particle Transmission Through Spherical Plate Electrostatic Analyzers." *Rev. Sci. Instrum.* 38, no. 5 (1967): 579-588.
Petit-Clerc, Y., and J.D. Carette. "The surface potential of metal surfaces under electron bombardment in high vacuum." *Vacuum* 18, no. 1 (1968): 7-16.
Pfaff, R.F., J.E. Borovsky, and D.T. Young, . *Measurement Techniques in Space Plasmas - Particles.* Vol. 102. Washington, DC: American Geophysical Union, 1998.
Polaschegg, H.D. "Optimization of the Parameters of the Ideal 180° Spherical Analyzer." *Applied Physics A: Materials Science & Processing* 9, no. 3 (1976): 223-227.
Poulin, A., and D. Roy. "Optimisation of the 180° hemispherical electrostatic deflector." *J. Phys. E: Sci. Instrum.* 11 (1978): 35-42.
Proca, G.A., and T.S. Green. "Minimum Image Size in a Parallel Plate Electrostatic Spectrograph." *Rev. Sci. Instrum.* 41, no. 12 (1970): 1778-1783.
Purcell, E.M. "The Focusing of Charged Particles by a Spherical Condenser." *Physical Review* 54 (1938): 818-826.
Read, F.H. "The parallel cylindrical mirror electron energy analyzer." *Rev. Sci. Instrum.* 73, no. 3 (2002): 1129-1139.
Read, F.H., D. Cubric, S. Kumashiro, and A. Walker. "The parallel cylindrical mirror analyzer: axis-to-axis configuration." *Nuclear Instruments and Methods in Physics Research A* 519 (2004): 338-344.
Reme, H., et al. "First multispacecraft ion measurements in and near the Earth's magnetosphere with the identical Cluster ion spectrometry (CIS) experiment." *Ann. Geophys.* 19 (2001): 1303.
Renfro, G.M., and H.J. Fischbeck. "Effects on focusing properties due to field fringing near the ends of the electrostatic cylindrical mirror analyzer." *Rev. Sci. Instrum.* 46 (1975): 620-624.
Risley, J.S. "Design Parameters for the Cylindrical Mirror Energy Analyzer." *Rev. Sci. Instrum.* 43, no. 1 (1972): 95-103.
Risley, J.S. "Magnetic Field Measurements Using an Electron Beam and an Electrostatic Analyzer." *Rev. Sci. Instrum.* 42 (1971): 267-268.
Ritchie, R.H., J.S. Cheka, and R.D. Birkhoff. "The spherical condenser as a high transmission particle spectrometer I. Point source." *Nuclear Instruments and Methods* 6 (1960): 157-163.
Rogers, F.T. "On the Theory of the Electrostatic Beta-Particle Analyzer. V." *Rev. Sci. Instrum.* 22, no. 10 (1951): 723-726.
Roy, D., and D. Tremblay. "Design of electron spectrometers." *Rep. Prog. Phys.* 53 (1990): 1621-1674.
Roy, D., and J.D. Carette. *Electron Spectroscopy for Surface Analysis.* Edited by H. Ibach. Berlin: Springer-Verlag, 1977.
Roy, D., and J.D. Carette. "Improvement of the Resolving Power and Transmission of Electrostatic Spectrometers." *J. App. Phy.* 42, no. 9 (1971): 3601-3615.
Roy, D., and J.D. Carette. "Methods of Measuring the Performance of an Electrostatic Spectrometer." *Rev. Sci. Instrum.* 42, no. 8 (1971): 1122-1127.
Roy, D., and J.D. Carette. "Optimum Deflection Angle for Cylindrical and Spherical Electrostatic Spectrometer." *Appl. Phys. Lett.* 16, no. 11 (1970): 413-416.
Roy, D., and J.D. Carette. "Spectrometres Electrostatiques. Partie III." *Can. J. Phys.* 49 (1971): 2138-2159.
Ruan, C.Y., S. Nguyen, and M. Fink. "Optimization of spherical deflecting analyzer with finite-size effects." *Rev. Sci. Instrum.* 70, no. 11 (1999): 4213-4220.

Rubio-Zuazo, J., and G.R. Castro. "First principle study of the properties of a Cylindrical Sector Analyzer: Complete calculation of the electron trajectory." *Journal of Electron Spectroscopy and Related Phenomena* 184 (2011): 440-451.

Rubio-Zuazo, J., M. Escher, M. Merkel, and G.R. Castro. "High Voltage-Cylinder Sector Analyzer 300/15: A cylindrical sector analyzer for electron kinetic energies up to 15 keV." *Rev. Sci. Instrum.* 81 (2010): 043304.

Rudd, M.E. "Analog Plotting System for Recording Energy Spectra of Low Energy Charged Particles." *Rev. Sci. Instrum.* 37 (1966): 971-973.

—. *Low Energy Electron Spectrometry.* Edited by K.D. Sevier. New York: Wiley-Interscience, 1972.

Sablik, M.J., D. Golimowski, J.R. Sharber, and J.D. Winningham. "Computer simulation of a 360° fieldofview ‘‘tophat’’ electrostatic analyzer." *Rev. Sci. Instrum.* 59, no. 1 (1988): 146-155.

Sagara, T., L. Boesten, S. Nishida, and K. Okada. "Resolution improvements for hemispherical energy analyzers." *Rev. Sci. Instrum.* 71, no. 11 (2000): 4201-4207.

SarEl, H.Z. "Criterion for Comparing Analyzers." *Rev. Sci. Instrum.* 41, no. 4 (1970): 561-564.

Sar-El, H.Z. "Cylindrical Capacitor as an Analyzer I. Nonrelativistic Part." *Rev. Sci. Instrum.* 38, no. 9 (1967): 1210-1216.

SarEl, H.Z. "Cylindrical Mirror Analyzer with Surface Entrance and Exit Slots. I. Nonrelativistic Part." *Rev. Sci. Instrum.* 42, no. 11 (1971): 1601-1606.

Sar-El, H.Z. "More on the spherical condenser as an analyzer I. Nonrelativistic Part." *Nuclear Instr and Methods* 42, no. 1 (1966): 71-76.

Sauvaud, J.A., et al. "The IMPACT SolarWind Electron Analyzer (SWEA)." *Space Sci. Rev.* 136, no. 1-4 (2008): 227-239.

Schmitz, W., and W. Melhorn. "Parallel plate analyser with second order focusing property." *J. Phys. E: Sci. Instrum.* 5 (1972): 64-68.

Siegbahn, K., N. Kholine, and G. Golikov. "A high resolution and large transmission electron spectrometer." *Nuclear Instruments and Methods in Physics Research Section A* 384 (1997): 563-574.

Siggel-King, M.R.F., R. Lindsay, F.M. Quinn, J. Pearson, G. Fraser, and G. Thornton. "TEARES: a toroidal energy- and angle-resolved electron spectrometer." *Journal of Electron Spectroscopy and Related Phenomena* 137-140 (2004): 721-729.

Simpson, J.A. "Design of Retarding Field Energy Analyzers." *Rev. Sci. Instrum.* 32, no. 12 (1961): 1283-1293.

Simpson, J.A. "High Resolution, Low Energy Electron Spectrometer." *Rev. Sci. Instrum.* 35, no. 12 (1964): 1698-1704.

Sise, O., T.J.M. Zouros, M. Ulu, and M. Dogan. "Novel and traditional fringing field correction schemes for the hemispherical analyser: comparison of first-order focusing and energy resolution." *Meas. Sci. Technol.* 18 (2007): 1853-1858.

Smeenk, R.G., R.M. Tromp, H.H. Kersten, A.J.H. Boerboom, and F.W. Saris. "Angle resolved detection of charged particles with a novel type toroidal electrostatic analyser." *Nuclear Instruments and Methods in Physics Research* 195, no. 3 (1982): 581-586.

Smith, Z.K., and J.R. Day. "A Mathematical Model of the Arc Pioneer 6⁄7 Plasma Probe." *Rev. Sci. Instrum.* 42, no. 7 (1971): 968-976.

Steckelmacher, W. "Energy analysers for charged particle beams." *J. Phys. E: Sci. Instrum.* 6 (1973): 1061-1071.

Stroscio, J.A., and W. Ho. "Design and performance of a doublepass highresolution electron energy loss spectrometer." *Rev. Sci. Instrum.* 57, no. 8 (1986): 1483-1493.

Szuszczewicz, E.P., and J.C. Holmes. "Surface contamination of active electrodes in plasmas: Distortion of conventional Langmuir probe measurements." *J. Appl. Phys.* 46, no. 12 (1975): 5134-5139.

Theodoridis, G.C., and F.R. Paolini. "Charged Particle Transmission through Cylindrical Plate Electrostatic Analyzers." *Rev. Sci. Instrum.* 39, no. 3 (1968): 326-330.

Theodoridis, G.C., and F.R. Paolini. "The Angular Response of Spherical Plate Electrostatic Analyzers." *Rev. Sci. Instrum.* 40, no. 5 (1969): 621-631.

Thomas, T.L., and E.L. Battle. "Effects of Contamination on Langmuir Probe Measurements in Glow Discharge Plasmas." *J. Appl. Phys.* 41, no. 8 (1970): 3428-3432.

Tokesi, K., L. Kover, and D. Varga. "A modified distorted field electrostatic analyzer." *Nuclear Instruments and Methods in Physics Research A* 348 (1994): 173-176.

Trubitsyn, A.A. "A cylindrical mirror analyser with high energy resolution." *Journal of Electron Spectroscopy and Related Phenomena* 73 (1995): 305-310.

Varga, D., K. Tokesi, and I. Rajta. "Design of an electrostatic electron spectrometer for simultaneous energy and angular distribution measurements." *Journal of Electron Spectroscopy and Related Phenomena* 76 (1995): 433-436.

Victor, A.L. "Design and Utilization of a Top Hat Analyzer for Hall Thruster Plume Diagnostics." *Ph.D. Dissertation.* University of Michigan, 2006.

Victor, A.L., T.H. Zurbuchen, and A.D. Gallimore. "Top hat electrostatic analyzer for far-field electric propulsion plume diagnostics." *Rev. Sci. Instrum.* 77 (2006): 013505.

Vilppola, J.H., J.T. Keisala, P.J. Tanskanen, and H. Huomo. "Optimization of hemispherical electrostatic analyzer manufacturing with respect to resolution requirements." *Rev. Sci. Instrum.* 64, no. 8 (1993): 2190-2194.

Vilppola, J.H., P.J. Tanskanen, B.L. Barraclough, and D.J. McComas. "Comparison between simulations and calibrations of a high resolution electroststatic analyzer." *Rev. Sci. Instrum.* 72, no. 9 (2001): 3662-3669.

Vilppola, J.H., P.J. Tanskanen, H. Huomo, and B.L. Barraclough. "Simulations of the response function of a plasma ion beam spectrometer for the Cassini mission to Saturn." *Rev. Sci. Instrum.* 67, no. 4 (1996): 1494-1501.

Wadey, W.G. "Magnetic Shielding with Multiple Cylindrical Shells." *Rev. Sci. Instrum.* 27, no. 11 (1956): 910-916.

Wang, K.L. "Optimum transport in charged particle analysers." *J. Phys. E: Sci. Instrum.* 5 (1972): 1193-1196.

Warmack, R.J., J.A.D. Stockdale, and R.N. Compton. "Apparatus for Energy, Angle, and Mass Analysis of Products from Alkali-Molecule Reactions." *International Journal of Mass Spectrometry and Ion Physics* 27, no. 3 (1978): 239-247.

Warmack, R.J., J.A.D. Stockdale, and R.N. Compton. "Ionizing collisions of cesium and potassium atoms with water." *J. Chem. Phys.* 68, no. 3 (1978): 916-925.

Warren, R.E., J.L. Powell, and R.G. Herb. "Electrostatic Analyzer for Selection of Homogeneous Ion Beam." *Rev. Sci. Instrum.* 18, no. 8 (1947): 559-563.

Wilson, R.G., and G.R. Brewer. *Ion Beams; With Applications to Ion Implantation.* John Wiley and Sons, Inc., 1973.

Wollnik, H., T. Matsuo, and H. Matsuda. "The Electrostatic Potential in a Toroidal Condenser." *Nuclear Instruments and Methods* 102, no. 1 (1972): 13-17.

Wollnik, Hermann. "Chapter 4.1 Electrostatic Prisms." In *Focusing of Charged Particles*, edited by Albert Septier, 163-202. New York: Academic Press, 1967.

Wuest, M., D. Evans, and R.V. Steiger, . *Calibration of Particle Instruments in Space Physics.* ISSI Scientific Report SR-007, 2007.

Yarnold, G.D., and H.C. Bolton. "The Electrostatic Analysis of Ionic Beams." *J. Sci. Instrum.* 26, no. 2 (1949): 38-40.

Yavor, M. *Advances in Imaging and Electron Physics.* Vol. 157. 2009.

Yavor, M.I., H. Wollnik, M. Nappi, and B. Hartmann. "Image aberrations of poloidal toroid electrostatic analyzers." *Nuclear Instruments and Methods in Physics Research A* 311 (1992): 448-452.

Yavor, S.Ya., and L.A. Baranova. "Optics of conical electrostatic analysing and focusing systems." *Nuclear Instruments and Methods in Physics Research Section A* 298, no. 1-3 (1990): 421-425.

Young, D.T. "Space Plasma Particle Instrumentation and the New Paradigm: Faster, Cheaper, Better." In *Measurement Techniques in Space Plasmas: Particles*, edited by R.F. Pfaff, J.E. Borovsky and D.T. Young, 1-16. Washington, D.C.: American Geophysical Union, 1998.

Young, D.T., A.G. Ghielmetti, E.G. Shelley, J.A. Marshall, J.L. Burch, and T.L. Booker. "Experimental tests of a toroidal electrostatic analyzer." *Rev. Sci. Instrum.* 58, no. 4 (1987): 501-508.

Young, D.T., et al. "2π-radian field-of-view toroidal electrostatic analyzer." *Rev. Sci. Instrum.* 59, no. 5 (1988): 743-751.

Zouros, T.J.M., and E.P. Benis. "Optimal energy resolution of a hemispherical analyzer with virtual entry." *Appl. Phys. Lett.* 86 (2005): 094105.